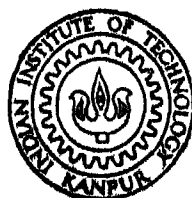


LASER EXCITED FLUORESCENCE AND LIFETIME STUDIES OF Dy^{3+} AND UO_2^{2+} IN SINGLE CRYSTALS

By
AREPALLI SIVARAM



DEPARTMENT OF PHYSICS

INDIAN INSTITUTE OF TECHNOLOGY KANPUR
DECEMBER, 1977

LASER EXCITED FLUORESCENCE AND LIFETIME STUDIES OF Dy^{3+} AND UO_2^{2+} IN SINGLE CRYSTALS

A Thesis Submitted
In Partial Fulfilment of the Requirements
for the Degree of
DOCTOR OF PHILOSOPHY

By
AREPALLI SIVARAM

to the

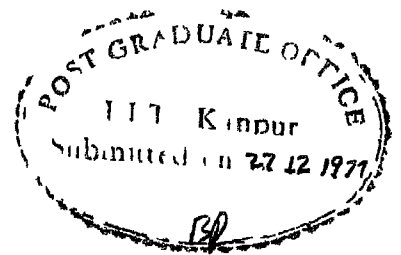
DEPARTMENT OF PHYSICS
INDIAN INSTITUTE OF TECHNOLOGY KANPUR
DECEMBER, 1977

117 1 1111
CENTRAL LIBRARY
Acc. No. **A 55479**

17 OCT 1978

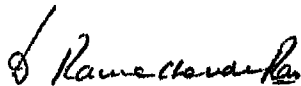
PHY-1977-D-SIV-LAS


To
My parents

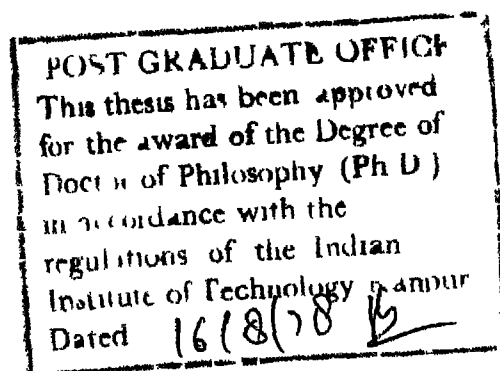


Certificate

This is to certify that the work presented in this thesis is the original work of Mr A Sivaram done under our joint supervision, and it is not submitted elsewhere for a degree


D Ramachandra Rao
Professor of Physics
I I T Kanpur

 Putcha Venkateswarlu
Dec 2, 1977
Putcha Venkateswarlu
Professor of Physics
I I T Kanpur



ACKNOWLEDGEMENTS

I would like to express my deep sense of gratitude to Professor Putcha Venkateswarlu and to Professor D Ramachandra Rao for introducing me to the field of solid state spectroscopy and for showing constant interest in my work as well as in my general well being

The lanthanum fluoride crystal used in the present work is loaned from Professor H P Broida, Univ of California, Santa Barbara I am very thankful to him

The calcium fluoride crystals were grown at B A R C , Bombay with the help of my colleague Mr H Jagannath I am indebted to Dr S Muralidhara Rao, Health Physics Division for his help in using their vacuum furnace for the crystal growth This is to acknowledge the interest shown by Dr S D Soman, Head, Health Physics Division and by Dr A K Ganguly, Director, Chemistry Division in my work

The lithium fluoride crystal containing uranium is loaned from Dr. A V R Warrier, Solid State Physics Laboratories Delhi I am also very thankful to him for many helpful discussions

My sincere thanks are due to Dr N A Narasimham, Head, Spectroscopy Division, B A R C , Bombay for the spectrochemical analysis of some of the crystals

I would like to thank Dr U V Kumar, Dr Bansilal and Mr. H Jagannath for their advice and readiness to help

me tackle many experimental difficulties I am also thankful to Dr K S Rama Sastry for the patient help rendered while working with the pulsed Argon ion laser

The friendship and co-operation of all the past and present members of the Molecular and Laser Spectroscopy (MOLS) group is gratefully acknowledged I am thankful for the co-operation extended by Central glass blowing section, Physics Electronics shop and Physics work shop

Thanks are due to Miss C Komala for patiently typing the rough drafts, to Mr B N Srivastava for the neat tracings and to Mr H K Panda for the careful cyclostyling work

It is a pleasure to thank my friends and many families of this Campus for their encouragement and unreserved help

Words are woefully inadequate to express my feelings towards my parents and to the other members of our big family for their perseverance in letting me pursue this ambition of mine The understanding nature and co-operation of my wife Swarajya Lakshmi has been very helpful and I would like to thank her for the neat and patient typing

The financial assistance from the Council of Scientific and Industrial Research, India and from the National Bureau of Standards, U S A , is gratefully acknowledged.

A SIVARAM

CONTENTS

	<u>Page</u>
Synopsis .	ix
Chapter 1 <u>INTRODUCTION</u> .	1
1.1 General . .	1
1.2 Static ion-lattice interaction .	3
1.2.1 Dynamic ion-lattice interaction . . .	5
1.3 Relaxation processes . .	9
References	13
Chapter 2 <u>EXPERIMENTAL DETAILS</u>	15
Abstract	15
2.1 Experimental set-up for the recording of fluorescence with the Argon ion laser	16
2.2 Experimental arrangement for fluorescence with N ₂ laser excitation	19
2.3 Set-up for lifetime measurements	21
2.3.1 Laser source . .	22
2.3.2 Electronics . . .	24
References	29
Chapter 3 <u>THE STEADY STATE AND TRANSIENT FLUORESCENCE SPECTRUM OF Dy³⁺ LaF₃</u> . . .	30
Abstract	30
3.1 Introduction	32
3.2 Experimental details	34

		<u>Page</u>
3.3	Fluorescence from G-level . . .	35
3 4	Lifetime of F-level . . .	39
3 5	Lifetime of G-level . . .	40
3 6	Radiative relaxation rates of F and G-levels . . .	41
3 7	Polarized fluorescence from the F-level . . .	45
	3.7.1 Crystal structure of LaF_3 and polarized lines . . .	51
	3 7.2 Discussion . . .	52
3 8	Conclusion	56
	References	57
Chapter 4	<u>THE STEADY STATE AND TRANSIENT FLUORESCENCE SPECTRUM OF $\text{Dy}^{3+} \text{CaF}_2$</u>	60
	Abstract	60
4 1	Introduction	61
4 2	Crystal structure of CaF_2 and analysis of the spectra of $\text{Re}^{3+} \text{CaF}_2$	64
4 3	Experimental details	68
4.4	General features of the fluorescence spectrum at 77 and 300°K	69
	4 4.1 Analysis and discussion	71
4.5	Temperature dependence of the 'cubic spectrum'	87

		<u>Page</u>
4 6	Variation of the fluorescence spectrum with excitation wavelength . .	91
4.7	High temperature fluorescence spectrum .	92
4.8	Conclusion .	97
	References .	98
Chapter 5	<u>THE STEADY STATE AND TRANSIENT FLUORESCENCE SPECTRUM OF LiF UO_2^{++} SINGLE CRYSTAL</u>	
	Abstract . . .	100
5 1	Introduction .	101
5 2	Experimental details .	105
5 3	Fluorescence spectrum at 77°K . .	106
5.4	Relaxation rates of F and C levels . .	113
5 5	Self-absorption and oscillator strength determination .	119
5 6	Conclusion .	123
	References . .	125

SYNOPSIS

The spectroscopic study of impurity ions in single crystals has been valuable for understanding the structure of solids and the ions themselves. The discovery of solid state lasers gave further impetus to these studies. The search for new laser material has particularly necessitated a detailed study of the excitation and deexcitation mechanisms of the impurity ions. The development of tunable and pulsed lasers has made these studies more feasible. This thesis presents the study of the steady state and the transient fluorescence of Dy^{3+} in LaF_3 and CaF_2 and of UO_2^{++} in LiF single crystals using Ar^+ and N_2 lasers.

The first chapter gives a brief introduction to the spectroscopy of rare earth ions and transuranium ions and outline of the different relaxation processes relevant to these classes of ions.

The experimental details are presented in Chapter 2. The spectra are recorded using a pulsed Ar^+ laser and a N_2 laser fabricated in the laboratory along with a CW Ar^+ laser (Spectra Physics, 165-03). The spectrophotometer used is assembled around a 0.75m Jarrell-Ash spectrograph and is fitted with an ITT No. FW 130 photomultiplier tube. Fluorescence excited by the N_2 laser is photographed using a Carl-Zeiss three prism spectrograph. The decay times are measured using a boxcar integrator (PAR, No. CW-1).

Chapter 3 presents the study of the steady state and the transient fluorescence spectrum of $\text{Dy}^{3+} \text{LaF}_3$ in the 4500-9000 Å region in the temperature range of 77 to 673°K. The spectrum shows significant polarization which is incompatible with the low site symmetry of the Dy^{3+} ion in LaF_3 crystal. An attempt is thereby made to explain the polarized lines by considering possible distortion towards higher site symmetry of the rare earth ion and also by the coupling of lattice phonons to the stark levels. However the observed polarization could not be explained completely.

This chapter also presents the fluorescence from G-level ($^4\text{I}_{15/2}$) which has so far not been reported in any lattice. The increase in intensity of this G-fluorescence with temperature is understood in terms of thermal population of this level from the F-level.

The decay time of F-level ($^4\text{F}_{9/2}$) is found to be ~ 1.39 msec throughout the temperature range of study, which signifies the purely radiative nature of the fluorescence decay. The G-level is found to show the same decay time. This observation also is in favour of the hypothesis of thermal mixing between the F and G levels. An estimate of the radiative relaxation rates has been made using a simplified model of four-level system.

The work on the fluorescence and lifetimes of the Dy^{3+} CaF_2 is presented in Chapter 4. The study is done in the 4500-9000 Å region, in the temperature range of 77 to 673°K using six concentrations of dysprosium (0.01 to 1.08% by wt. of DyF_3 in CaF_2). At 77°K, five groups of lines are observed, all of them originating from F-level ($^4\text{F}_{9/2}$). These studies show that there are at least two kinds of Dy^{3+} -centers, one with fluorescence decay time (τ) of ~ 1.3 msec (A-center) and another with ~ 3.5 msec (B-center). The energy level schemes for both these centers are presented. The lines belonging to the B-center increase in intensity as the Dy-concentration is increased. The variation of intensity with Dy-concentration and their line positions match with the cubic center reported by earlier workers. The lines belonging to the A-center match well with the tetragonal center, also reported earlier. The earlier work on cubic center was done upto 6700 Å and that on tetragonal center upto 5800 Å only.

In these crystals fluorescence from the G-level ($^4\text{I}_{15/2}$) is observed from both the centers in the temperature range of 300 to 673°K. Here also, as in LaF_3 , the lifetime of F- and G-levels are independent of temperature and are found to be the same within experimental errors thereby indicating the thermalization taking place between these two levels for the two centers observed.

In chapter 5, the fluorescence and lifetime studies of Uranium activated LiF in the temperature range of 77 to 673°K are presented. The fluorescence spectrum in the 5200 Å region, which has also been reported by earlier workers, consists of two zero-phonon lines (F_0 and C_0) coming from the first excited electronic state (${}^3\Delta_u$) of Uranyl ion (UO_2^{++}) along with four vibrational side bands ($\nu_{vib}^1 \sim 800 \text{ cm}^{-1}$). The fluorescence observed in the present study at wavelengths less than 5200 Å is not yet understood.

New fluorescence is observed in 7500 Å region which shows a 750 cm^{-1} vibrational quantum. From the energy level considerations and from earlier reported decrease of vibrational quantum energy associated with excited electronic states, this fluorescence has been tentatively assigned as due to ${}^3\pi_u \rightarrow {}^3\Delta_u$ transition.

The lifetimes measured in the temperature range of 77 to 673°K are found to be different for different regions of the spectrum. The zero-phonon lines (F_0 and C_0) and their vibrational satellites show a lifetime of $\sim 600 \mu\text{sec}$ at 77°K, while the lines in the 7500 Å region, show a lifetime of $\sim 2000 \mu\text{sec}$. It is observed that these decay times vary with temperature. A simple model is proposed to explain the temperature variation of decay times of F_0 , C_0 and their vibrational satellites involving the thermalization of the excited electronic levels corresponding

to F_0 and C_0 . The radiative rate of F_0 is found to be of the order of $1.5 \times 10^5 \text{ sec}^{-1}$ on the basis of this model.

The higher energy zero-phonon line (F_0) is found to show self-absorption. From the observed decrease in intensity and the 'hump-separation' the oscillator strength is calculated to be $\sim 2 \times 10^{-6}$, signifying the forced electric dipole nature of this transition.

In conclusion, the results of the steady state and the transient fluorescence studies of Dy^{3+} in LaF_3 and CaF_2 and UO_2^{++} in LiF single crystals have been presented. The radiative relaxation rates of $\text{Dy}^{3+} \cdot \text{LaF}_3$ are obtained using a four-level model. The spectrum of $\text{Dy}^{3+} \cdot \text{CaF}_2$ system is interpreted as due to different centers. A simplified model is proposed to understand the temperature variation of decay times of UO_2^{++} in LiF . The oscillator strength is estimated from the observed self-absorption of F_0 -fluorescence of this system. The polarization features of Dy^{3+} fluorescence in LaF_3 can probably be understood by performing experiments at 4.2°K and by carrying out the Zeeman studies.

CHAPTER 1

INTRODUCTION

1.1 General

In recent years, the spectroscopic investigations of lanthanide and actinide ions have gained considerable attention as these ions are found to be good lasants. A detailed study of the excitation and deexcitation mechanisms of these ions in single crystals is helpful in the search for new laser materials as well as to understand the structural and dynamical properties of the crystals. Several techniques like absorption, fluorescence, EPR, etc. have been used to evaluate the energy levels and energy transfer processes of these ions in single crystals. This thesis represents an attempt to study the steady state and the transient fluorescence spectra of Dy^{3+} in LaF_3 and CaF_2 and of UO_2^{2+} in LiF single crystals using Ar^+ and N_2 lasers.

The normal electronic configurations of neutral lanthanides (actinides) consist of a closed shell of xenon (radon) structure, $4f^N$ ($5f^N$) electrons and two or three loosely bound electrons. Trivalent state is the normal excitation state* for lanthanide (actinide) ions. The

*Stable divalent ions like Sm^{2+} , Eu^{2+} , U^{2+} , tetravalent ions like Ce^{4+} , U^{4+} , Np^{4+} and hexavalent ions like U^{6+} are also reported in literature.

optical spectra of these ions generally consist of several groups of sharp lines. The relative positions of the centers of gravity of these groups are not found to alter much from host to host thereby reflecting the weak influence of the environment (which is usually in the form of crystal field) on the ions. The observed lines of triply ionized lanthanides (actinides) are associated with transitions among the levels of $4f^N$ ($5f^N$) configurations. Shielding from the crystal field is provided by the $5s^2 5p^6$ ($6s^2 6p^6$) orbitals. However, the shielding of actinide ions is small compared to lanthanide ions and probably because of this, the chemical properties of actinides are considerably different from those of lanthanides. Thus the actinides are found to form stable molecular complexes such as UO_2^{2+} , NpO_2^{2+} , etc., reflecting the covalent bonding while lanthanides retain their ionic character¹⁾. When the lanthanide (actinide) ions are doped in crystals, the free ion energy levels of the ions are split into a number of Stark components. The number of components and the extent of splitting depends on the strength and symmetry of the static part of the ion-lattice interaction. The dynamical part of the ion-lattice interaction involving phonons of the lattice gives rise to the thermal dependence of the transitions and results in energy exchange processes between the ion and the lattice.

1.2 Static Ion-lattice Interaction

The Hamiltonian of the system can be written as

$$H = H_0 + V_0 \quad (1.1)$$

where V_0 represents the static interaction of the ion with the crystalline environment and H_0 is free ion Hamiltonian which is represented in the usual notation by

$$H_0 = \sum_{i=1,N} \left(\frac{\hbar^2}{2m} v_i^2 - \frac{ze^2}{r_i} \right) + \sum_{i>j=1,N} \frac{e^2}{r_{ij}} + \sum_{i=1,N} \zeta_i \vec{L}_i \cdot \vec{S}_i \quad (1.2)$$

V_0 can be expanded in terms of spherical harmonics as

$$V_0(r_1, \theta_1, \phi_1) = \sum_{l,m} A_{lm} r_1^{-l} Y_l^m(\theta_1, \phi_1) \quad (1.3)$$

In the central field approximation (zero-order approximation), all states of a given configuration f^N have the same energy. Part of this degeneracy is removed with the inclusion of interelectronic repulsion and spin orbit interaction. The electronic repulsion term gives rise to different electronic states (called multiplets) and the spin orbit interaction further splits these states into levels having different J values. The levels finally have only one good quantum number J . When the ion is embedded in a crystal, the extent to which the $(2J+1)$ -fold degeneracy of these levels is lifted depends upon the symmetry of the crystal field. By knowing the site symmetry of the ion in the lattice, it is possible to predict the

number of Stark components into which the J level is split and the transformation properties of the corresponding wave functions using group theory. Several site symmetries for the ions are possible when they are accommodated in a lattice (e.g. CaF_2) having aliovalent cations

The spectral lines of the lanthanide (actinide) ions doped in crystals in the optical region are associated with transitions among the levels of $4f^N$ ($5f^N$) configuration and are found to involve electric dipole radiation. The intra-configurational transitions due to electric dipoles are forbidden because of the parity rule within the free ion energy levels. However, these transitions become allowed through configurational mixing (e.g. $4f^N$ and $4f^{N-1} 5d$) brought about by the ion-lattice interaction and hence are called forced electric dipole transitions. In the case of static crystal field interaction with the ion, the crystal field has to be non-centrosymmetric to bring about this admixture of different configurations. When the crystal field has a center of inversion (i.e., centrosymmetric), the dynamic crystal field interaction with the ion through the lattice phonons can bring about the configurational mixing. The oscillator strengths (f) of the forced electric dipole transitions are very small and are of the order of 10^{-6} whereas for allowed electric dipole transitions²⁾, f is of the order of 10^{-3} .

1 2.1 Dynamic Ion-lattice Interaction

This interaction is reflected in the following experimental observations

(1) The presence of spectral lines which are allowed by the simultaneous interaction of the ionic system with both lattice vibrations and the radiative field,

(2) The presence of radiationless processes in crystals, by which an ion in an excited state decays by transferring its energy to phonons, and

(3) The dependence of the width and the position of the spectral lines on the temperature. The Hamiltonian describing the total system (ion + lattice) can be written as²⁾

$$H = H_{\text{latt}} + H_{\text{ion}} + H_{\text{int.}} \quad (1.4)$$

where

$$H_{\text{ion}} = H_0 + H_{\text{cryst}}$$

$$H_{\text{latt.}} = \sum_k \hbar \omega_k (a_k^\dagger a_k + 1/2), \text{ summed over all } 3N \text{ oscillators of the lattice,}$$

$$H_{\text{int}} = \text{interaction Hamiltonian}$$

The crystalline field is due to the charges of the (ligand) ions surrounding the lanthanide (actinide) ion, therefore a distortion of the ligand ions affects the crystal field. Such a distortion is a function of the local strain and the crystal field potential can be

expressed as

$$V_{\text{cryst}} = V_0 + V_1\varepsilon + V_2\varepsilon^2 + \quad (1.5)$$

where V_0 , the static term is included in the Hamiltonian H_{ion} as H_{cryst} , which has been discussed earlier. V_1 , V_2 , etc. are the coupling parameters which are functions of the coordinates of the electrons of the lanthanide (actinide) ion and of the static distances of this ion and the ligand charges

The interaction Hamiltonian can thus be written as

$$H_{\text{int}} = V_1\varepsilon + V_2\varepsilon^2 + \quad . \quad (1.6)$$

The different terms in H_{int} give rise to the different processes (V_1 for first order process etc.) involving emission or absorption of one phonon (for first order process), two phonons etc. The relative importance decreases as one considers higher and higher order processes. All these processes involving lattice phonons are temperature-dependent²⁾

Vibronic transitions observed in the optical spectra of lanthanide (actinide) ions belong to the first order process. An indication of the vibronic character of the transitions is given by the close fitting of the fluorescence lifetimes of vibronic lines and the lifetimes of the zero-phonon (pure electronic) lines. Also, the

thermal shift of the peaks of the vibronic lines is equal to the shift of the zero-phonon line. They show the same Zeeman effect as the zero-phonon line³⁾ Vibronic transitions can be easily detected by their temperature dependence and from group theoretical analysis⁴⁾ The vibronic transition between two levels i and j depend essentially on the matrix element

$$[\langle \psi_f^{\text{elec}} | e^{i\vec{k} \cdot \vec{r}} \vec{p} \cdot \vec{\pi}_k^\lambda | \psi_j^{\text{elec}} \rangle] \times [\langle \psi_j^{\text{elec}} | v_p | \psi_i^{\text{elec}} \rangle] \quad (1.7)$$

where $\vec{\pi}_k^\lambda$ is the polarization of the photon,

$e^{i\vec{k} \cdot \vec{r}} \vec{p}$ is the electric multipole radiation operator,

v_p is the operator representing the vibrational mode involved

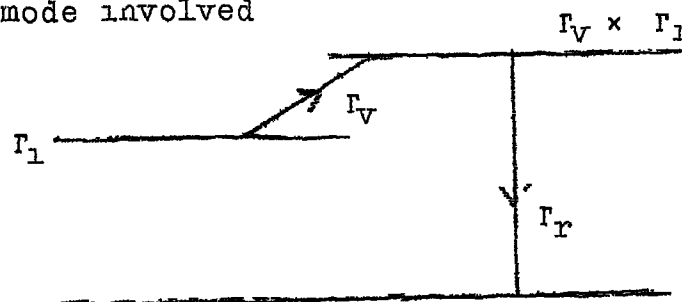


Fig. 1.1

The selection rules for vibronic transitions can be illustrated by considering Fig. 1.1. Γ_i and Γ_f denote the representations of the initial and final levels of the vibronic transition, Γ_v is the representation of the active vibrational mode and Γ_r is the representation of the radiation operator. The transition is allowed if

the direct product representation ($\Gamma_L \times \Gamma_V \times \Gamma_R$) contains Γ_f . In general, it is possible that phonons with all possible wave vectors (\vec{k}) can participate in these transitions^{5,6}). It is observed that phonons belonging to high symmetry points in the Brillouin Zone are predominant in the vibronic transitions⁶). Thus, the representations of the phonons at these special points have to be reduced into a sum of irreducible representations of the site symmetry group of the lanthanide (actinide) ion and the selection rules can then be derived which would also give polarization features of the vibronic transitions.

Second order and higher order processes (multi-phonon processes) are found to be responsible for the non-radiative relaxations of the ion between two levels. The relative importance of the contributions of the different processes decreases as the order of the process increases. All these processes are temperature dependent and give rise to the observed thermal broadening of the spectral lines which results in homogeneous broadening⁶ (Lorentzian line shape). In the case of lanthanides, in which the crystal field produces splitting of the 'J-levels' that is smaller than kT_D (T_D is the Debye temperature), the multi-phonon

* The broadening of lines observed at very low temperatures where thermal vibrations are quenched is attributed to microscopic strains in the crystal. This inhomogeneous broadening results in a 'Gaussian line shape'.

relaxation processes may produce a shortening of the lifetime of a certain level and give a homogeneous 'lifetime broadening' contribution. In actinides, where the crystal field effects are large, one observes large thermal dependences of 'band' (line) positions, band widths and band areas because of the changing crystal field with temperatures²⁾.

1.3 Relaxation Processes

Ions in excited levels can relax to lower levels radiatively as well as nonradiatively. The observed lifetime of an excited level is the inverse of the sum of the probabilities for all possible transitions (radiative and nonradiative) to all the lower levels,

$$\text{i.e., } \tau_1^{-1} = \sum_j \omega_{1j}^r + \sum_j \omega_{1j}^{nr} \quad (1.8)$$

where ω_{1j}^r (ω_{1j}^{nr}) is the probability of radiative (non-radiative) transition from level 1 to level j

The radiative relaxation of the lanthanide (actinide) ions is mostly due to forced electric dipole transitions which become allowed because of configurational mixing, as has been discussed earlier (Sec 1.2). The calculation of the transition probabilities for forced electric dipole transitions thus involves the sum over the levels of a large number of configurations. Judd⁷⁾ and Ofelt⁸⁾ have shown that the electric dipole transition

probability can be expressed in terms of a small number of intensity parameters which are characteristic of the host lattice. Using this theory, the observed spectral intensities and radiative lifetimes can be explained satisfactorily⁹⁻¹²⁾

There are number of ways in which a nonradiative relaxation can take place. The ion interacts with the lattice and relaxes to the lower levels by spontaneous emission of phonons in the multiphonon relaxation process^{13,14)}. In the ion-ion interaction relaxation process, the energy transfer takes place between the excited ion and the other ions in the ground state through multipole (dipole-dipole, quadrupole-dipole etc.) interactions or exchange interactions with or without the assistance of lattice phonons^{15,16)}. Another well known process is the migration of the excitation energy among the ions until a quenching center is encountered¹⁷⁾. In addition to these, other processes like cooperative energy transfer have been observed which involve more than two ions^{18,19)}.

The multiphonon relaxation process, which plays the dominant role in the nonradiative relaxation contribution of the decay times for low concentrations of the ions, has been very well studied. The spontaneous emission of the lattice phonons takes place during the transition of the ion between two energy levels. With increasing

temperature, the multiphonon relaxation is contributed by stimulated emission of phonons also

The rate of spontaneous emission of phonons has been observed to depend exponentially on the energy separation of the levels. It is characteristic of the lattice and is independent of the ion. It is given by²⁰⁾

$$\omega = C \exp(-\alpha / \Delta E) \quad (19)$$

where C and α are constants characteristic of the lattice and ΔE is the energy separation between the levels. The rates calculated from this equation are found to be within ± 50 percent of the experimentally observed values.

The rate of multiphonon transitions vary with temperature due to the stimulated emission of phonons from the thermally excited phonon modes of the lattice. The phonon mode whose frequency is close to the cut-off frequency of the phonon spectrum of the lattice (Debye-phonon) has been found to play a dominant role in the relaxation process^{13,14,20,21)}. The observed multiphonon transition rate (MPTR) of a Stark manifold at any temperature is a weighted (thermal) average of the individual rates of the thermally accessible Stark levels.

It is observed that when the ions are pumped into higher levels and the observed fluorescence is from lower levels, the decay rates of the lower levels are influenced by those of higher levels and their branching

ratios The branching ratio for transitions from level i to level j is given by

$$\beta = \frac{\omega_{ij}}{\sum_j \omega_{ij}} \quad (1.10)$$

where ω_{ij} is the transition rate (radiative + nonradiative). The 'buildup-times' (t_{max}) observed as 'peaks' in the fluorescence decay-curves reflect these effects. From the observed t_{max} , the branching ratios and the transition rates of different higher levels can be obtained by monitoring the decay of the fluorescence from the lower level^{2,22)}. By solving the rate equations of the system of levels, one can thus get all the dynamical characteristics of the different excited levels. Transient fluorescence study is thus helpful in understanding the different excitation and deexcitation processes that take place amongst the energy levels of the ion.

Analysis of the steady state and the transient fluorescence spectra of ions in crystals is the aim of the most of the current studies, and a vast amount of literature exists on these topics. Only a cursory review of some of the salient features necessary for this thesis is presented here.

REFERENCES

- 1 G H Dieke, 'Spectra and energy levels of Rare Earth Ions in Crystals', Interscience Publ , NY (1963)
- 2 B Di Bartolo, 'Optical Interactions in Solids', John Wiley and Sons (1963)
- 3 Y K. Chow, Z. Phys 124, 52 (1948)
- 4 W.M Yen, W.C Scott and A.L Schawlow, Phys Rev A136, 271 (1964)
- 5 R Loudon, Proc. Phys. Soc. 84, 379 (1964).
- 6 M J. Weber and R F Schaufele, Phys Rev. A138, 1544 (1965)
7. B R. Judd, Phys Rev 127, 150 (1962)
8. G.S Ofelt, J Chem. Phys. 37, 511 (1962)
9. W F Krupke, Phys Rev. 145, 325 (1966)
10. M.J. Weber, Phys. Rev. 157, 262 (1967).
- 11 M.J Weber, Phys. Rev. 171, 283 (1968).
12. M J. Weber, T.E Varitomos and B H Matsinger, Phys Rev B8, 47 (1973).
13. A. Kiel, 'Quantum Electronics' (Ed. P. Grivet and N. Bloembergen), Columbia Univ. Press, NY (1964), Vol. 1, p 765
- 14 T E Fong, H.V Lauer and C.R. Chilver, J. Chem Phys. 63, 366 (1975) and references contained therein
- 15 J Miyakawa and D L. Dexter, Phys. Rev. B1, 2961 (1970) and references contained therein
- 16 N Yamada, S. Shionoya and T. Kishida, J. Phys. Soc Japan 32, 1577 (1972).

- 17 M Yokota and O. Tanimoto, J. Phys. Soc Japan 22, 779 (1967)
- 18 W Ostermayer and L J Van Vliet, Phys. Rev B1, 4208 (1970)
- 19 L D Litvanova, I.G Saizkulov and A L Stolov, Sov Phys. Solid State 11, 750 (1969).
- 20 L A. Riseberg and H. I Moos, Phys. Rev 174, 429 (1968).
21. D. Partlow and H I Moos, Phys Rev. 157, 252 (1967).
- 22 S.A. Pollack, J Chem. Phys 38, 2521 (1963)

CHAPTER 2

EXPERIMENTAL DETAILS

ABSTRACT

A pulsed N_2 laser and a pulsed Ar^+ laser both fabricated in the laboratory along with a commercial CW Ar^+ laser (Spectra-Physics), are employed for recording the fluorescence spectra and for the measurement of lifetimes of the fluorescence levels. The spectrometer used is assembled around a 0.75 m plane grating spectrograph, fitted with a $1W$ 130 photomultiplier tube. The wavelength accuracy is $\sim 1.5 \text{ \AA}$. The fluorescence excited by the N_2 laser is photographed using a Carl-Zeiss three prism spectrograph.

For transient (lifetime) studies, a boxcar integrator is used. Initially the experiments were conducted by chopping the CW Ar^+ laser output by a rotating prism to obtain light pulses of $\sim 10 \text{ }\mu\text{sec}$ width with a repetitive rate of 20 to 170 pps. Latter work is carried out with the pulsed Ar^+ laser fabricated in the laboratory. In this case, the pulse widths can be varied from 2 to 50 μsec with a maximum repetition rate of 50 pps. The N_2 laser is employed whenever it yielded strong fluorescence. The N_2 laser could be operated with a maximum of 70 pps and a pulse width of $\sim 80 \text{ nsec}$.

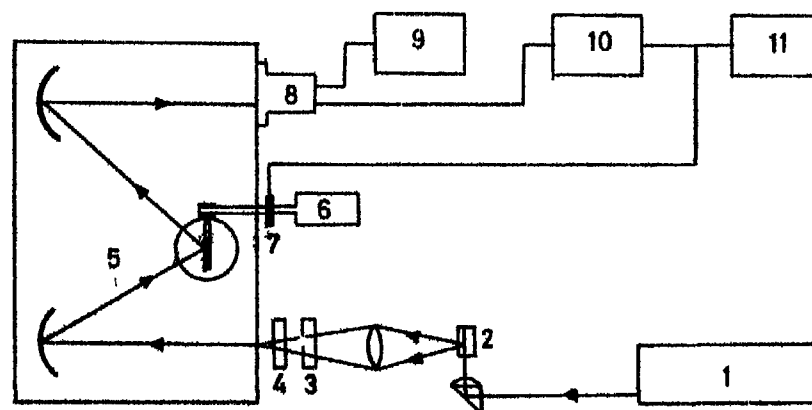
2.1 Experimental set up for the recording of fluorescence with the Argon ion laser

The steady state fluorescence spectra excited by the CW Ar^+ laser are recorded by the experimental set up¹⁾ shown in Fig 2.1

The Ar^+ laser used is a Spectra-Physics, No 165-03. It is capable of operating at any of the nine spectral lines, which can be selected by an intra-cavity tuning prism

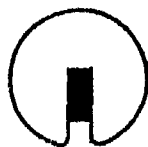
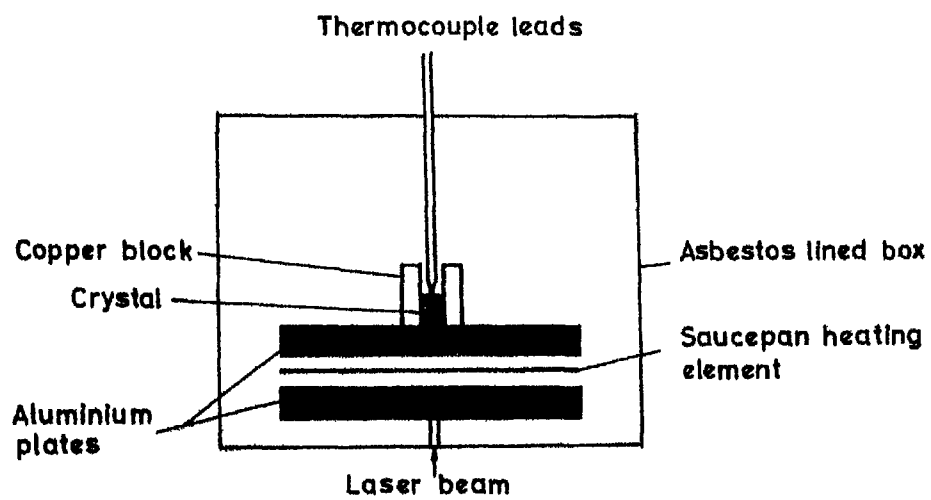
The laser beam is made vertical and focused on to the crystal under study by a right angled prism, lens combination. Standard demountable cold-finger dewars are fabricated for measurements at 77°K. The lower portion of the cryostat has five windows, four on four sides and the fifth at the bottom. The heater assembly²⁾ shown in Fig 2.2 is used for high temperature measurements (300 to 600°K). The laser light enters the crystal from the bottom as shown and the fluorescence is collected perpendicular to the plane of paper.

The emitted fluorescence light is collected by a double convex lens of 2'' focal length and 2'' aperture. This lens is so chosen as to overfill the collimating mirror of the 0.75 m, f/6.3 plane grating spectrograph (Jarrell-Ash, Model No. 75-000). This spectrograph which uses an asymmetric Czerny-Turner mounting, has a worm and gear arrangement to rotate the grating table. One revolution of the grating shaft results in a 0.1 degree rotation



- | | |
|-----------------|-------------------------|
| 1 Laser | 7 Cam and Microswitch |
| 2 Crystal | 8 Photomultiplier tube |
| 3 Polarizer | 9 H V Power supply |
| 4 Filter | 10 Picoammeter |
| 5 Monochromator | 11 Strip chart recorder |
| 6 Motor | |

FIG 21 BLOCK DIAGRAM OF THE RECORDING SPECTROPHOTOMETER
(Ref 1)



Top view of crystal holder

FIG 22 HEATER ASSEMBLY
(Ref 2)

of the grating. A mechanical counter indicates the setting, in hundredths of a degree. The grating is rotated using a reversible d.c. motor (Bodine, No. NSH-12RG), fed by a regulated 115 V d.c. power supply (Minarik electronics, No. 1214). The speed of the motor can be varied in six steps between 0.5 and 3 rpm, which results in scanning speeds of 26 to 156 Å/minute for a 1200 grooves/mm grating. The grating used is blazed at 5000 Å and has 1200 grooves/mm. A precision bilateral slit (Jarrell-Ash, No. 12-000) is mounted in place of the plate holder using the same clamping arrangements.

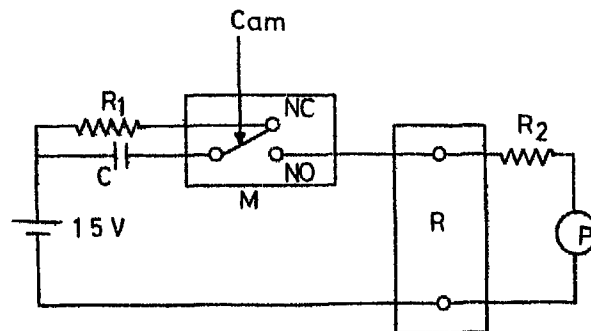
To eliminate second order spectra and also to minimise the scattered laser radiation, Corning glass filters are used. To study the polarization characteristics of the fluorescence, a polaroid sheet is used below 6500 Å and a Glan-Thompson prism beyond 6500 Å.

A photomultiplier tube (PMT, No. FW 130) is fixed directly in front of the exit slit. The response of the FW 130 tube is S-20 and its dark current at 1300 V at room temperature is ~10 nA, which obviates the necessity of 'PMT-cooling' unlike other photomultipliers. The high voltage required for the tube is obtained from a stabilised high voltage power supply.

The current from the PMT (for steady state experiments) is measured by a picoammeter (Keithley, No. 417),

which has a full scale range variable between 3×10^{-5} amps and 3×10^{-14} amps in a 3, 1, 0 1 and 0 3 sequence. In the current ranges below 3×10^{-3} amps, a low pass filter with time constant continuously variable from 0 to 3 secs can be used for noise rejection. The d c component of the dark current of the PIT can be subtracted out using the 'Current Suppress'. The picoammeter has an output of 3 V for full scale deflection, which is used to drive the strip chart recorder (Varian Model No G-14A-2). The recorder has two chart speeds of 2.5 cms and 10 cms/min giving a dispersion of 0.26 Å to 1.56 Å/mm for the various speeds of the grating rotation (1.0 Å/mm is generally used).

A provision is also made to obtain a 'wavelength marker' on the chart for every rotation of the grating shaft (Fig. 2.3). A cam attached to the grating drive shaft closes the microswitch [Desbo (India), No MVR6] contact once every rotation and connects a 1.5 V dry cell across the recorder terminals through a capacitor. The capacitor allows only a sharp spike of voltage to pass through, at the instant the contact is closed. During the off period of the microswitch, the capacitor is discharged through the resistor R_1 to make it ready for the next marker. R_2 is an isolation resistor inserted in the picoammeter output lead to prevent the shunting of the 1.5 V pulse by the low output impedance of the picoammeter.



M = Microswitch-(Kesbo No MVR-6)

NC = Normally closed contact

NO = Normally open contact

R = Recorder

P = Picoammeter

C = $\sim 0.1 \mu\text{F}$

$R_1 = \sim 10 \text{ K}\Omega$

$R_2 = \sim 50 \text{ K}\Omega$

**FIG.2 3 SCHEMATIC DIAGRAM OF THE WAVELENGTH
MARKER CIRCUIT**

Since the output impedance of the recorder is $1\text{M}\Omega$, this series resistance R_2 does not reduce the voltage received by the recorder significantly

By recording the spectra of standard sources like the low-pressure discharges of Ar, He-Ne, and Cs, the positions of the markers could be calibrated and are repeatable to $\pm 1 \text{ \AA}$. Usually the spectra are recorded several times and the calculated wavelength of the spectral lines rarely differ from each other by more than 1 \AA and the rms deviation (of 5 repetitions) is less than 0.5 \AA .

Some preliminary work on the fluorescence spectrum of $\text{Dy}^{3+} \text{LaF}_3$ using Ar^+ laser excitation on a Spex No 1400 double monochromator was done by Professor P Venkateswarlu in association with Dr. J J. Kim at the University of California, Santa Barbara. These results were used by the author during the initial stages of work. All the recordings and the numbers reproduced in this thesis are however, obtained by the author on the setup assembled here.

2.2 Experimental arrangement for fluorescence with N_2 laser excitation

The optical arrangement is shown in Fig 2.4. The length of the N_2 laser plasma tube is 80 cms and the optimum pressure for the commercial nitrogen gas used is 40 mm of Hg at an excitation voltage of 12 KV d.c.. The spark gap is flushed continuously with air at a pressure

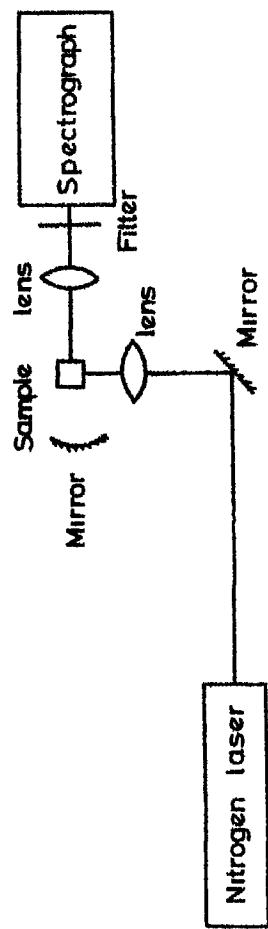


Fig 2 4 Optical arrangement for photographing the spectrum with N_2 laser

(Ref 3)

of ~ 2 bar. The pulse repetition rate can be controlled by triggering the spark gap with a trigger generator. However, this is not used for the present work and the spark gap is fired in a self-quenched mode where the repetition rate depends on the applied voltage. The laser pulse generated has a width of 8 nsec with an estimated peak power >100 KW. The repetition rate used is ~ 25 pps.

The cross section of the laser beam is a rectangle of dimensions $4 \times 10 \text{ mm}^2$. It is reflected upwards by a front coated (aluminum) mirror and is focused into the crystal by a quartz lens (2" dia, 1" focus). Fluorescence from the crystal is collected in a perpendicular direction and is focused on the entrance slit of the spectrograph. A Carl-Zeiss three prism spectrograph is used to photograph the spectrum. The dispersion varies from 47 \AA/mm at 4500 \AA to 220 \AA/mm at 9000 \AA . A slit width of 30μ is used in all the regions. The exposure times are a few hours. Eastman Kodak 103a-M and F plates are used. Cesium and Potassium lamps are used as standards in the region 5250 to 9000 \AA and Iron arc in the region below 5250 \AA . The plates are measured on a Carl-Zeiss Model B Abbe comparator which has a least count of 1μ . The positions of the broad (broader than 30μ slit) lines are obtained by taking densitometer traces of the plates on a Carl-Zeiss microdensitometer used with an

attached strip chart recorder. The errors in the wavelength values are $\pm 1.0 \text{ \AA}$.

2.3 Set up for lifetime measurements

The transient fluorescence is also measured by the same spectrophotometer (Sec 2.1) as is used for the steady state fluorescence. The block diagram is shown in Fig 2.5 (When pulsed Ar^+ and N_2 lasers are used for the decay time measurements, the prism is stationary and the scattered beam is sensed by the photocell/photodiode.) In this case, the output of the PMT is fed to a boxcar integrator through an emitter follower. For very weak signals, an amplifier is used before the boxcar. The trigger pulses needed for triggering the boxcar are obtained from an oscilloscope which in turn is triggered by the output of a photo tube (RCA, No. 929) or a photodiode (HP, No 5082-4207) which senses a fraction of the laser beam. The trigger pulses from the CRC are also used to start a digital counter [Yamuna (India), Model 614]. The moving gate from the boxcar is used to stop the counter so that the time elapsed between the instant the boxcar is triggered and the continuously moving boxcar gate can be noted from the counter. The output of the boxcar is fed to a strip chart recorder (Varian, Model G-14A-2). The 'markers' in this case are obtained in the following way. The counter is used in the 'display hold' mode and the readings are

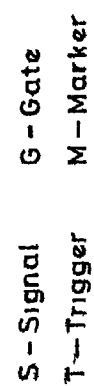


Fig 2 5 Block diagram of the life-time measurement set-up

taken only when the counter is 'reset'. This reset voltage is tapped out of the counter and used to provide a mark on the chart paper (Fig 2.6)

2.3.1 Laser source

Initial experiments are done using the C^{II}Ar^+ laser. The continuous laser beam is chopped using a right angled prism mounted on a universal motor (Bodine, Model NSE-13). The prism could achieve a top speed of 10,000 rpm when a voltage of 110 V is applied to the motor. The rise time of the pulse (from 10 percent of the total power to 90 percent) can be calculated and is given by

$$T_{10-90} = \frac{0.2\lambda}{a\omega} \quad (2.1)$$

where a is the radius of the beam before focusing and ' ω ' denotes the angular velocity of the prism. For $\lambda = 4880 \text{ \AA}$, $a = 1 \text{ mm}$, and $\omega = 3000 \text{ rpm}$, $T_{10-90} = 2 \text{ \mu sec}$. A typical laser pulse is shown in Fig. 2.7. This arrangement is used to study the lifetimes (τ) of only Dy^{3+} LaF_3 at 77°K and at 300°K . In this case, τ is $\sim 1 \text{ msec}$ and so, the speed of the motor is kept minimum to give a repetition rate of $\sim 20 \text{ pps}$.

In the later experiments, the author could use a pulsed Ar^+ laser of peak power $\sim 30 \text{ W}$. This is fabricated in the laboratory in association with Drs K. S. Ramasastry and U. V. Kumar. Its design is similar to the Hughes Model

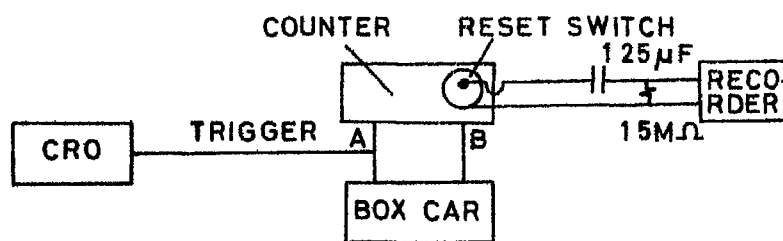


FIG 2.6 EVENT MARKER CIRCUIT

Time base = 0.2 milli-sec
Gate width = 1 micro-sec
Scan time = 30 minutes
Time constant = 0.1 milli-sec

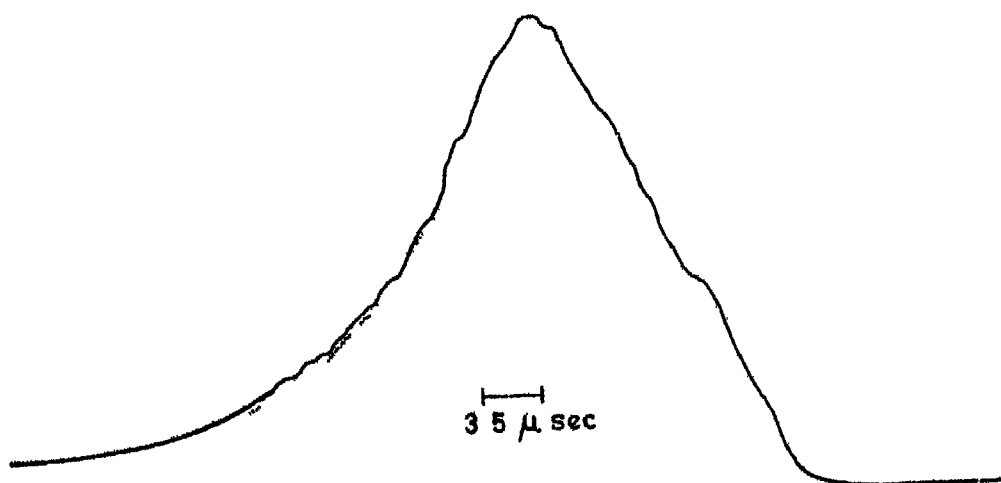


FIG 2.7 A TYPICAL LASER PULSE

No 3030 H pulsed Ar^+ laser The pulse width of this laser can be varied from 10 μsec to 50 μsec and the repetition can be varied upto 60 pps. The laser discharge tube is a Corning (India) glass capillary of 6 mm I D and one meter length (Fig 2.8) It is terminated on either ends with quartz windows set at Brewster's angle It is connected on one side to a large gas ballast tube of 2" I D and 30" length The electrodes are co-axial type and are made of Moovar The laser is excited by d.c. voltage pulses of 750 to 2000 V coupled to the tube through an artificial transmission line made up of several L C sections as shown in fig. 2.9 and is triggered externally The current pulse width can be varied by changing the number of sections of the L C network. The equivalent resistance of the tube is $\sim 2.5 \Omega$ The laser resonator is formed by two multi-layer dielectric coated mirrors (Spectra Physics Co) of 2 meter radius of curvature, separated by about 1.5 meters The mirrors are broad band mirrors with one percent and four percent transmission peaked at about 4700 \AA The multi- λ beam has maximum intensity at a pressure of $\sim 15 \mu$, though there is slight variation for individual laser lines A 60° glass prism is placed inside the cavity near the one percent mirror side for intracavity tuning of wavelength. Also, different modes can be obtained by placing a variable aperture inside the cavity. But, it is found

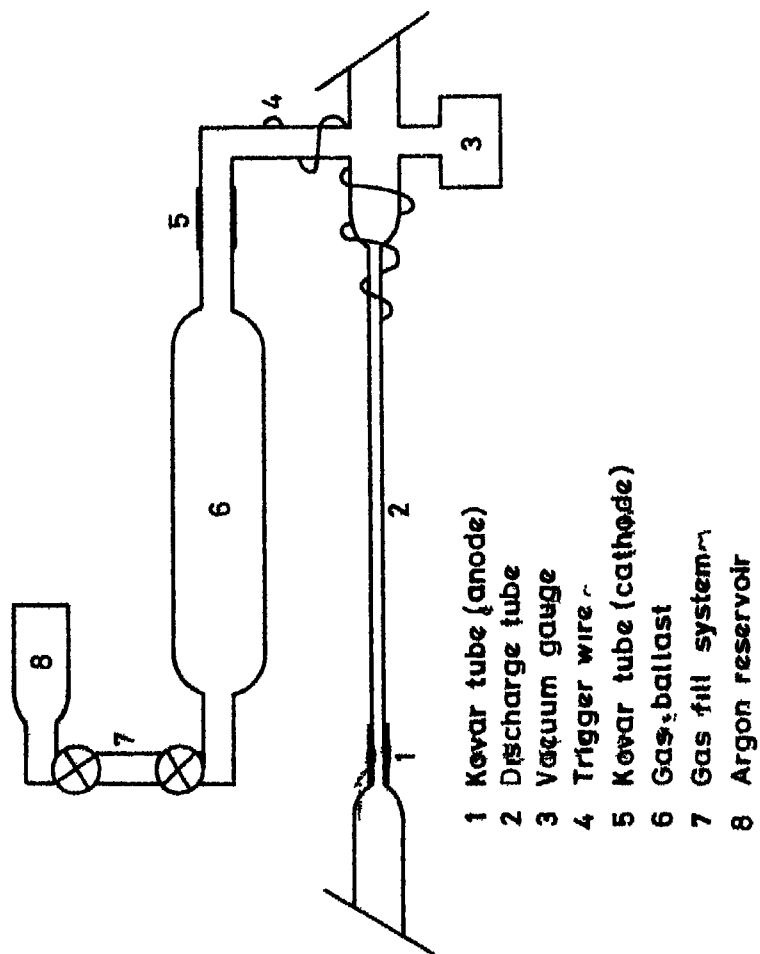


Fig.2 8 Pulsed Ar⁺ laser tube

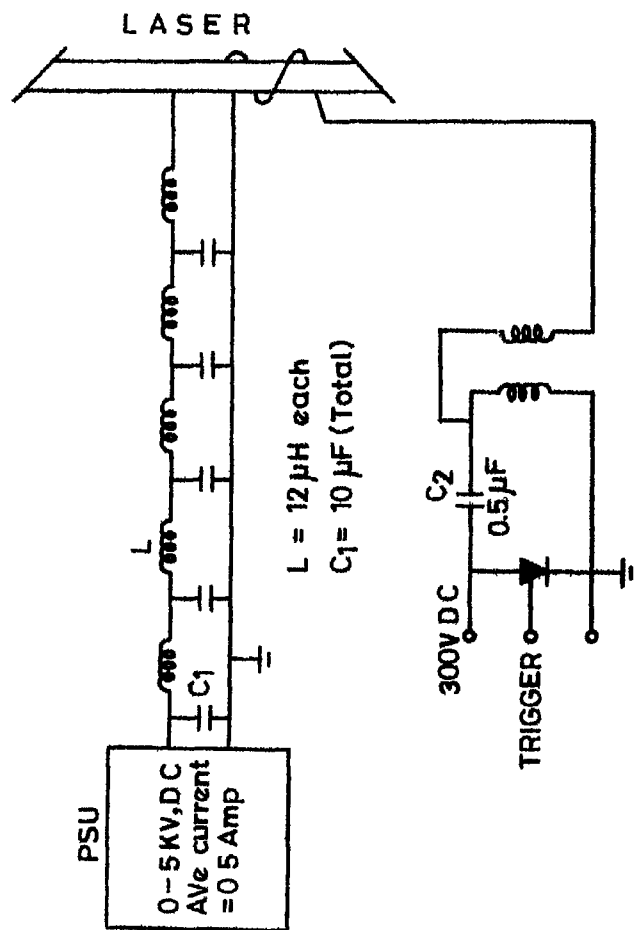


FIG 2.9 L - C NETWORK

that in the lowest TE₁₀₀ mode, the intensity is very low and so, the laser is used as such without any aperture controller. This laser is used to study the decay times of only the LiF UO₂⁺⁺ system in the present work, as the intensity of the fluorescence is very strong compared to the other two systems under study

The transient fluorescence of Dy³⁺ CaF₂ crystals is studied by using the N₂ laser which is described earlier

2.3.2 Electronics

The output from the PNT is fed to an a c coupled amplifier (Tektronix Model 1121, 5 Hz to 17 MHz), through an emitter follower. The emitter follower (Fig 2.10), with a large input impedance (20K to 2000K Ω) and an output impedance of 50 Ω is used to avoid the distortion of the pulse due to impedance mismatch. The gain of the a c coupled amplifier could be varied between 5 and 100 in 8 steps with the help of an input attenuator

A boxcar integrator (PAR, Model CW-1) is used for signal integration. This instrument ⁴⁾ samples the input transient signal with a variable width, variable delay gate. The gate can be scanned employing different scan rates across a variable time base suitable for the input signal. The signal passed by the gate is averaged by variable time constant integrators, the output of which is the average of some number of repetitions of the input

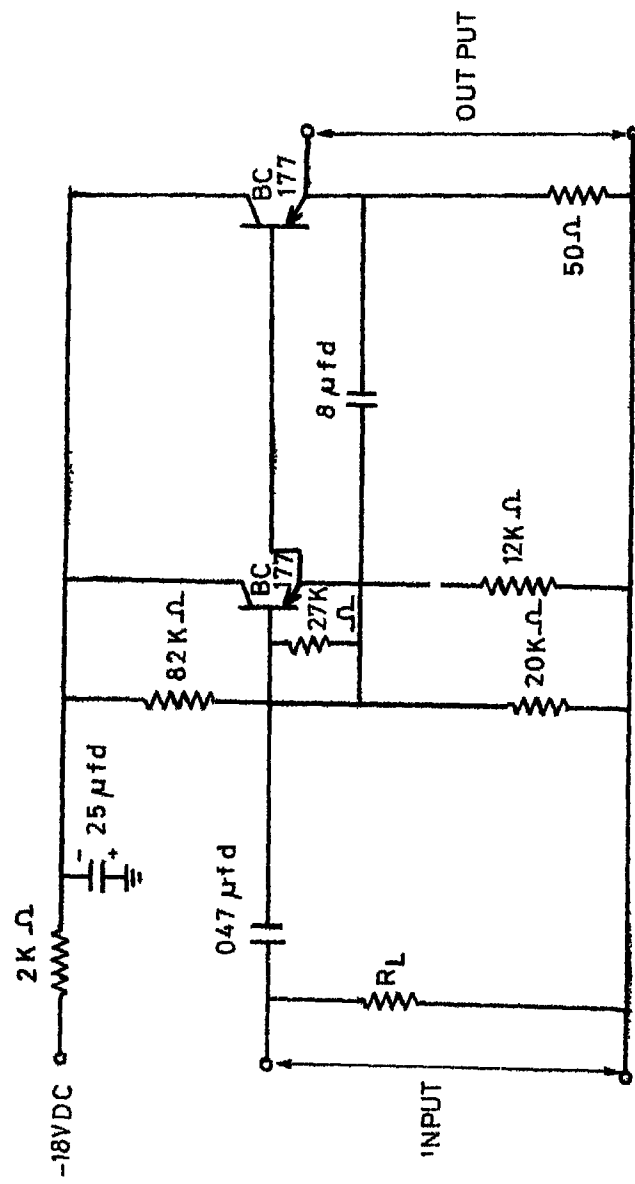


FIG 2.10 EMITTER FOLLOWER

signal over the gate width interval. Because the average value of noise over a large number of repetitions is zero, an improvement in S/N ratio occurs which is given by

$$\text{SNIR} = \left[\frac{2 \times \text{Time constant (sec)}}{\text{Gate width (sec)}} \right]^2 \quad (2.2)$$

To obtain a resolution equal to the selected aperture time (gate width), a minimum scan period (MSP) is to be used, which is

$$\text{MSP (minutes)} = \frac{\text{Time constant (sec)} \times \text{Time base (sec)}}{12 \times \text{Trigger freq. (/sec)} \times [\text{Gate width (sec)}]^2} \quad (2.3)$$

The averaging time constant can be varied from 100 μsec to 100 sec in 1-3 sequence, while the time base duration is adjustable between 10 μsec to 1 sec in 1-2-5 sequence. The gate width is continuously variable from 1 μsec to 0.11 sec.

The boxcar has ± 10 V output for driving potentiometric recorders. A varian G-14A-2 recorder with two chart speeds of 4"/min and 1"/min is used.

While using the CW Ar^+ laser, for lifetime measurements, the light reflected from the rotating prism is sensed by a phototube (RCA, No. 929), biased at -250 V, d.c. The amplified output of the phototube is

taken through a cathode follower (Fig 2 11), and is used to trigger the CRO (Tektronix, No 545B). The delayed triggered pulse from the CRO is used to trigger the boxcar integrator as well as to start a digital counter [Yasuna (India), No 614]. The delay is chosen to match the time period between the instant the laser beam strikes the photo tube and the instant it falls on the crystal under study.

While using the pulsed Ar^+ and the N_2 laser a part of the beam is sensed by a photodiode (H P No 5082-4207) biased at -18 V d.c (Fig 2 12), the output of which is used to trigger the CRO, the boxcar integrator and the counter simultaneously.

The moving gate from the boxcar integrator is used to stop the digital counter, thus giving the location of the gate across the fluorescence signal. The 'display time' switch is kept at ' ∞ ' thereby disabling the counter and the time interval can be noted whenever needed by pressing the 'Reset' switch. About 20 V is always available across this switch. On pressing the switch, this voltage is grounded and the resultant spike of voltage is used for marking the events on the chart (Fig. 2 6). The values of the capacitor and the resistor are chosen by trial and error to get a marker of about 1 cm height. A typical decay curve is shown in Fig. 2.13

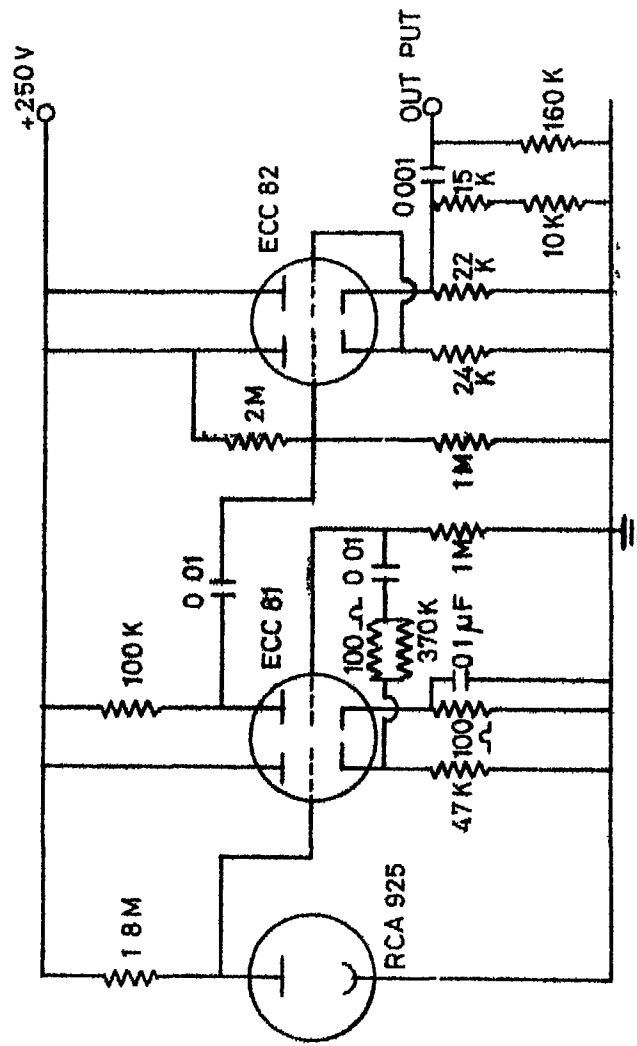


FIG 211 PHOTO-CELL AMPLIFIER

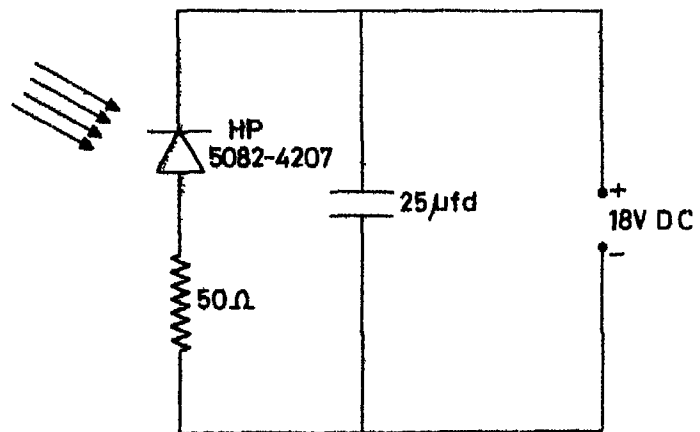


Fig 2.12 Photodiode detector

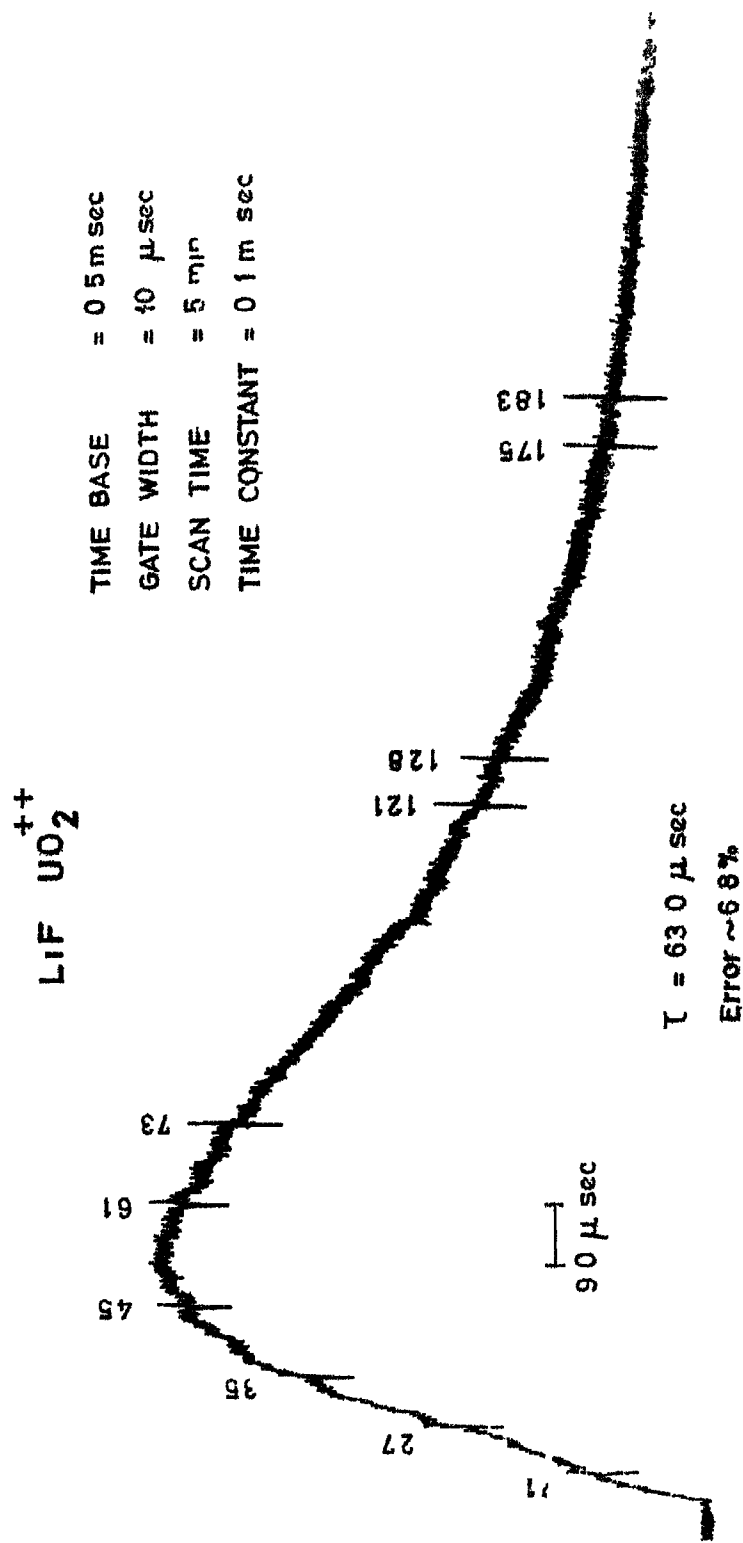


FIG 2 13 A TYPICAL DECAY CURVE .

2.4 The Crystals used

A single crystal of LaF_3 Dy (0.5 percent) from Optovac Co., has been loaned from Professor H P Broida, University of California, Santa Barbara. Excitation with Ar^+ laser has shown the presence of Pr^{3+} as an additional impurity and N_2 laser excitation has shown the presence of Nd^{3+} as a third impurity. The presence of Nd^{3+} is not detectable with Ar^+ laser.

Single crystals of CaF_2 Dy $^{3+}$ are grown in a vacuum Bridgman furnace in the Bhabha Atomic Research Centre (BARC), Bombay by the author in association with Mr H Jagannath of this laboratory and Dr. S. Muralidhara Rao of the Health Phys Division, BARC. The furnace is designed and fabricated by Dr. S. Muralidhara Rao and it can be operated upto 1600°C . There is a provision in the furnace to grow a batch of crystals at a time in a graphite crucible so as to ensure identical growth conditions. For the present work, the author has grown a batch of seven crystals. The activator (DyF_3) concentrations are 0.0, 0.01, 0.03, 0.09, 0.27, 0.54 and 1.08 percent by wt of the host material CaF_2 . A small amount of PbF_2 is added to the charge to remove traces of oxygen. The absence of oxygen is reflected in the transparency and the lack of greenish tinge of the CaF_2 Sm^{3+} crystals grown by this method. In the CaF_2 Dy $^{3+}$ crystals, the oxygen-activated spectra are not found. Small pieces are cut from these

1/4'' dia, 2'' long rods and are used after polishing. By comparing the observed fluorescence spectra in these crystals excited with various lines of the CW Ar⁺ laser with the spectra recorded in a similar manner by exciting CaF₂ Nd³⁺ and CaF₂ Pr³⁺ crystals, the presence of Pr³⁺ as well as Nd³⁺ could be confirmed.

The LiF UO₂⁺⁺ (<250 ppm) crystal is loaned to the author by Dr A V R. Varrier, Solid State Physics Laboratory, Delhi. The crystal is cleaved so as to get (100) faces and is used after polishing.

REFERENCES

- 1 D Ramachandra Rao, U V. Kumar, Bansil Lal and P Venkateswarlu, J Instr Soc of India 6, 5 (1976).
2. Bansil Lal, Ph D Thesis, IIT, Kanpur, India (1977)
- 3 D. Ramachandra Rao, H. Jagannath, & Chakrapani and P. Venkateswarlu, Ind J Phys 50, 267 (1976).
H Jagannath, Ph D Thesis, IIT, Kanpur, India (1977).
- 4 Instruction Manual, Borcor Integrator Model CW-1, Princeton Applied Research Corporation, USA
5. K S. Rama Sastry and D Ramachandra Rao, Technical Report, 'Fabrication of Q-switched Ruby Laser', IIT, Kanpur, India (1976).

CHAPTER 3
THE STEADY STATE AND TRANSIENT FLUORESCENCE
SPECTRUM OF $\text{Dy}^{3+}.\text{LaF}_3$

ABSTRACT

The steady state and transient fluorescence spectra of 0.5 percent $\text{Dy}^{3+} \text{LaF}_3$ are studied in the 4500 to 9000 Å region in the temperature range of 77 to 673°K. The positions and the relative intensities of the fluorescence lines agree well with the ones reported earlier, except for the observation of a new group of lines arising from G-level ($^4\text{I}_{15/2}$). The fluorescence from G-level of Dy^{3+} has so far not been reported in any lattice. This fluorescence is barely detectable at 300°K and the intensity is found to increase as the temperature is raised. From the energy level positions and from the observed rate of variation of intensity, it is concluded that the G-level is thermally populated from F-level which is primarily excited by the 4765 Å laser line.

The decay time of the F-level ($^4\text{F}_{9/2}$) is found to be ~1.39 msec throughout the temperature range of study (77 to 673°K), thereby signifying the purely radiative nature of the fluorescence decay. The G-level ($^4\text{I}_{15/2}$) is also found to show the same decay time throughout (i.e. 300 to 673°K). The build up time of the fluorescence (with N_2 laser excitation) is compatible with the

expected rates of populating the F and G levels via the multiphonon transitions from higher levels. A simplified four-level model is used to obtain the radiative transition rates of F and G levels. The radiative transition rate of $^4F_{9/2}$ is found to be $\sim 720 \text{ sec}^{-1}$ and that of $^4I_{15/2}$ is calculated to be less than $1.5 \times 10^3 \text{ sec}^{-1}$.

The fluorescence spectrum shows significant polarization which is incompatible with the low site symmetry of the ion. An attempt is thereby made to explain the polarized lines by considering possible distortion towards higher site symmetry and also by the coupling of lattice phonons to the Stark levels of the ion. It is concluded that the site symmetry of the Dy^{3+} ion in LaF_3 is very likely higher than C_{2v} .

3.1 Introduction

Trivalent dysprosium (Dy^{3+}) is a Kramer's ion with a valence electron configuration of $4f^9$ and a ${}^6\text{H}_{15/2}$ ground state. The free ion levels are split into $(2J+1)/2$ Kramer's doublets by a crystalline field of any site symmetry less than cubic.

The absorption, fluorescence and the lifetimes of Dy^{3+} in various lattices have been studied extensively by several authors. Gobrecht^{1,2)} investigated the spectrum of $\text{Dy}_2(\text{SO}_4)_3 \cdot 8\text{H}_2\text{O}$ in the powder form. These spectra were rerecorded with high dispersion (5 Å/mm) at 20°K by Meehan and Nutting³⁾. Rosa⁴⁾ used single crystals and powders of $\text{Dy}_2(\text{SO}_4)_3 \cdot 8\text{H}_2\text{O}$, $\text{Dy}(\text{NO}_3)_3 \cdot 6\text{H}_2\text{O}$, $\text{Dy}(\text{BrO}_3)_3 \cdot 9\text{H}_2\text{O}$ and $\text{Dy}(\text{C}_2\text{H}_5\text{SO}_4)_3 \cdot 9\text{H}_2\text{O}$ for study at 85°K. Hoogschagen et al⁵⁾ have done the absorption studies of Dy^{3+} ion in some aqueous solutions. The absorption and fluorescence spectra of $\text{DyCl}_3 \cdot 6\text{H}_2\text{O}$ were recorded by Dieke and Singh⁶⁾ at 4.2°K using a 21 ft. concave grating with a dispersion of 1.2 Å/mm and a Wadsworth spectrograph with a dispersion of 5 Å/mm. Zeeman effect studies were also done by them and the levels upto 21,000 cm^{-1} were established. Gramberg⁷⁾ investigated the absorption spectra of $\text{Dy}(\text{C}_2\text{H}_5\text{SO}_4)_3 \cdot 9\text{H}_2\text{O}$, $\text{DyCl}_3 \cdot 6\text{H}_2\text{O}$ and $\text{Dy}(\text{NO}_3)_3 \cdot 6\text{H}_2\text{O}$ between 21,000 cm^{-1} and 26,220 cm^{-1} and discussed the magnetic properties of these salts. Crosswhite and Dieke⁸⁾ have

established the energy levels of DyCl_3 upto $37,000 \text{ cm}^{-1}$ by the Zeeman study of the absorption and fluorescence spectra at 4.2°K . The first theoretical interpretation of Dy^{3+} ion was due to Jørgensen⁹⁾ The calculations were systematized by Elliott et al¹⁰⁾, Judd¹¹⁾, Wybourne^{12,13)} and Axe and Dieke¹⁴⁾ Lifetime studies of the excited states of Dy^{3+} in LaCl_3 were made by Barasch and Dieke¹⁵⁾ Moos and his co-workers¹⁶⁻¹⁸⁾ have measured the lifetimes of Y, X, W, A, B, D and E levels of this system in detail and studied the multiphonon relaxation rate as a function of energy gap and temperature They have also studied the relaxation rates for the 3, J and E levels of Dy^{3+} LaBr_3 ^{17,18)}

Fry et al¹⁹⁾ (hereafter referred to as FCRM) have reported the absorption and fluorescence spectra of Dy^{3+} LaF_3 at 4.2°K . The absorption spectrum was recorded in the $3000\text{--}30000 \text{ \AA}$ range and the fluorescence was recorded in the $4500\text{--}11000 \text{ \AA}$ region. The energy levels below $24,000 \text{ cm}^{-1}$, established with the aid of intermediate coupling calculations, are shown in Fig 5.1. They have observed fluorescence only from the $F(4, 9/2)$ level while in other hosts, fluorescence was observed from some higher as well as lower levels^{16,20)}. Also, the observed number of transitions in fluorescence and absorption of Dy^{3+} LaF_3 only indicate that the site symmetry of rare earth ion is non cubic In LaF_3 crystal,

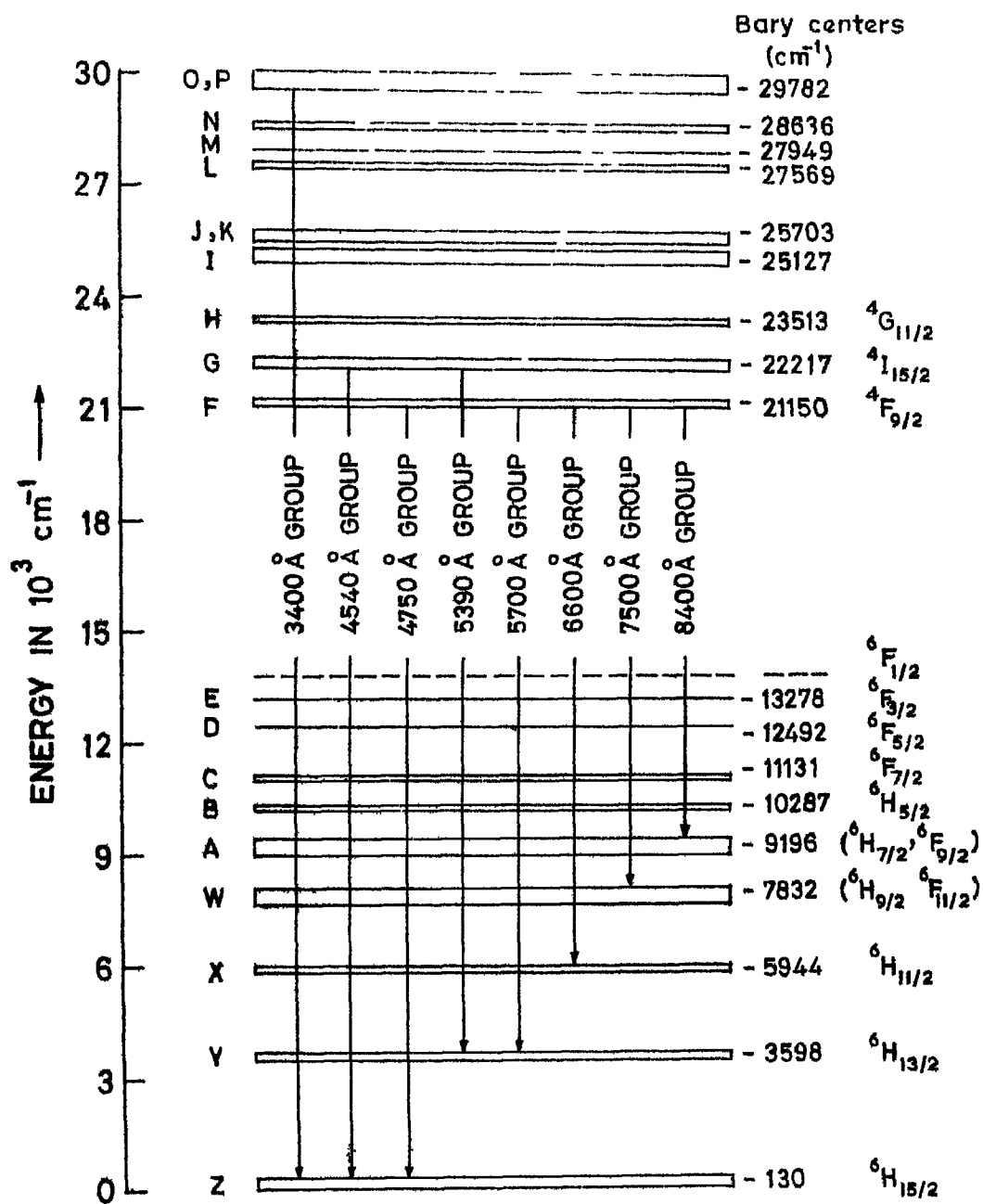


FIG 31 ENERGY LEVEL DIAGRAM OF Dy^{3+} LaF_3
(Ref 19)

the rare earth ion can have at least four different non cubic site symmetries (D_{3h} , C_{2v} , C_2 or C_s) according to the different structures proposed for LaF_3 ²¹⁻²⁸). No attempt was, however, made by FCRM to determine the exact site symmetry by recording the polarization of various lines. The present work reports the observation of new fluorescence from the G-level ($^4I_{15/2}$) as well as the polarization features of the fluorescence from F-level of Dy^{3+} LaF_3 . Fluorescence from the G-level has so far not been reported in any lattice. The lifetimes of the F and G-levels are also measured in the temperature range of 77 to 673°K. An attempt is made to understand these values along with the observed 'build-up times', assuming thermal mixing of the F and G-levels and the radiative as well as non radiative relaxation rates are calculated.

3.2 Experimental Details

The steady state and transient fluorescence spectra are recorded using Ar^+ and N_2 lasers as described in Chapter 2. The decay times are measured using a mechanically chopped CW Ar^+ laser excitation as well as N_2 laser. The high temperature fluorescence is recorded using the heater assembly (Sec. 2.1).

A single crystal of LaF_3 containing 0.5 percent by wt. of Dy^{3+} used for the present study is loaned from Professor H. P. Broida of University of California, Santa Barbara, U.S.A. . The crystal is originally bought from

Optovac Inc., USA. It is of very good optical quality and its dimensions are $10 \times 7 \times 4 \text{ mm}^3$, c axis being parallel to 4 mm side. The c axis has been checked by using a polarization microscope. An unknown but small quantity of Pr^{3+} as well as still smaller quantities of Nd^{3+} are detected from the excitation of fluorescence with Ar^+ and N_2 lasers.

3.3 Fluorescence from G-level

The observed 'G-fluorescence', $G(^4I_{15/2}) \rightarrow Z(^6H_{15/2})$ at three different temperatures using 4765 Å excitation is shown in Figure 3.2. The polarization features are shown in Figure 3.3. The spectrum is similar with N_2 laser excitation and is detectable only above 300°K. It is barely identifiable with 4580 Å excitation because of its immediate neighbourhood of this laser line. A 'slow-scan' spectrum with 4765 Å excitation is shown in Figure 3.4. G → Y fluorescence is shown in Figure 3.5. The wavelengths, relative intensities and the assignments of the observed transitions of G → Z and G → Y groups are given in Table 3.1. The increase in integrated intensities of G → Z fluorescence with temperature is shown in Figure 3.6. It is seen that the integrated intensities at temperature T°K can be written as

$$I_T = I_0 \exp(-\Delta E/kT) \quad (3.1)$$

with $\Delta E = 1140 \pm 70 \text{ cm}^{-1}$. k is the Boltzmann factor.

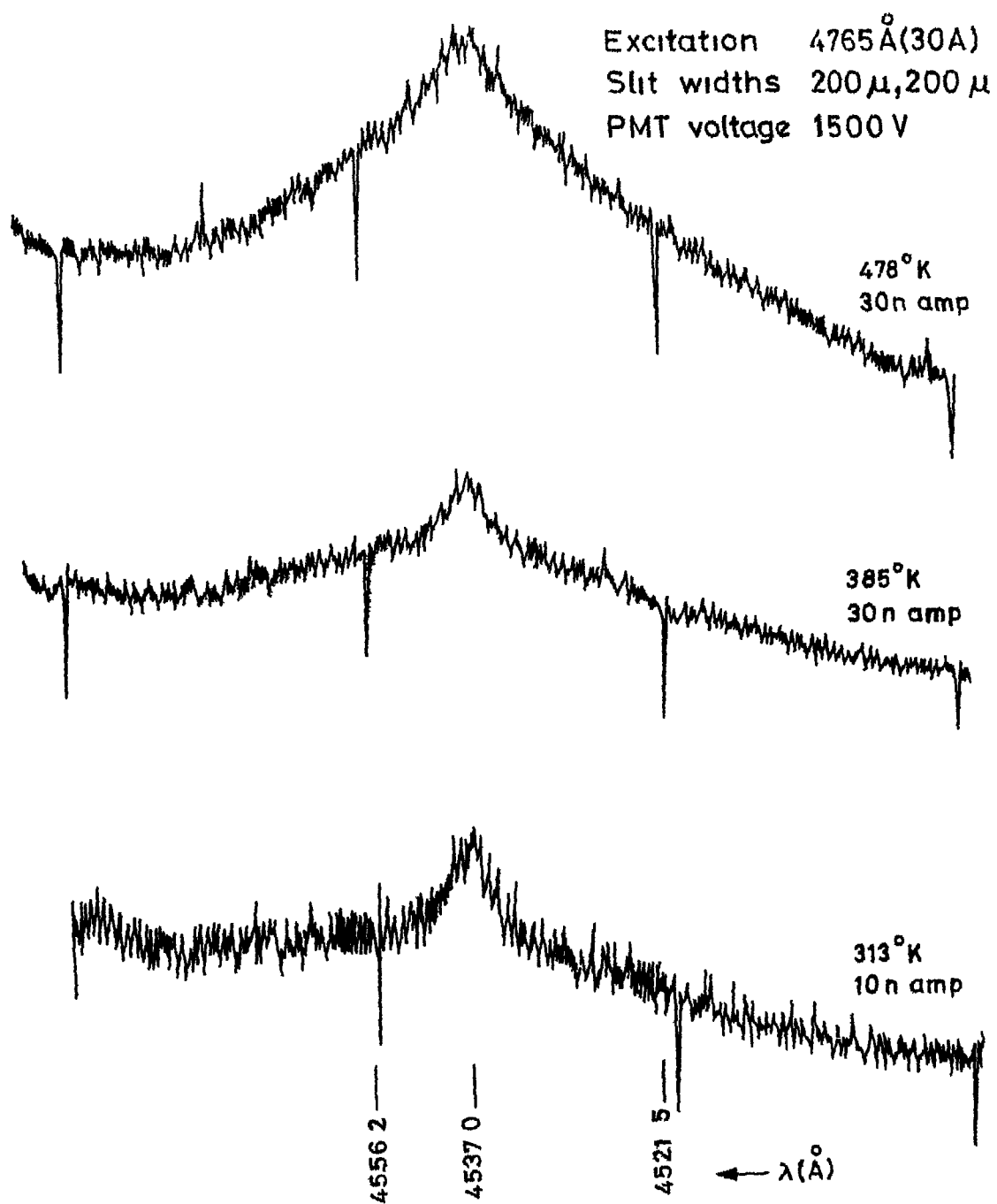


FIG. 3 2 High temperature fluorescence of $\text{Dy}^{3+} \text{LaF}_3$,
 4765\AA excitation, $G(^4I_{15/2}) \rightarrow Z(^6H_{15/2})$ Group

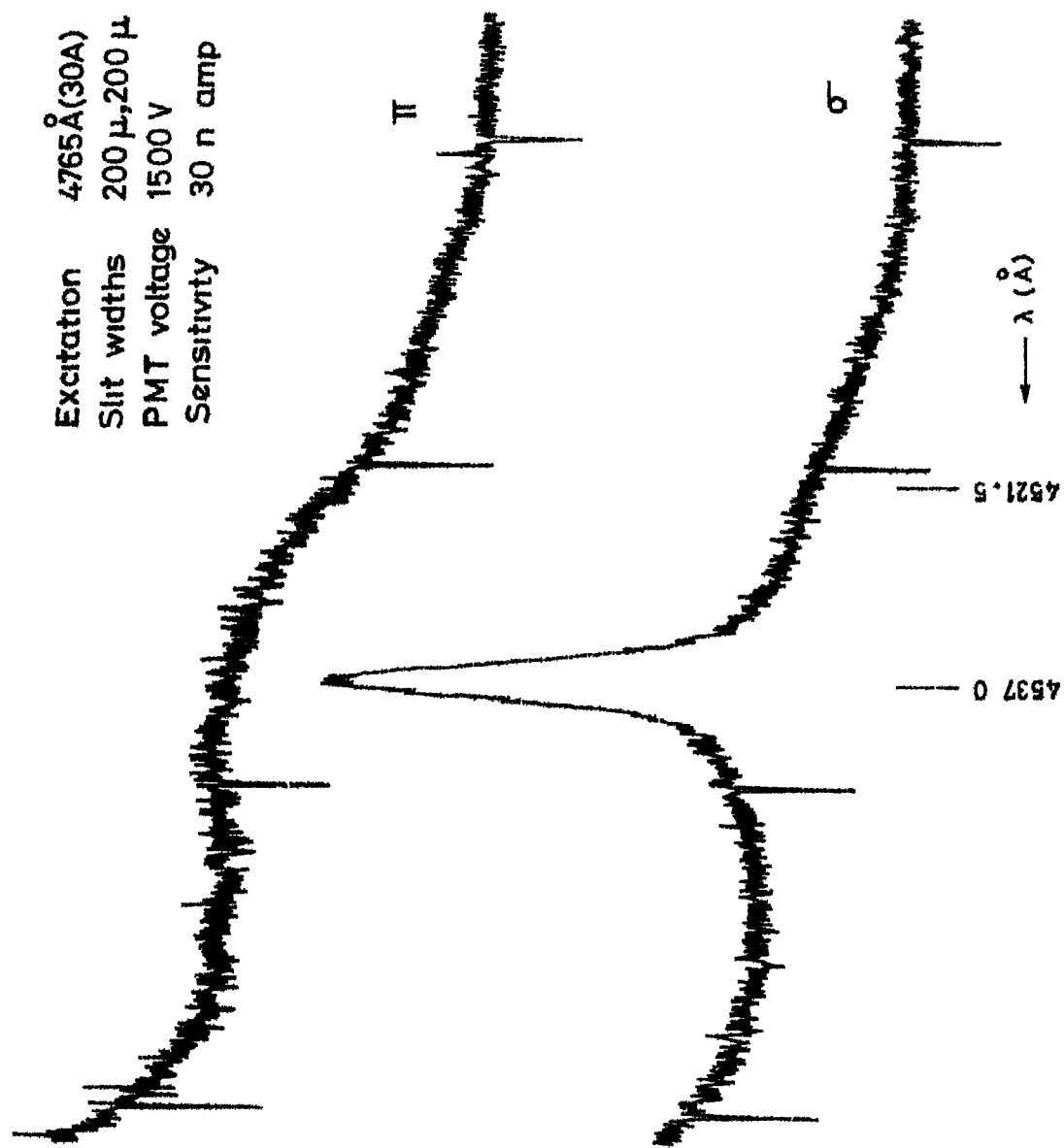


Fig 3 3 LaF_3 Dy^{3+} fluorescence at 300 $^\circ\text{K}$, 4765 \AA excitation,
 $G(^4I_{15/2}) \longrightarrow Z(^6H_{15/2})$ Group.

Excitation 4765Å (30Å)
 Slit widths 200 μ , 200 μ
 PMT voltage 1500 V
 Sensitivity 10 n amp

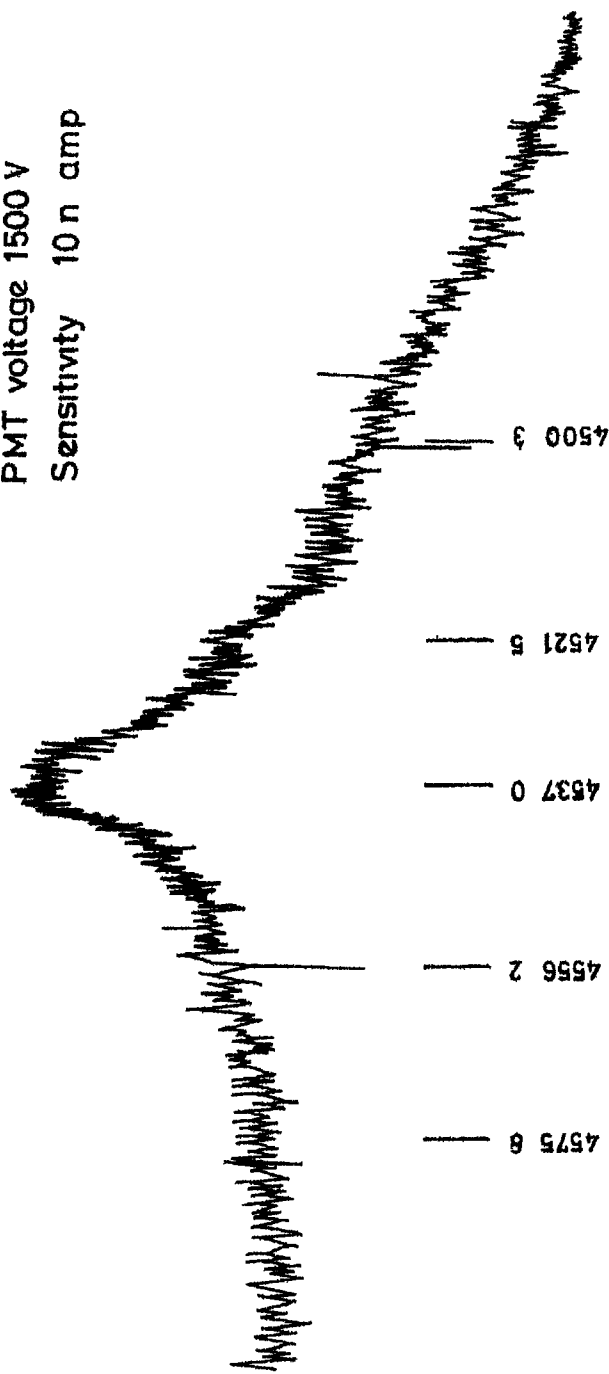


Fig 3 4 LaF_3 Dy^{3+} fluorescence at 300 °K ; 4765Å excitation ,
 $\text{G} (^4\text{I}_{15/2}) \longrightarrow \text{Z} (^6\text{H}_{15/2})$ Group

Excitation N₂ laser
 PMT voltage 2000 V
 Slit width 300 μ , 200 μ
 Sensitivity 300 n amp

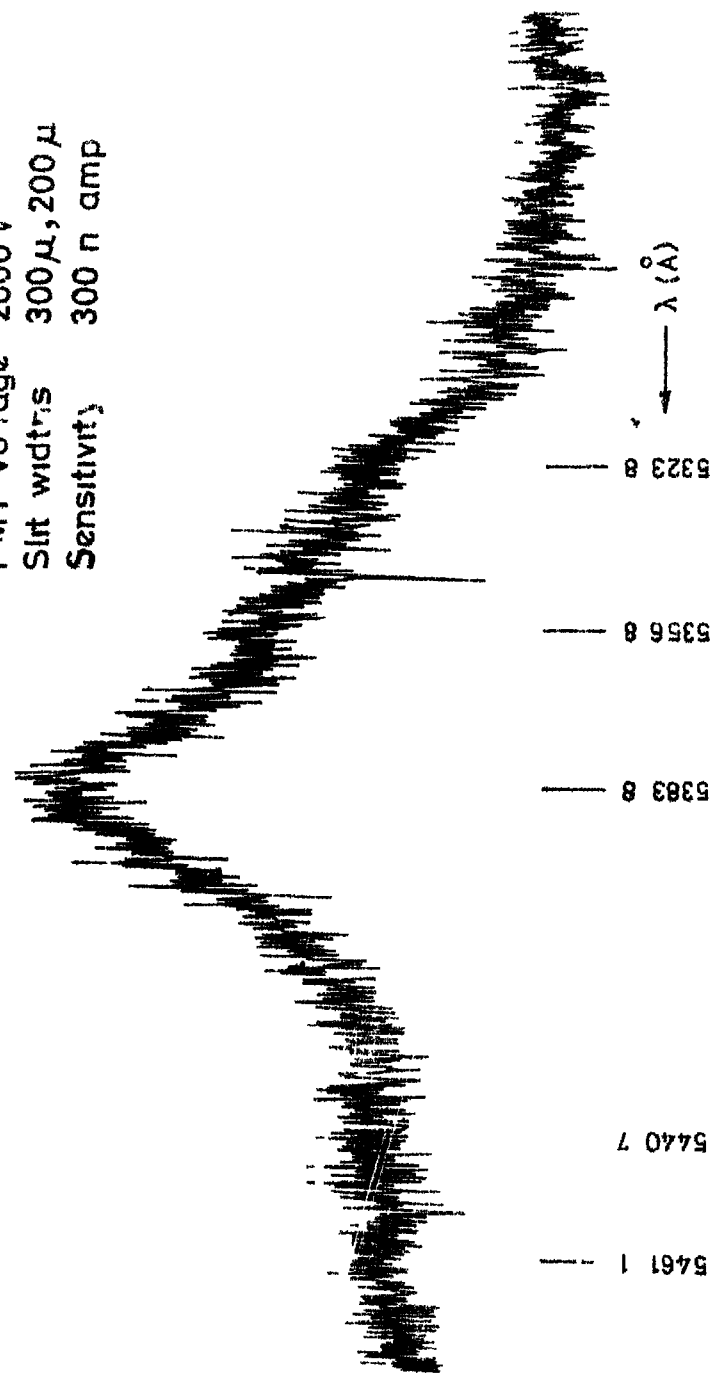


Fig 35 Dy³⁺ LaF₃ fluorescence at 573°K, N₂ laser excitation,



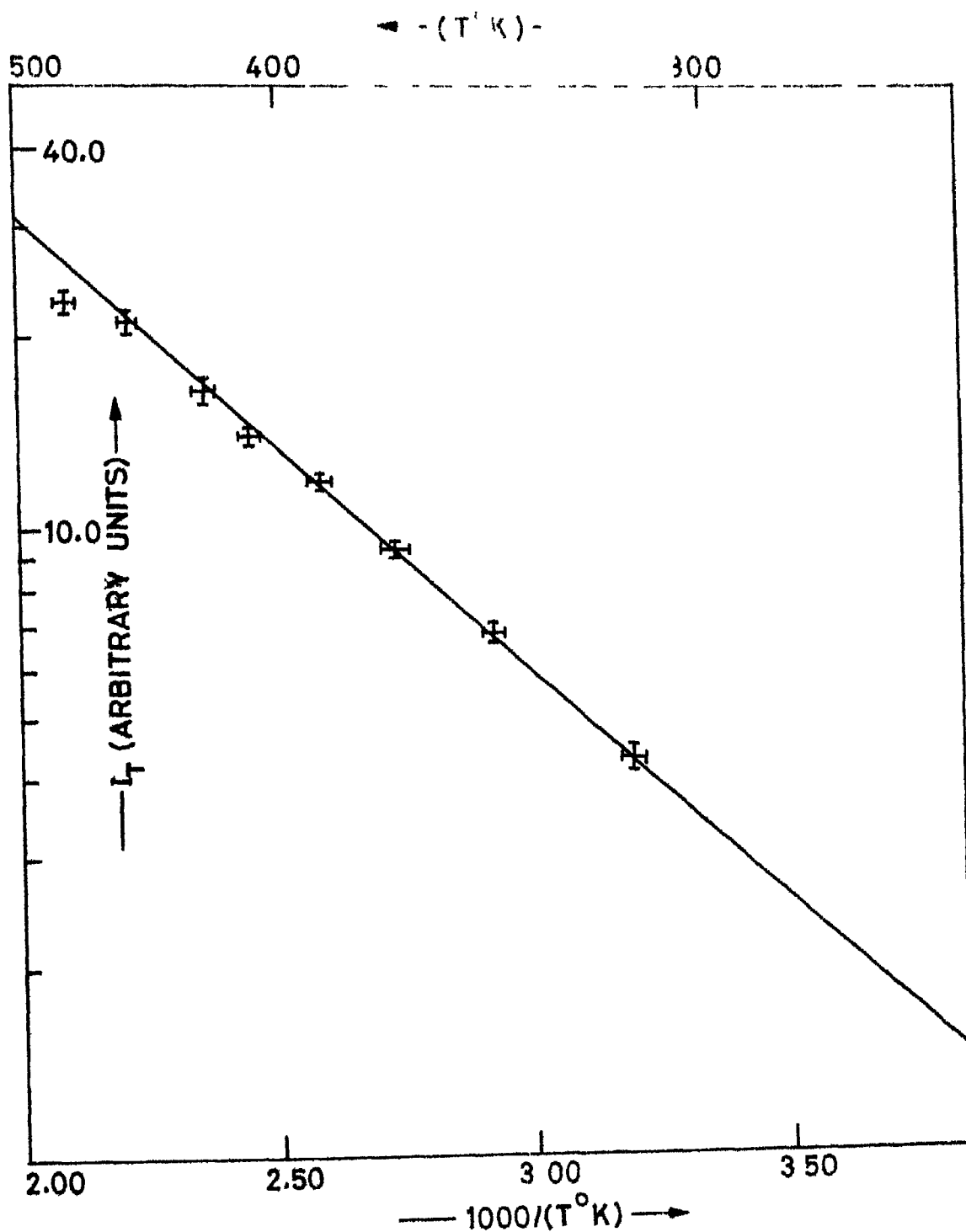


FIG.3 6 TEMPERATURE VARIATION OF INTEGRATED INTENSITY OF $G(^4I_{15/2}) \rightarrow Z(^6H_{15/2})$ FLUORESCENCE

Table 3 1
High-temperature fluorescence spectrum of $\text{Dy}^{3+} \text{LaF}_3$

Wavelength (Å)	Energy (cm^{-1})	Intensity* (arb. units)	Transition
			Assignments
4500.3	22215	38 VB	$^4F_5 \rightarrow Z_1, G_6 \rightarrow Z_3, G_7 \rightarrow Z_4$
4521.5	22110	57 SR	$^4F_2 \rightarrow Z_2, G_6 \rightarrow Z_6$
4537.0 ^φ	22035	90 M	$^4F_5 \rightarrow Z_5, G_3 \rightarrow Z_4, ^4F_7 \rightarrow Z_7$
4556.2	21942	61 VB	$G_2 \rightarrow Z_5, G_1 \rightarrow Z_3$
4575.8	21848	53 VVB	$G_1 \rightarrow Z_5, G_3 \rightarrow Z_7$
5323.3	18778	28 VB	$G_6 \rightarrow Y_1, G_7 \rightarrow Y_2$
5356.8	18663	47 VB	$G_6 \rightarrow Y_5, G_3 \rightarrow Y_1, G_4 \rightarrow Y_2$
5383.8	18569	80 M	$G_5 \rightarrow Y_6, G_4 \rightarrow Y_4, Y_5$
5440.7	18375	28 VVB	$G_5 \rightarrow Y_5, G_1 \rightarrow Y_4$
5461.1	18306	26 VVB	$G_1 \rightarrow Y_6$

φ This line is σ-polarized. Polarization characteristics could not be recorded for $G \rightarrow Y$ fluorescence because of the very weak intensity.

The numbers indicate relative intensities of the lines in each group in an arbitrary scale and the letters S, M, B, VB, VVB, SR stand for sharp, medium, broad, very broad, very very broad and shoulder transitions.

The energy mismatch between 4765 \AA (20981 cm^{-1}) excitation and the lowest Stark level (F_1) of 'F' is 77 cm^{-1} and thus only those levels which are at least 70 cm^{-1} above the ground state will participate in the excitation. The increased intensity of 'F-fluorescence' as temperature is changed from 77 to 300°K closely follows the expected increase (> 2.5) in the population of 69 cm^{-1} level (Z_2) of the ground state. But, when the crystal is heated further above 300°K , the integrated intensity remains almost the same and reduces slightly beyond 450°K . The present experiments (Sec. 3.4) showed the lifetimes of F-level to be constant ($\sim 1.39 \text{ msec}$) throughout the temperature range of 77 to 673°K , indicating that the multiphonon transition rates do not influence the fluorescence decay. The decrease in 'F-fluorescence' is thus not expected.

The 'G-fluorescence' on the other hand is not detectable at 77°K and starts appearing at about 300°K and its intensity increases with further rise in temperature (Fig. 3.6).

The Stark levels of G can be populated in two ways, (a) by direct excitation into the G-level by the laser line and (b) by the excitation of the ions into the F-level by the laser and subsequent thermal population of G-level from 'F'.

(a) The 4765 \AA (20981 cm^{-1}) excitation falls short of the lowest Stark level of G ($\sim 22020 \text{ cm}^{-1}$) by 1039 cm^{-1}

and from the energy level diagram (Fig. 3.1), no level is to be seen having this much energy. The ground state (${}^6\text{H}_{15/2}$) extends upto 307 cm^{-1} (Z_7) only and the next excited level is at 3502 cm^{-1} (Y_1 of ${}^6\text{H}_{13/2}$). The Boltzmann factors for the Y levels can explain neither the increase in G-fluorescence nor the decrease in F-fluorescence. This mechanism of direct excitation into the G-level by the laser lines can thus be ruled out as invalid.

(b) The separation of centers of gravity of the F- and G levels is 1070 cm^{-1} and agrees well with the observed 'effective energy gap, ΔE ' (Fig. 3.6) of $1140 \pm 70\text{ cm}^{-1}$. Also, thermal population of G from F at 77°K is about six orders of magnitude less than that at 300°K which thus explains the non-detectability of G-fluorescence at 77°K . As the temperature is raised beyond 300°K , the increased intensity of G-fluorescence closely follows the expected thermal population of G from F. Thus, 'drain-out' of the F-population by thermalization with G qualitatively explains the decrease in intensity of F-fluorescence beyond 450°K . Also, from the decay time measurements of G-fluorescence (Sec. 3.6), this can be clearly seen as being represented by the thermalization rate, $W_{F \rightarrow G}$ (Eq. 3.3), which at 77°K is much smaller than the multiphonon transition rate of the G-level, $W_{G \rightarrow F}$.

3 4 Lifetime of F-level

The lifetime of the F-level is measured using both the Ar^+ and N_2 lasers in the temperature range of 77 to 673°K (Sec 2 3). The transient fluorescence signal is found to increase initially, reach a maximum (at t_{max}) and then decay exponentially. The decay time is observed to be ~ 139 msec, corresponding to a decay rate of $\sim 720 \text{ sec}^{-1}$ throughout the temperature range of study. This is easily understood as follows. The level $^4\text{F}_{9/2}$ is separated from the next lower level $^6\text{F}_{1/2}$ by at least 6000 cm^{-1} (The $^6\text{F}_{1/2}$ level in LaF_3 is however not reported so far). Hence the multiphonon transition rate (MPTR) can be expected to be small from the empirical band-gap rule²⁹), and the other non radiative processes like ion-ion interaction can be assumed to be negligible because of the low concentration of dysprosium (0.5 percent).

The buildup time (t_{max}) observed while using the Ar^+ laser excitation is $\sim 80 \text{ } \mu\text{sec}$. This is attributable to the finite rise time ($\sim 25 \text{ } \mu\text{sec}$) of the laser pulse itself at the low speeds of the prism-motor used (Sec 2 3). With N_2 laser excitation (rise time $< 8.0 \text{ nsec}$), the buildup times observed are $\sim 100 \text{ } \mu\text{sec}$ at 77°K and $\sim 60 \text{ } \mu\text{sec}$ at 673°K. This 'build-up' is due to the population of F level from upper levels by radiative or non-radiative processes. The N_2 laser (29656 cm^{-1}) lifts the ions from the ground

state into 'O and P levels'²⁰⁾, from which only weak fluorescence is observed³⁰⁾ No detectable fluorescence is observed from any of the intermediate levels As the concentration of dysprosium is low, one need to consider only the multiphonon relaxation as the important non-radiative process by which the ions in 'O and P levels' can relax to F-level The MPTR for the different energy gaps between the intermediate levels can be estimated from the band-gap rule²⁹⁾ However, it is to be noted that these values can be ± 50 percent of the observed values. The maximum energy level separation in $\text{Dy}^{3+} \text{LaF}_3$ ¹⁹⁾, is $\sim 1500 \text{ cm}^{-1}$ (between L and 'J and K' levels) which contributes a MPTR of $\sim 2 \times 10^5 \text{ sec}^{-1}$ and a $t_{\text{max}} \sim 30 \text{ } \mu\text{sec}$ The effect of the other intermediate energy gaps is to increase the t_{max} The exact value of t_{max} can only be obtained by writing the rate equations for all the intermediate levels. The observed t_{max} ($\sim 100 \text{ } \mu\text{sec}$) can thus be attributed to multiphonon transitions from the upper levels to F level. Also, the decrease in the t_{max} with increase in temperature is also understandable because MPTR do increase with increasing temperatures.

3 5 Lifetime of G-level

The G-level is separated from F (i e , G_1-F_5) by $\sim 800 \text{ cm}^{-1}$. At 77°K , the estimated MPTR is $\sim 10^7 \text{ sec}^{-1}$. No detectable fluorescence is observed from this level at 77°K . At 300°K and above, G-fluorescence has been observed

by both Ar^+ and N_2 lasers (Sec. 3.3) It is found to show a decay time of ~ 1.4 msec throughout the temperature range of 300 to 673°K This value is same as that of F-level

3.6 Radiative Relaxation Rates of F and G levels

At room temperature and above, a small population exists in the G-level due to thermalization from F, as has already been discussed in Sec. 3.3 The redistribution of the Dy^{3+} ion population in the two levels at thermal equilibrium affects the decay rates of the levels The effective decay rate would be a weighted average of the two levels.

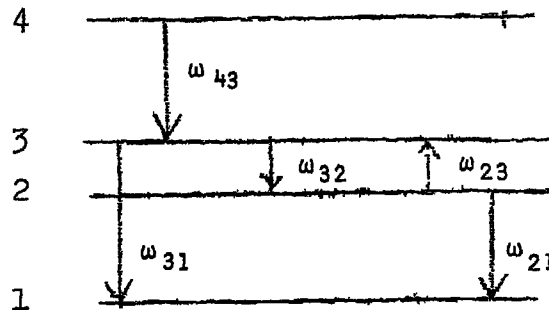
The G-level ($^4\text{I}_{15/2}$) decays by both radiative and multiphonon transitions. Also, the level is populated from 'F' by thermalization. The rate of thermalization w_{th} at a temperature $T^\circ\text{K}$ is given by ³¹⁾

$$w_{th} = w_{MPT} \exp(-\Delta E/kT) \quad (3.2)$$

where w_{MPT} is the rate of multiphonon transitions between the F and G levels and ΔE is the energy separation between the two levels

Intensity of fluorescence vs time and the effective decay rate can be obtained by solving the rate equations. Since a large number of levels exist above $^4\text{I}_{15/2}$ and below $^4\text{F}_{9/2}$, a simple model of a four level system is assumed to obtain the solution, in which '1' represents all the levels below $^4\text{F}_{9/2}$ Levels '2' and '3' represent the levels $^4\text{F}_{9/2}$ and $^4\text{I}_{15/2}$ respectively and level '4' represents an effective

level above $^4I_{15/2}$ from which Dy^{3+} ions relax by non radiative transitions to levels 2 and 3.



The following nomenclature is followed

ω_{42} = Multiphonon transition rate of level 4

ω_{32} = Multiphonon transition rate of level 3

ω_{23} = Rate of excitation of level 3 by thermalization from level 2

ω_{31} = Radiative transition rate of level 3

and ω_{21} = Radiative transition rate of level 2

The rate equations are

$$\dot{n}_4 = -\omega_{43}n_4$$

$$\dot{n}_3 = \omega_{43}n_4 + \omega_{23}n_2 - (\omega_{31} + \omega_{32})n_3 \quad (3.3)$$

$$\dot{n}_2 = \omega_{32}n_3 - (\omega_{21} + \omega_{23})n_2$$

Following the standard procedures of using Laplace transforms for the solution of differential equations, and making the following assumptions, viz ,

$$\omega_{32} > \omega_{43} \gg \omega_{21}, \omega_{31} \quad (3.4)$$

and

$$\omega_{23} \geq \omega_{31} \quad (3.5)$$

the solutions are

$$n_4(t) = N \exp(-\omega_{43}t) \quad (3.6)$$

$$n_3(t) = \frac{\omega_{43} N}{(\alpha - \beta)(\alpha - \omega_{43})(\omega_{43} - \beta)} [(\alpha - \omega_{43})(\omega_{21} + \omega_{23} - \beta) \exp(-\beta t) + (\alpha - \beta)(\omega_{43} - \omega_{21} - \omega_{23}) \exp(-\omega_{43}t)] \quad (3.7)$$

and

$$n_2(t) = \frac{\omega_{43} N \omega_{32}}{(\alpha - \beta)(\alpha - \omega_{43})(\omega_{43} - \beta)} [(\alpha - \omega_{43}) \exp(-\beta t) - (\alpha - \beta) \exp(-\omega_{43}t)] \quad (3.8)$$

where

$$\alpha = \omega_{32}(1 + \exp(-\Delta E/kT)) + \left[\frac{\omega_{21} \exp(-\Delta E/kT) \exp(-\omega_{43}t)}{1 + \exp(-\Delta E/kT)} \right] \quad (3.9)$$

$$\beta = \frac{\omega_{21} + \omega_{31} \exp(-\Delta E/kT)}{1 + \exp(-\Delta E/kT)} \quad (3.10)$$

The level 3 (Equation 3.7) decays as a sum of two exponentials and level 2 (Equation 3.8) decays as a difference of two exponentials and the 'tails' of both the decay curves have the same time constant β . The level 3 also decays

as a difference of two exponentials for temperatures such that $\omega_{32} \exp(-\Delta E/kT) > \omega_{43}$. In the present case this condition is satisfied above room temperature

The degeneracy of the levels 2 and 3 has not been considered while obtaining equation (3 10) With this correction

$$\beta = \frac{g_2 \omega_{21} + g_3 \omega_{31} \exp(-\Delta E/kT)}{g_2 + g_3 \exp(-\Delta E/kT)} \quad (3 11)$$

The validity of the assumptions made can be checked by estimating the various transition rates From the experimental results,

$$\beta = 720 \text{ sec}^{-1} \quad (3 12)$$

and $\omega_{43} \sim 5 \times 10^4 \text{ sec}^{-1}$

ω_{32} can be estimated from the band gap rule²⁹⁾ and it comes out to be $\sim 5 \times 10^6 \text{ sec}^{-1}$ Also $\exp(-\Delta E/kT)$ varies from 7×10^{-3} at 300°K to 0.1 at 673°K , and the equation (3 3) yields ω_{23} to be greater than β , in this range of temperature At 77°K , from equation (3 11),

$$\beta = \omega_{21} \ll \omega_{43} < \omega_{32}$$

The radiative transition rate of $^4F_{9/2}$ is thus, 720 sec^{-1} . It is not possible to calculate the value of ω_{31} from the present experimental results as the range of temperature over which the decay rates have been measured is not sufficient The maximum temperature 673°K reached is not

large enough to give a value of β which is significantly different from ω_{21} unless $\omega_{31} \gg \omega_{21}$. The experimental results suggest that ω_{31} and ω_{21} are of the same order. The upper limit of ω_{31} can be estimated from equation (3.11) taking into account the maximum possible experimental inaccuracy in the measurements, which is 10 percent in the present case. (A variation in the decay time more than 10 percent can be easily detected in the present set up). The value of the upper limit of ω_{31} comes out to be $1.5 \times 10^3 \text{ sec}^{-1}$ thereby justifying the assumptions made (Eqs 3.4 and 3.5).

3.7 Polarized fluorescence from F-level

The fluorescence spectrum has been recorded at 77°K in the wavelength region of 4500 to 9000 Å using various excitations of the CW Ar^+ laser and the N_2 laser. The fluorescence observed is similar to the one reported by FCRM. In addition, transitions from the upper Stark levels of F are also observed because the lowest temperature attained in the present work is only 77°K . The observed fluorescence groups (F → Z, Y, X, W, A) are indicated in the energy level diagram shown in Fig. 3.1.

The spectrum is recorded using mainly 4727 Å (21149 cm^{-1}) and 4765 Å (20981 cm^{-1}) excitations. The energies of these laser lines match approximately with the fluorescing F-level and thus these excitations yield fluorescence of intensity at least one order of magnitude more

than that obtained by using other laser lines. Many lines in the observed fluorescence spectrum show partial polarization and some lines are even completely polarized. The crystal is aligned carefully in all these measurements, but it is observed that the amount of polarization is not very sensitive for slight misalignments. The spectra are shown in Figs 3.7 to 3.11. The 4750 Å group is recorded using N₂ laser. When this group is recorded with the Ar⁺ laser, the Dy³⁺ fluorescence is obscured by the fluorescence of Pr³⁺ which is also excited. (In other regions of Dy³⁺-fluorescence, there is no such interference from Pr³⁺-fluorescence). With N₂ laser excitation, Pr³⁺ is not excited as evidenced by the absence of the Pr³⁺-fluorescence. However, the fluorescence spectra recorded with N₂ laser have comparatively small S/N ratio (because of the pulsed excitation) and thus only the strong 4750 Å group is recorded with this.

All the fluorescence groups are corrected only for the polarization of the grating and not for PMT response etc. Thus, comparison of intensities of different lines can only be made amongst each group of lines and not between lines belonging to different groups. The numbers under the 'σ' and 'π' columns in Table 3.2 denote relative intensities in the two polarizations, and when the intensity could not be determined, it is indicated by a blank (—).

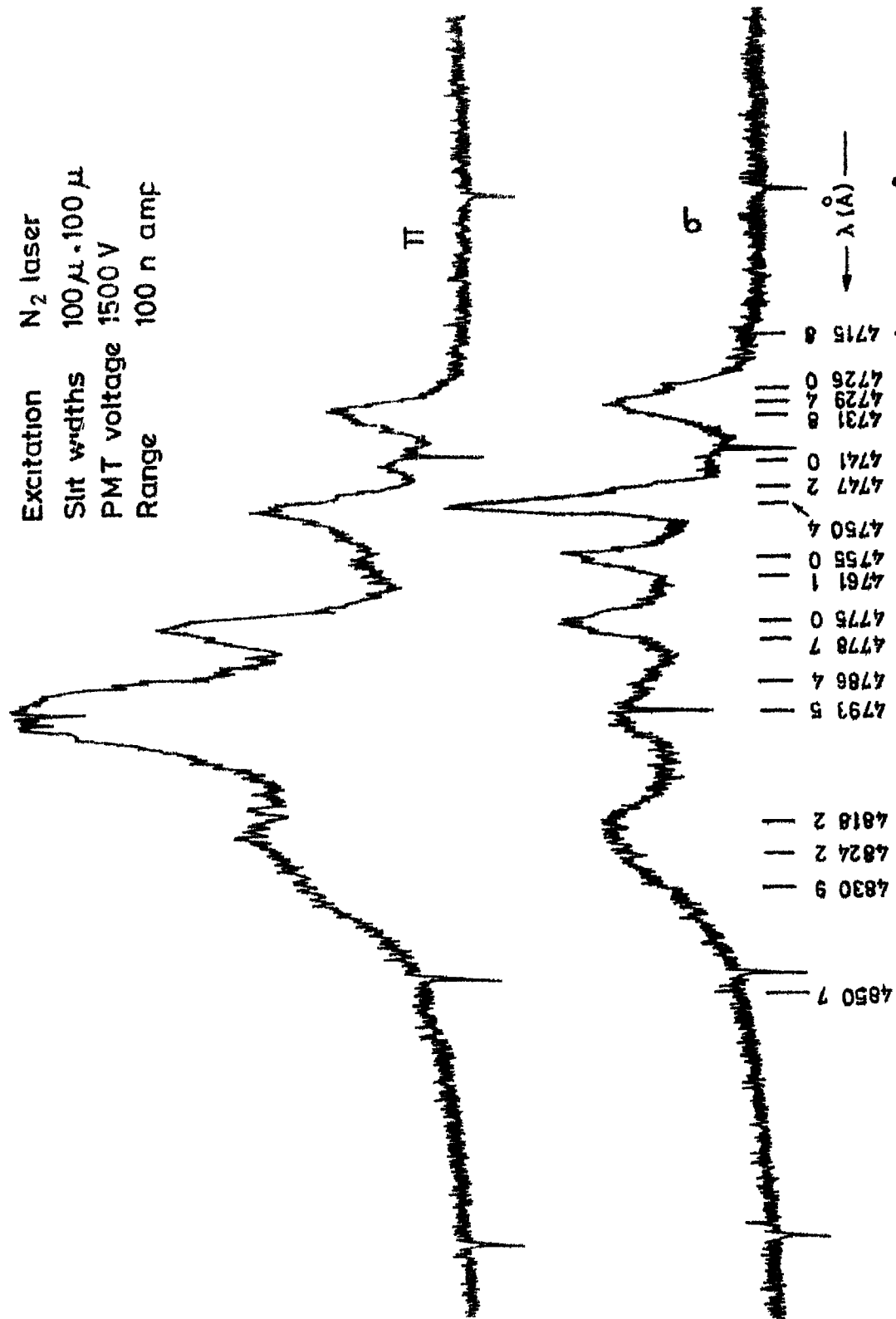


Fig 3 7 Dy³⁺ LaF₃ fluorescence at 77°K, N₂ laser excitation, F(⁴F_{5/2}) → Z(⁶H_{15/2}) Group.

Excitation $4765 \text{ \AA} (30 \text{ A})$
 Slit widths $100 \mu, 50 \mu$
 PMT voltage 1500 V
 Range 300 n amp

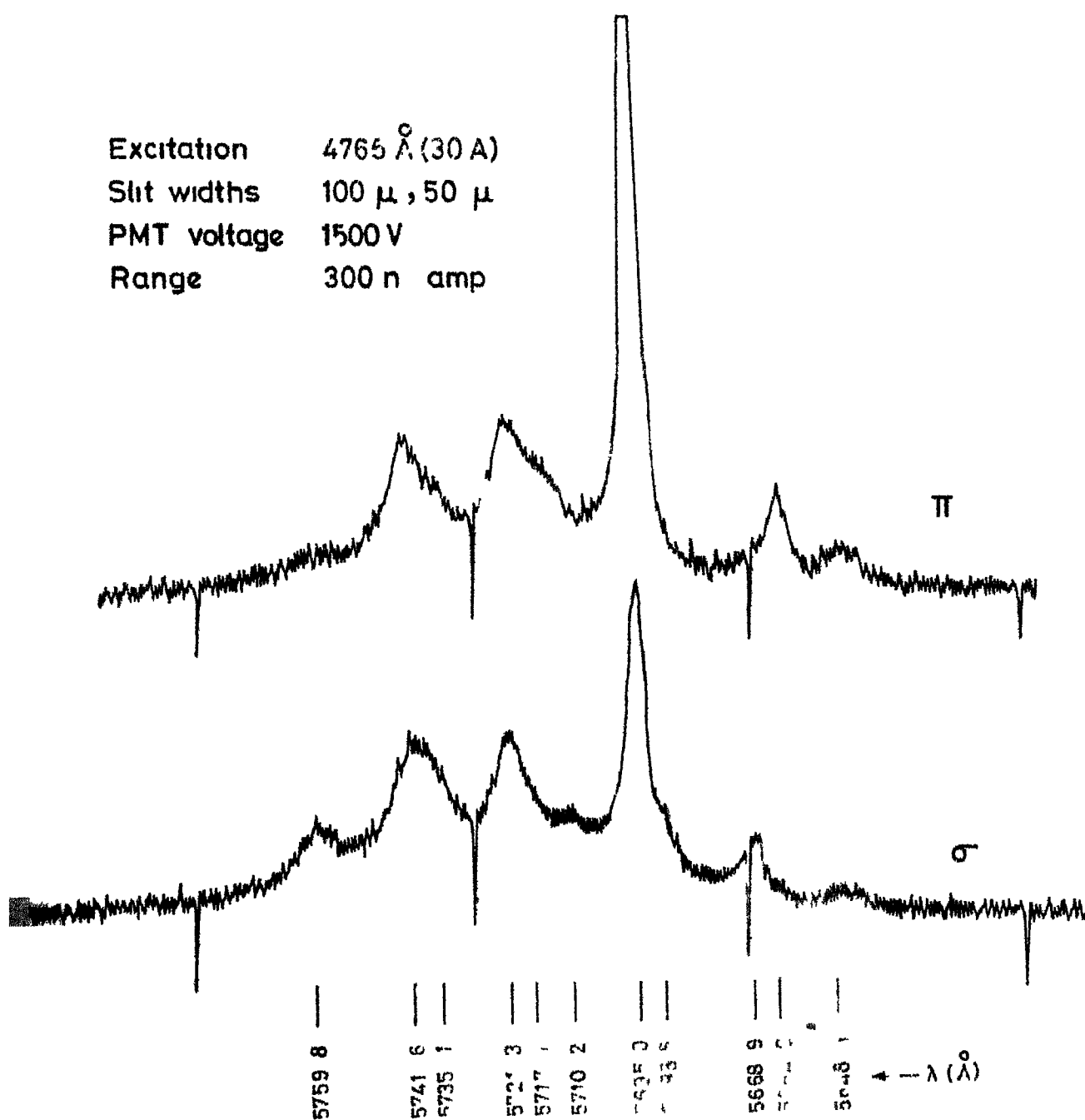
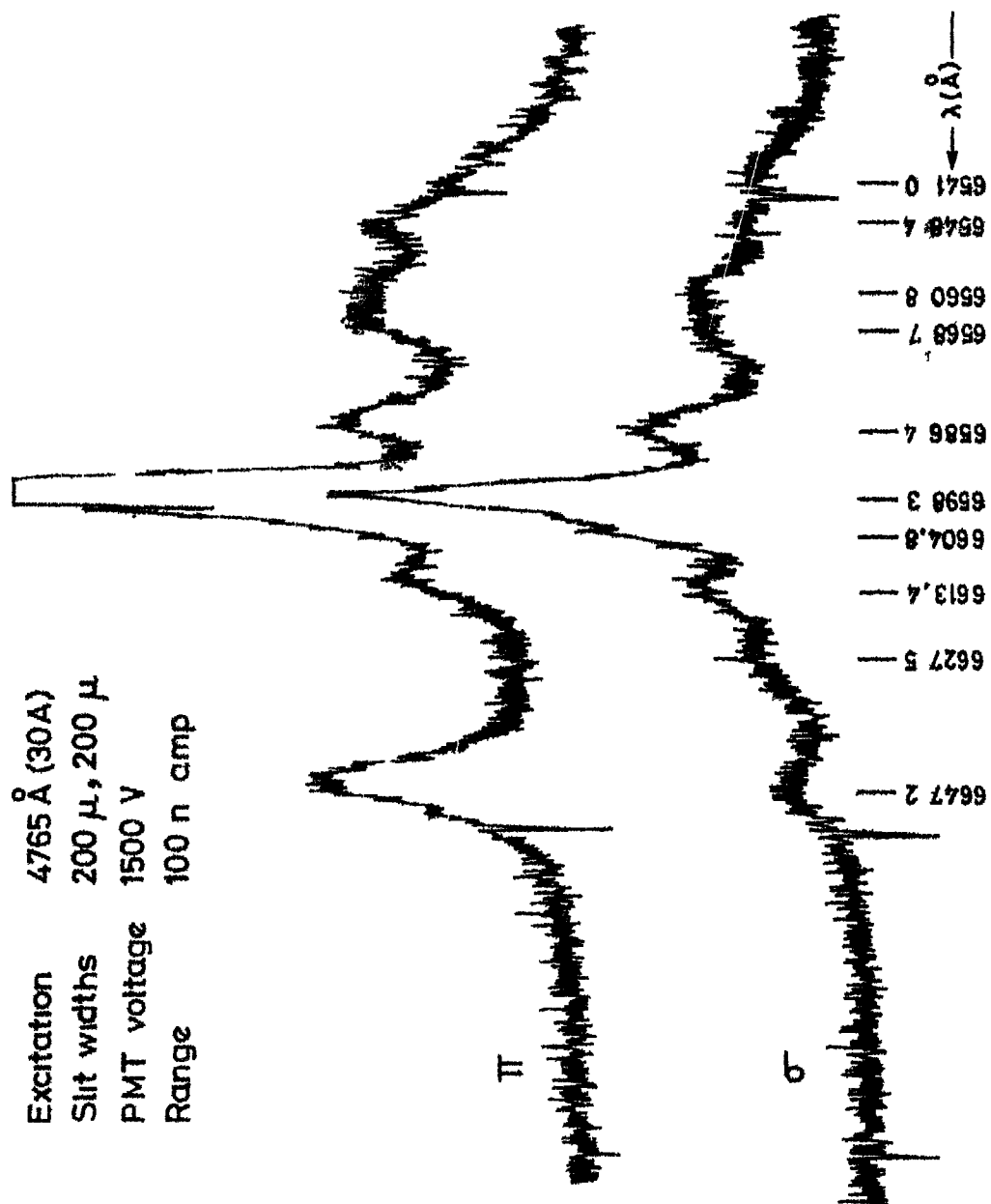


Fig 3 8 $\text{Dy}^{3+} \text{LaF}_3$ fluorescence at 77°K 4765 \AA excitation,
 $\text{F}(^4\text{F}_{9/2}) \longrightarrow \text{Y}(^6\text{H}_{11/2})$ group



Excitation 4765 Å (30A)
 Slit widths 200 μ , 200 μ
 PMT voltage 1500 V
 Range 100 n amp

Fig 39 Dy³⁺ LaF₃ fluorescence at 77°K, 4765 Å excitation;
 $F(^4F_{5/2}) \rightarrow X(^6H_{11/2})$ Group.

Excitation 4765 Å (30 Å)
 Slit widths 200 μ, 100 μ
 PMT voltage 1500 V
 Range 100 n c/mμ

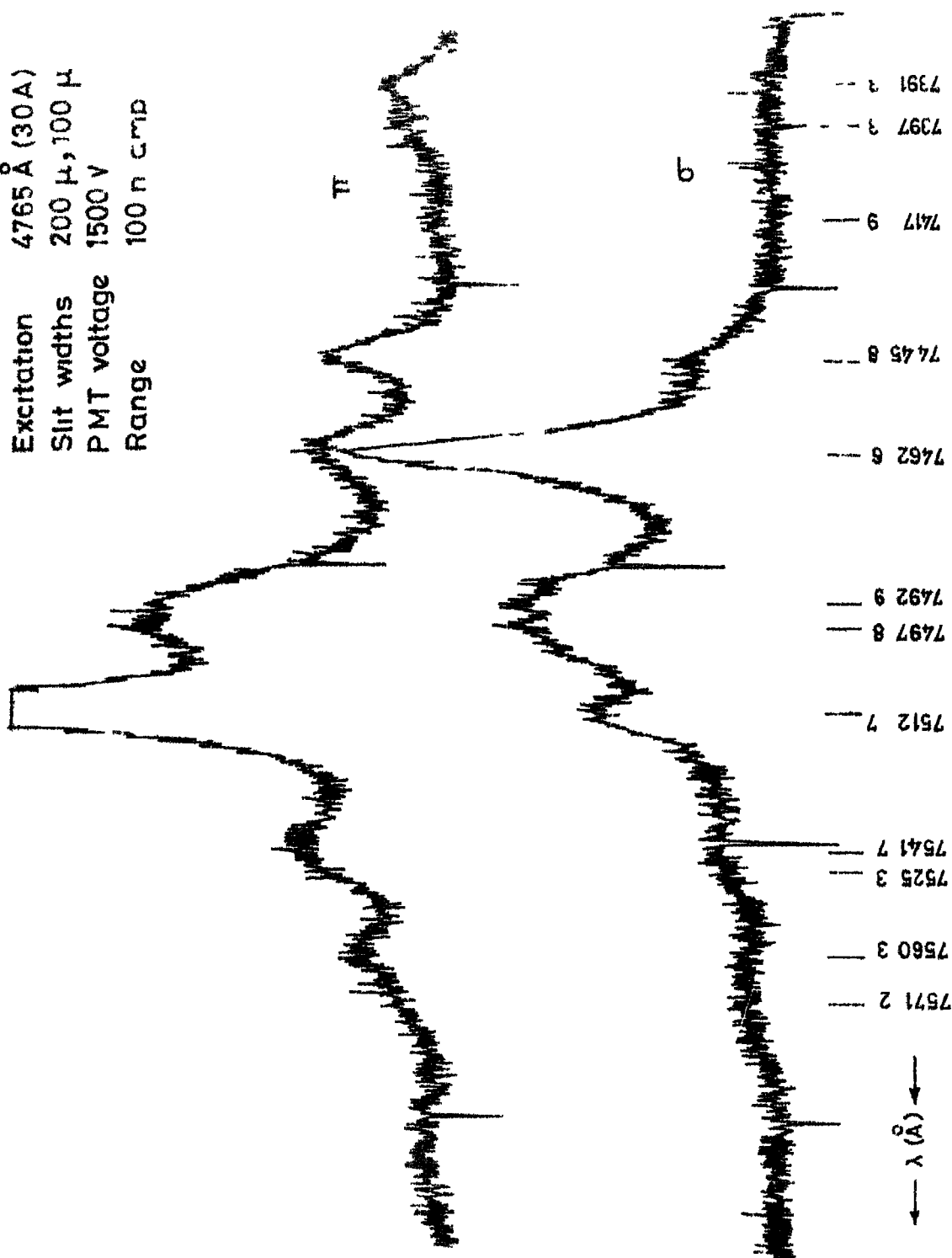


Fig 310 Dy³⁺ LaF₃ fluorescence at 77°K, 4765 Å excitation,
 $F(^4F_{9/2}) \rightarrow W(^6H_{9/2}, ^6F_{11/2})$ Group.

Excitation 4765 Å (30A)
 PMT voltage 1500 V
 Range 30 n amp

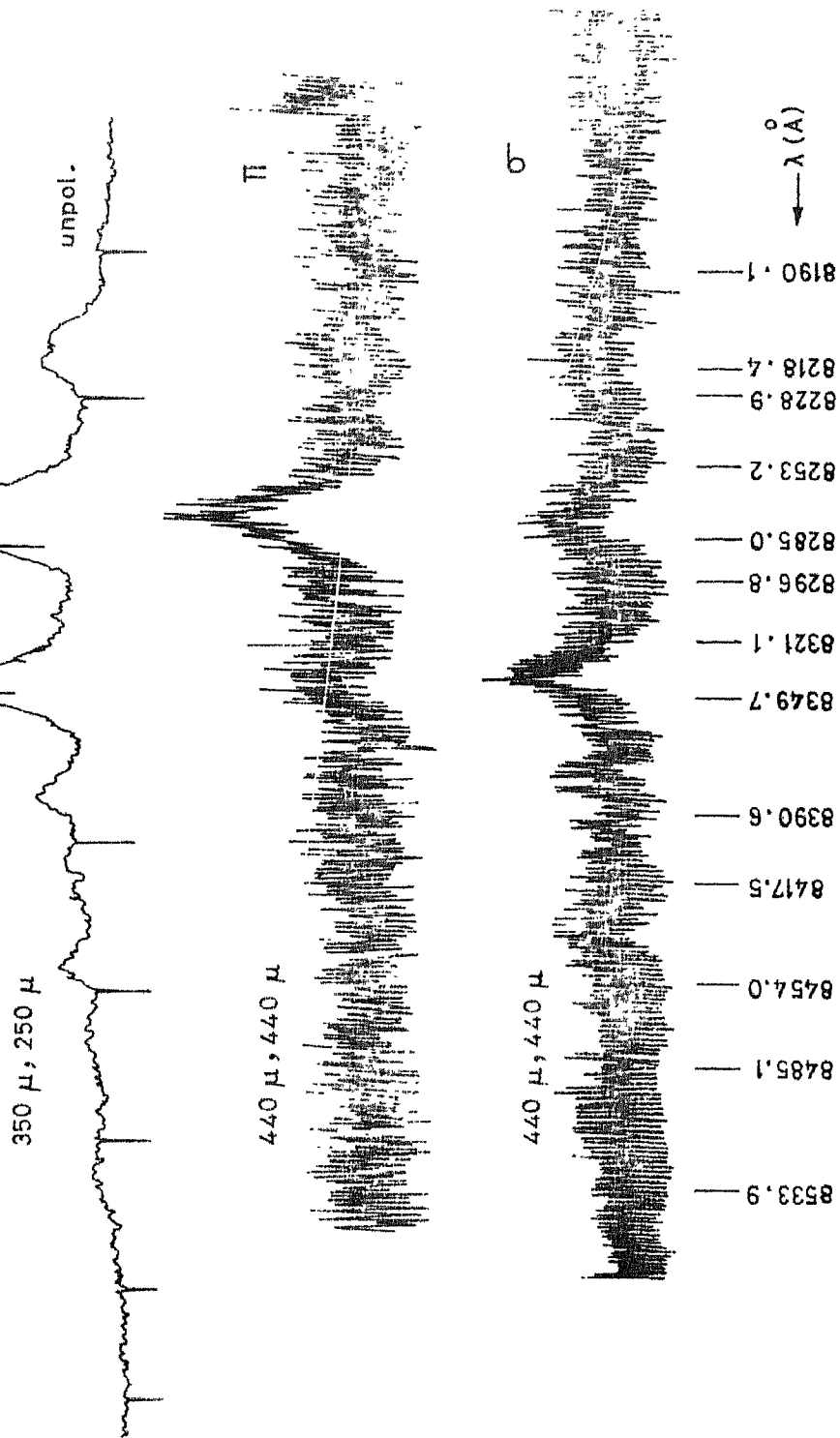


Fig. 3.11 Dy³⁺:LaF₃ fluorescence at 77°K; 4765 Å excitation;
 $F(^4F_{9/2}) \rightarrow A(^6H_{7/2}, ^6F_{9/2})$ Group.

Table 3 2
Fluorescence spectrum of $\text{Dy}^{3+} \text{LaF}_3$ at 77°K

Wavelength (Å)	Energy (cm^{-1})	Polarization	
		σ	π
4703.4	21255	vW	vW
4715.8	21199	4	vW
4726.0	21154	25	0
4729.4	21138	36	30
4731.8	21128	27	22
4741.0	21087	13	16
4747.2	21059	29	29
4750.4	21045	69	49
4755.0	21025	0	29
4761.1	20993	46	24
4772.1	20949	49	--
4775.0	20939	46	77
4778.7	20920	0	54
4786.4	20887	--	--
4793.5	20856	35	104
4803.8	20811	0	56
4818.2	20749	43	58
4824.2	20723	--	50
4830.9	20694	--	42
4835.3	20676	--	29
4850.7	20610	--	13

Table 3 2 (.Contd.)

Wavelength (Å)	Energy (cm ⁻¹)	Polarization	
		σ	π
5648.3	17699	4	5
5664.0	17650	5	24
5668.9	17634	24	8
5688.8	17572	26	11
5695.0	17554	130	315
5710.2	17507	21	26
5717.1	17486	17	0
5721.3	17473	90	84
5735.1	17431	0	35
5741.6	17411	90	66
5759.8	17357	41	15
6541.0	15284	3	5
6548.4	15267	5	9
6553.7	15254	vw	vw
6560.8	15238	9	8
6568.7	15220	6	10
6571.6	15213	vw	vw
6586.4	15179	24	24
6598.3	15149	54	64
6604.8	15136	28	27
6613.4	15117	18	16

Table 3.2 (. .Contd)

Wavelength (Å)	Energy (cm ⁻¹)	Polarization	
		σ	π
6627.5	15035	12	0
6647.2	15040	9	24
7370.2	13564	vw	vw
7391.3	13526	5	9
7397.3	13515	4	8
7417.9	13477	vw	vw
7445.8	13427	20	14
7462.6	13396	77	16
7492.9	13342	54	32
7497.8	13333	50	34
7512.7	13307	38	68
7541.7	13256	14	20
7545.3	13250	vw	vw
7560.3	13223	7	13
7571.2	13204	7	9
7600.2	13154	5	7
7610.1	13137	vw	vw
7652.9	13065	vw	vw
7697.6	12987	vw	vw

Table 3 2 (Contd.)

Wavelength (Å)	Energy (cm ⁻¹)	Polarization	
		σ	π
8085 1	12365	-	
8190 1	12207	-	-
8218 4	12164	-	-
8228 9	12149	-	-
8253.2	12113	-	-
8270.6	12038	-	-
8285.0	12067	38	50
8296.8	12050	-	-
8321.1	12014	-	-
8340 4	11987	-	-
8349 7	11973	57	15
8390.6	11915	-	-
8417.5	11877	-	-
8454 0	11826	-	-
8485 1	11783	-	-
8524 8	11727	-	-
8533.9	11715	-	-
8598.1	11627	-	-

3 7.1 Crystal structure of LaF_3 and polarized lines

Various crystal structures (D_{3d}^4 , D_{6h}^3 , C_{6v}^3 , have been proposed so far for LaF_3 ²¹⁻²⁷⁾ There are only minor differences in these The site symmetry of La^{3+} ion is determined to be orthorhombic (C_{2v} , C_2 or C_s) in all these models Under all these site symmetries, all the Kramer's wave functions (i e., for odd electron systems) belong to a single species and no selection rules exist nor should there be any polarization. A highly symmetric D_{6h}^4 structure has also been proposed²⁸⁾, D_{3h} being the site symmetry of the La^{3+} ion Later studies however do not agree with this²³⁻²⁷⁾.

It is observed that the spectra of other Kramer's ions in LaF_3 , however, are partially polarized³²⁻³⁶⁾ Wong et. al.³²⁾ reported polarized lines in the optical absorption of Nd^{3+} in LaF_3 and suggested that the polarization might be due to the coupling of six RE^{3+} ions into two groups Krupke and Gruber³³⁾ observed that many lines of Er^{3+} LaF_3 exhibit partial polarization and some lines appear only either in the σ - or π -spectrum. They suggested that the site symmetry of RE^{3+} might have a slight distortion towards trigonal symmetry such as D_{3h} Some transitions in Sm^{3+} LaF_3 show strong polarization as reported by Rast et al³⁴⁾. Polarized lines are observed in the absorption as well as in the fluorescence spectrum of

CENTRAL LIBRARY
 Acc. No. **55479**

Nd^{3+} LaF_3 , but no explanation could be found^{35,36)}

3 7.2 Discussion

As has been mentioned, the polarization of the spectral lines is not expected for any of the pure electronic transitions in C_{2v} , C_2 or C_s site symmetries of the Kramer's ion in LaF_3 lattice. Polarization of the spectral lines could also arise mainly because of the two following possibilities, viz., (a) distortion of the site symmetry of the rare earth ion from C_{2v} to higher symmetries like D_{3h} and (b) coupling of phonons to the Stark levels of the ion.

(a) When the lattice is slightly distorted so that the Re^{3+} ion is situated more symmetrically, the highest symmetry the RE^{3+} ion can exhibit is D_{3h} . In this point group, the Stark levels of the Kramer's ion are represented by any of three irreducible representations $E_{1/2}$, $E_{3/2}$ or $E_{5/2}$ ³⁷⁾. The relevant selection rules and the term splittings are shown in Table 3.3. As the 'axial spectrum' is similar to the ' σ -spectrum' in the present system, the transitions would have forced electric dipole nature³⁸⁾. Since, all the transitions from F_1 to lower levels are observed at 4.2°K, one can safely assume that F_1 belongs to $E_{5/2}$ irreducible presentation. Thus, from group theoretical considerations one would expect from F_1 ,

Table 3 3
Selection rules and term splittings in
 D_{3h} double group

D_{3h}	$E_{1/2}$	$E_{3/2}$	$E_{5/2}$
$E_{1/2}$	-	T_{xy}, T_z	T_{xy}
$E_{3/2}$	T_{xy}, T_z		T_{xy}
$E_{5/2}$	T_{xy}	T_{xy}	T_z
$J = 7/2$	1	2	1
9/2	1	2	2
11/2	2	2	2
13/2	3	2	2
15/2	3	2	3

3π 's and 5σ 's in 4750 Å group

2π 's and 5σ 's in 5700 Å group

2π 's and 4σ 's in 6600 Å group

4π 's and 7σ 's in 7500 Å group

3π 's and 6σ 's in 8400 Å group

Also, another Stark level of F must belong to $E_{5/2}$,

($\Gamma_{9/2} = E_{1/2} + 2E_{3/2} + 2F_{5/2}$) which has to yield transitions with identical characters compared to Γ_1 . Considering the four groups (F → Z, Y, X, W) where the polarization is studied in detail, it's difficult to find the other Stark level uniquely. One can thus only state that F_1 must be a $E_{5/2}$

(b) The other source of polarization is due to vibronic transitions. The phonons of the host lattice can get coupled to the Stark levels of the impurity ion, thereby changing the symmetry species of the Stark level under consideration. The representation of the vibronic level (i.e., phonon-coupled Stark level) is given by the direct product of the representations of the Stark level and of the lattice phonon,

$$\text{i.e.,} \quad \Gamma_{\text{vibronic}} = \Gamma_{\text{Stark}} \times \Gamma_{\text{Phonon}} \quad (3.13)$$

The lattice phonons, which are nothing but 'normal modes of vibration' of the host lattice transform according to

the irreducible representations of the space group of the lattice. These irreducible representations of the space group are then reduced in terms of the irreducible representations of the site symmetry group of the impurity ion so as to arrive at (Γ_{phonon}) ion site and then only they can be coupled to the Stark level of the impurity ion³⁹⁾. It is observed that phonons with all possible wave vectors (\vec{k}) can participate in the vibronic transitions and the peaks in the vibronic spectrum usually appear for phonons at points of high symmetry in the Brillouin Zone of the host lattice⁴⁰⁾. Accordingly, the irreducible representations of the phonons at these special points have to be reduced into a sum of irreducible representations of the site symmetry group of the impurity ion.

When C_{2v} site symmetry is considered for phonon-coupling, the vibronic levels are also represented by the single irreducible representation $E_{1/2}$.

$$(\Gamma_{A_1}, \Gamma_{A_2}, B_1 \text{ or } B_2 \times \Gamma_{E_{1/2}} = \Gamma_{E_{1/2}})$$

and the direct product $\Gamma_{E_{1/2}} \times \Gamma_{E_{1/2}}$ contains all the irreducible representations of the normal C_{2v} point group

$$(i.e., \Gamma_{E_{1/2}} \times \Gamma_{E_{1/2}} = \Gamma_{A_1} + \Gamma_{A_2} + \Gamma_{B_1} + \Gamma_{B_2}).$$

Thus, no polarization is expected from any vibronic transitions also.

When D_{3h} site symmetry is considered and the

selection rules etc are derived for vibronic transitions, it is found that the π -polarization could be expected only between the stark levels belonging to the irreducible representation of $E_{5/2}$. Also, this in turn, is possible only for the special points in the Brillouin Zone⁴¹⁾ which have the symmetries of D_{6h} , D_{3h} , or C_{6v} (i.e., Δ , A , K and H points only). However, for each spectral line, there exist number of vibronic transitions (more than twenty) and unique assignment is once again not found to be possible. The representations as well as energies of phonons are available from the Raman, Infrared and optical spectral data reported earlier^{24, 42-44)}.

3.3 Conclusion

High temperature study resulted in the observation of a new fluorescing level (G , $^4I_{15/2}$). Transient fluorescence study yielded radiative relaxation rates of F and G levels. By increasing the power of the W_2 laser, one can extend these studies, to the higher levels also. From the polarization features of the fluorescence data, it can be concluded that the site symmetry of the rare earth ion in LaF_3 is very likely higher than C_{2v} . However the present experiments are to be repeated at $4.2^\circ K$ and should be supplemented by polarization data of the absorption for better understanding.

REFERENCES

- 1 H Gobrecht, Ann Phys 28, 673 (1937)
- 2 ibid 31, 755 (1938)
- 3 E J Meehan and G C Nutting, J Chem Phys 7, 1002 (1939).
- 4 A I Rosa, Ann Phys. 43, 161 (1943)
- 5 J Hoogschagen, T G. Scholte and S Kruyer, Physica
11, 504 (1946).
- 6 G H Dieke and S. Singh, J Opt Soc Am 46, 495, (1956)
- 7 G Gramberg, Z. Physik 159, 125 (1960)
- 8 H H Crosswhite and G.H Dieke, J Chem Phys
35, 1535 (1961)
9. C F Jørgensen, Acta Chem Scand 11, 981 (1957)
- 10 J P Elliott, B.R Judd and W A Runciman, Proc Roy
Soc 240, 509 (1957)
11. B R Judd, Proc Phys Soc. 74, 330 (1959)
12. B G Wybourne, J. Chem Phys 36, 2301 (1962)
- 13 B G Wybourne, 'Spectroscopic Properties of Rare Earth
Ions', Interscience Publ , N Y (1965)
14. J D Axe and G.H Dieke, J Chem Phys 37, 2364 (1962).
15. G E. Barasch and G H Dieke, J Chem Phys 43,
983 (1965).
16. L A Riseberg, W B Gandrud and H. W Moos, Phys Rev
159, 262 (1967).
- 17 L A Riseberg and H.W. Moos, Phys Rev Lett 19,
1423 (1967)
- 18 W B Grandrud and H.W. Moos, J. Chem. Phys 49,
2170 (1968).

- 19 J L Fry, H H Caspers, H E Rast and S A Miller,
J Chem Phys 48, 2342 (1968)
- 20 G H Dieke 'Spectra and Energy Levels of Rare Earth Ions
in Crystals', Interscience Publ , N Y (1968)
- 21 J Oftedal, Z Phys Chem 5, 272 (1929).
- 22 ibid 13, 190 (1931)
- 23 M Mansman, Z, Anorg. Allgem Chem 331, 98 (1964)
- 24 R.P Bauman and S P S Porto, Phys Rev 161, 842 (1967)
- 25 J I Baker and R S. Kubins, Proc Phys Soc 78,
1353,(1961).
26. C de Rango, G. Tsoucaris and Ch Zelwer, C R Acad
Sci 263, 64 (1965).
27. V K Sharma, J Chem Phys 54, 496 (1971)
- 28 K Schlyter, Arkiv. Kemi 5, 73 (1952)
- 29 L A Riseberg and H W. Iloos, Phys Rev 174, 429 (1968)
- 30 H Jagannath, Ph D Thesis, IIT Kanpur, India (1976)
- 31 F I Fong, H V Lauer and C R Chilver, J Chem Phys
63, 366 (1975)
- 32 E Y Wong, O M Stafsudd and D R Johnston, Phys Rev.
131, 990 (1963).
33. W Trupke and J.B Gruber, J Chem Phys, 39, 1024 (1963)
34. H.L Rast, J L Fry and H.H Caspers, J Chem Phys
46, 1460 (1967)
- 35 H.H Caspers, H.E. Rast and R.A, Buchanan, J Chem
Phys, 42, 3214 (1965)
36. U V Kumar, Ph. D Thesis, IIT Kanpur, India (1975).

- 37 The Double Group Representations are tabulated by
G F Koster, 'Solid State Physics' (Ed. Seitz and
Turnbull) Academic Press, N Y (1957), Vol 5, P 173
38. D S Mc Clure, 'Electronic Spectra of Molecules and
Ions in Crystals' Academic Press, N Y (1969), p 37
- 39 B Di Bartolo, 'Optical Interactions In Solids', John
Wiley and Sons, N Y (1968), p 399
- 40 M J Weber and R L Schaufele, Phys Rev, 138,
1544 (1965)
- 41 'The Irreducible Representations of Space Groups',
(Ed J. Zak) Benjamin Inc, N Y (1969), Sec 7.5
42. H E Rast, H H. Caspers and S A Miller, Phys Rev
171, 1051 (1968)
- 43 M.M Yen, W.C Scott and A.L. Schawlow, Phys Rev 136
271 (1964)
- 44 P Venkateswarlu, Proc of Nuclear Phys and Sol State
Phys Symp. held at Bangalore, India (1973), p 158.

CHAPTER 4
THE STEADY STATE AND TRANSIENT LUMINESCENCE
SPECTRUM OF $\text{Dy}^{3+} \text{CaF}_2$

ABSTRACT

The fluorescence and the decay times of $\text{Dy}^{3+} \text{CaF}_2$ are studied in the 4500 to 9000 Å region, using a Cl Ar^+ laser and a pulsed N_2 laser in the temperature range of 77 to 673°K. At 77°K, five groups of lines are observed, all of them originating from the F-level ($^4\text{F}_{9/2}$) of Dy^{3+} . These studies show that there are at least two kinds of Dy^{3+} -centers, one with fluorescence decay time(τ) of ~ 1.3 msec (A-center) and another with $\tau \sim 3.5$ msec (B-center). The energy level schemes for both these centers are presented. The lines belonging to the A-center match well with the tetragonal center reported earlier and those of B-center match well with the cubic center also reported earlier. The earlier work on cubic center was in the region of 4700 to 6700 Å and that on tetragonal center was in the region of 4700 to 5800 Å only.

The present work reports also the observation of new fluorescence from the G-level ($^4\text{I}_{15/2}$) in the temperature range of 300 to 673°K. Approximate Stark level positions of G could be obtained from this study. The decay times indicate a thermal mixing of F and G levels for the two centers.

4 1 Introduction

The study of spectroscopic properties of Dy^{3+} in CaF_2 has been an active field of investigation over the last two decades¹⁻¹³). Dy^{3+} ion occupies Ca^{2+} ion site and depending upon the compensating ion and its vicinity from the Dy^{3+} ion, several Dy^{3+} centers having different site symmetries are possible. Various centers of Dy^{3+} have been identified and the energy level schemes are available in the literature. The presence and relative dominance of different centers change from sample to sample depending highly upon the growth conditions, heat treatment and concentration of the impurity ion.

The first attempt to identify the centers was by Rabiner¹⁾ who studied fluorescence spectrum at 77°K. The crystals were grown in a reducing atmosphere, using NaF in the melt. On the basis of the number of Stark components observed, he concluded that the spectrum was mainly due to cubic centers. Three groups were observed all of which originate from a single fluorescing level which was wrongly designated by him as $^6\text{F}_{11/2}$. The absorption, luminescence and excitation spectra were studied by Voronko et al²⁾. Three different centers were identified in crystals containing different amounts of oxygen. The absorption spectrum at room temperature was reported and only the principal group positions were identified for the three centers.

The centers in the crystals containing oxygen (Type II and III) were also seen to display strong Dy^{3+} -luminescence at 77°K when excited into the absorption bands near 2000 Å. The fluorescence spectrum (FS) as well as thermoluminescence spectrum (TLS) was studied by Liss and Staebler³⁾ The number of lines as well as their separations in the FS and TLS of γ -irradiated samples fitted very well with the calculated ground state energy levels for a cubic center⁴⁾ It was later observed by Merz and Pershan⁵⁾ that the low temperature 'glow-peaks' (80 to 280°K) of X-irradiated crystals were due to cubic centers, while tetragonal centers accounted for the high temperature (280 to 450°K) glow-peaks in the TLS

The first systematic study to identify the different centers in the fluorescence spectrum was done by Luks et al⁶⁾ (hereafter referred to as LSS) who performed the experiments at 4.2°K. Spectra due to four different centers (A, B, C and D) had been observed. The isolation of Stark structure belonging to each center was performed both by comparing the spectra of a number of crystals of varying dysprosium concentration and by grouping of lines with identical decay times (Sec 4.2). At 77°K, the A-center showed a decay time (τ) of 1.3 msec, B-center of 2.9 msec, C-center of 6.6 msec and D-center of 6.4 msec. The study was done in 4800 Å and 5700 Å regions only and the energy

level schemes involving transitions from the Stark levels of ${}^6F_{11/2}$ to those of ${}^6H_{15/2}$ and ${}^6H_{13/2}$ were proposed for B, C and D centers. The spectrum due to A-centers contained too few lines to construct the energy level scheme. The C-centers were identified to be cubic centers by comparing the spectra with those of earlier workers, as well as by its sharp increase in intensity when Na^+ ion was introduced⁷⁾. The B-center was later identified to be tetragonal center⁸⁾ by the comparison of luminescence spectra obtained using different methods of exciting the rare earth ion (e.g. x-ray luminescence, Cathod luminescence etc.). The D-center was assigned to rhombic center from its appearance when Na^+ ion was introduced in the melt⁷⁾. This work was extended to SrF_2 , BaF_2 and CdF_2 hosts also^{9,10)}. The upper free ion level from which luminescence originates was identified to be ${}^4F_{9/2}$ and not ${}^6F_{11/2}$. Crystal field parameters were calculated for cubic centers. An energy level diagram for cubic centers was presented, showing the levels of ${}^6H_{15/2}$, ${}^6H_{13/2}$, ${}^6H_{11/2}$ and ${}^4F_{9/2}$. Energy level scheme was also given for the orthorhombic center (which was designated as rhombic center in Ref. 6) involving the levels ${}^6H_{15/2}$, ${}^6H_{13/2}$ and ${}^4F_{9/2}$.

High resolution FLS was reported by Schlesinger and Swan¹¹⁾ along with FLS and excitation spectra for Dy^{3+} CaF_2 at 77°K. The crystal field parameters were calculated including J-mixing for both cubic and tetragonal

centers^{12,13)} For the tetragonal centers, they have assumed that all the fluorescence, at 77°K, was originating from a single Stark level of $^4F_{9/2}$ in contradiction with the two close lying Stark levels (separated by 27 cm^{-1} only) reported by LSS⁶⁾.

In the present study, the $\text{Dy}^{3+}\text{CaF}_2$ system is reinvestigated using Ar^+ and F_2 lasers as the excitation sources. Transitions from F-level ($^4F_{9/2}$) to W($^6H_{9/2}$, $^6F_{11/2}$) and A($^6H_{7/2}$, $^6F_{9/2}$) levels are also observed. The identification of centers is done using the concentration series method and the decay time methods (Sec 4.2). Two centers are mainly observed and the probable energy level schemes are presented. The present study also reports the fluorescence from G-level ($^4I_{15/2}$) to Z-level ($^6H_{15/2}$). The 'G-fluorescence' is not reported earlier for Dy^{3+} in any host.

4.2 Crystal structure of CaF_2 and analysis of the spectra of $\text{RE}^{3+}\text{CaF}_2$

CaF_2 has a fluorite structure¹⁴⁾ It consists of a simple cubic lattice of fluorine ions (F^-) in which alternate 'body-center' positions are occupied by the divalent cation (Ca^{2+}). The cation sites occupied or unoccupied have eight fold coordination resulting in O_h symmetry and the F^- ion sites have four fold coordination resulting in T_d symmetry.

When rare earth ions are doped in CaF_2 , they are usually present as trivalent ions (RE^{3+}) and substitute Ca^{2+} ion. In the absence of oxygen or other impurities, the excess +ve charge is compensated by F^- ions which occupy interstitial positions (usually at the body-center positions of the vacant cation sites). Depending on the vicinity of this compensating F^- ion, the site symmetry of the RE^{3+} ion changes from cubic to monoclinic¹⁵⁾ When oxygen is present, the substitution of O^{2-} in the place of F^- can also provide charge compensation and when hydrogen or deuterium is diffused in, H^+ ions can in turn be replaced by H^- or D^- ions^{16,17)}. Thermodynamic treatments of the existence of different centers are available in the literature¹⁸⁻²⁰⁾.

The complex spectra of the fluorescence of rare earth ions in fluorites which arise due to the simultaneous existence of different centers can be analysed in five ways (a) Concentration series method, (b) Varying the growth conditions, (c) Study with different excitations, (d) Decay times method and (e) Resonant excitation method.

(a) Concentration Series Method

The procedure is to look for lines in the spectrum whose relative intensity remains constant in all the crystals with different rare earth ion concentrations²¹⁾. All such lines can be assumed to belong to one center.

At any particular concentration of the rare earth ion, several such centers can co-exist. With a change in concentration, the relative intensities of one center relative to another center can change. At very low concentrations, cubic centers are usually predominant. As the concentration is increased, new lines appear which belong to centers other than cubic. Thus, using crystals with increasing rare earth ion concentrations (i.e. concentration series), the lines belonging to each center can be identified. It is to be noted that the 'concentration series' has to be grown under identical growth-conditions.

(b) Varying the Growth Conditions

It is observed that when crystals are grown under high vacuum conditions, with adequate F^- ions, the crystals contain predominantly tetragonal centers²²⁾. The reason for this is however, not satisfactorily explained. It is found that the presence of +ve compensator ions like Na^+ , K^+ etc in the melt, results in the increase of cubic and orthorhombic centers⁷⁾. The +ve compensator ion replaces Ca^{2+} ion in the third or sixth coordination sphere of the RE^{3+} ion. In the former situation, the site symmetry should be orthorhombic and in the latter situation, tetragonal. But, because the sixth coordination sphere is far away, the interaction between the Na^+ , etc and RE^{3+} ions is so small that the cubic symmetry

of the field is not distorted. One can thus identify the cubic centers by their increase in intensity and the orthorhombic centers by their appearance and corresponding increase in intensity as the concentration of the +ve compensator is increased. Also, thermal history of the crystal reflects in the relative abundance of different centers. For example, it is observed that rapid cooling (quenching) produces predominantly cubic center, while the crystals obtained by slow cooling contain very small number of cubic centers²³⁾.

(c) Study with different Excitations

The fluorescence of rare earth ions in fluorites can be excited with X-rays (X-luminescence) electron beam (Cathodo-luminescence), UV, visible and infrared photons (Photoluminescence) and also by varying the temperature of the γ -irradiated crystals (Thermoluminescence)⁸⁾.

It's observed that some centers are selectively excited when a particular type of excitation is used. For example, when an electron beam is used, as a result of electron hole recombination, Dy^{3+} ions not associated with a compensator ion (which acts as electro +ve defect) in its immediate neighbourhood are excited and the cubic spectral lines increase in intensity⁹⁾.

(d) Decay Times Method

It is observed that transitions involving the

Stark levels of one center show the same decay time throughout the different groups of the fluorescence spectrum. The isolation of Stark structure belonging to each center can thus be carried out by identifying the lines with identical decay times⁶⁾.

(e) Resonant Excitation Method

Powerful tunable dye lasers can be used to excite the rare earth ions of a particular site resonantly and this technique allows the unambiguous interpretation and classification of the spectral lines belonging to different centers. Fluorescence from a single site can be obtained if no overlap occurs between absorption lines of different sites²⁴⁾

In addition to resonant excitation method, the concentration series method along with the decay time method is found to be very useful in identifying different centers.

4.3 Experimental Details

The steady state fluorescence spectra are recorded using the Ar^+ and N_2 lasers as described in Chapter 2. The microdensitometer traces of the photographs taken with N_2 laser excitation are essentially the same as the fluorescence spectra recorded using the Ar^+ laser throughout the wavelength region of study. In the 4700 Å region, the Dy^{3+} fluorescence spectrum

photographed with the N_2 laser is used to separate out the Pr^{3+} -fluorescence which interferes with Dy^{3+} -fluorescence (Sec. 3.7). Also, in the 3500 Å region where the sensitivity of the photomultiplier tube used falls very rapidly, the spectra obtained with N_2 laser are used for identification of the lines.

The decay times are measured using N_2 laser (Chapter 2). Because of the very weak intensity, the decay times could not be measured for the 8500 Å group. The high temperature fluorescence is recorded using the heater assembly described earlier (Sec. 2.1).

The crystals used are $Dy^{3+}CaF_2$ (0.01, 0.03, 0.09, 0.27, 0.54 and 1.08 percent by wt of DyF_3 in CaF_2) single crystals, and are grown by Bridgman's method in a vacuum furnace at BARC, Bombay. The crystals are found to contain Nd^{3+} and Pr^{3+} as additional impurities (Sec. 2.4).

4.4 General Features of the Fluorescence Spectrum at 77 and 300°K

Five groups of fluorescence from $Dy^{3+}CaF_2$ are observed at 77°K (Figs. 4.1 to 4.6) using the 3371, 4580, 4658, 4727 and 4765 Å excitations. The groups are assigned to the following transitions on comparison with the earlier reported fluorescence spectrum of $Dy^{3+}CaF_2$ ⁶⁻⁹⁾ and that of $Dy^{3+}LaF_3$ ²⁵⁾ (Chapter 3).

4700 Å group	$F(4F_{9/2}) \rightarrow Z(6H_{15/2})$
5700 Å group	$(4F_{9/2}) \rightarrow V(6H_{13/2})$
6500 Å group	$F(4F_{9/2}) \rightarrow \Delta(6H_{11/2})$
7500 Å group	$F(4F_{9/2}) \rightarrow I(6H_{9/2}, 6F_{11/2})$
8500 Å group	$F(4F_{9/2}) \rightarrow A(6H_{7/2}, 6F_{9/2})$

The relative intensities and positions of the transitions are observed to be the same with 3371, 4580 and 4765 Å excitations. The relative intensities with 4727 Å and 4658 Å excitations, however, are found to be different in the 5700 and 6500 Å groups. In both these groups, the transitions with shorter wavelengths differ much in intensity from the other transitions compared to the relative intensities of the transitions in the same groups observed with the other excitations (Sec 4 6)

The dependance of the fluorescence spectrum on the concentration of Dy^{3+} is also studied. A set of six crystals with varying concentrations (Sec 4 3) grown under identical conditions are used. The spectra showed the presence of two types of transitions. Some of the transitions do not show any variation in the relative intensities with a change in Dy^{3+} -concentration (Type A). Transitions belonging to the other type (Type B) show an increase in intensity with concentration relative to the transitions of type A. Some of the transitions belonging to type B are the lines at 4802.2 Å, 4919.5 Å,

spectrum with concentration is suggestive of the cubic centers. Also, the line positions match well with the reported values. However, the present study yields a value of 3.5 msec as against 6.6 msec observed by LSS⁶⁾

The groups of transitions in the 6500, 7500 and 8500 Å regions have not been reported earlier for tetragonal center and the 7500 and 8500 Å groups of cubic center are also not reported earlier. Assuming the presence of only two centers - cubic and tetragonal in the present spectra, the energy level schemes for both the centers are given to explain most of the observed transitions. It is, however, to be noted that the scheme for cubic center is tentative as the number of transitions belonging to this center are rather small in number.

4800 Å Group

Forty one transitions are observed in this group at 77°K (Fig. 4.1) with 4580 Å excitation. The wavelengths and the intensities are shown in Table 4.1. Some of the transitions could be due to the presence of Pr^{3+} as an additional impurity in small quantities. Six transitions due to Pr^{3+} are identified by comparing the spectrum with that obtained by N_2 laser excitation.

LSS, have reported earlier this group for different centers at 4.2°K. The present spectra agree well with the reported spectrum for tetragonal centers.

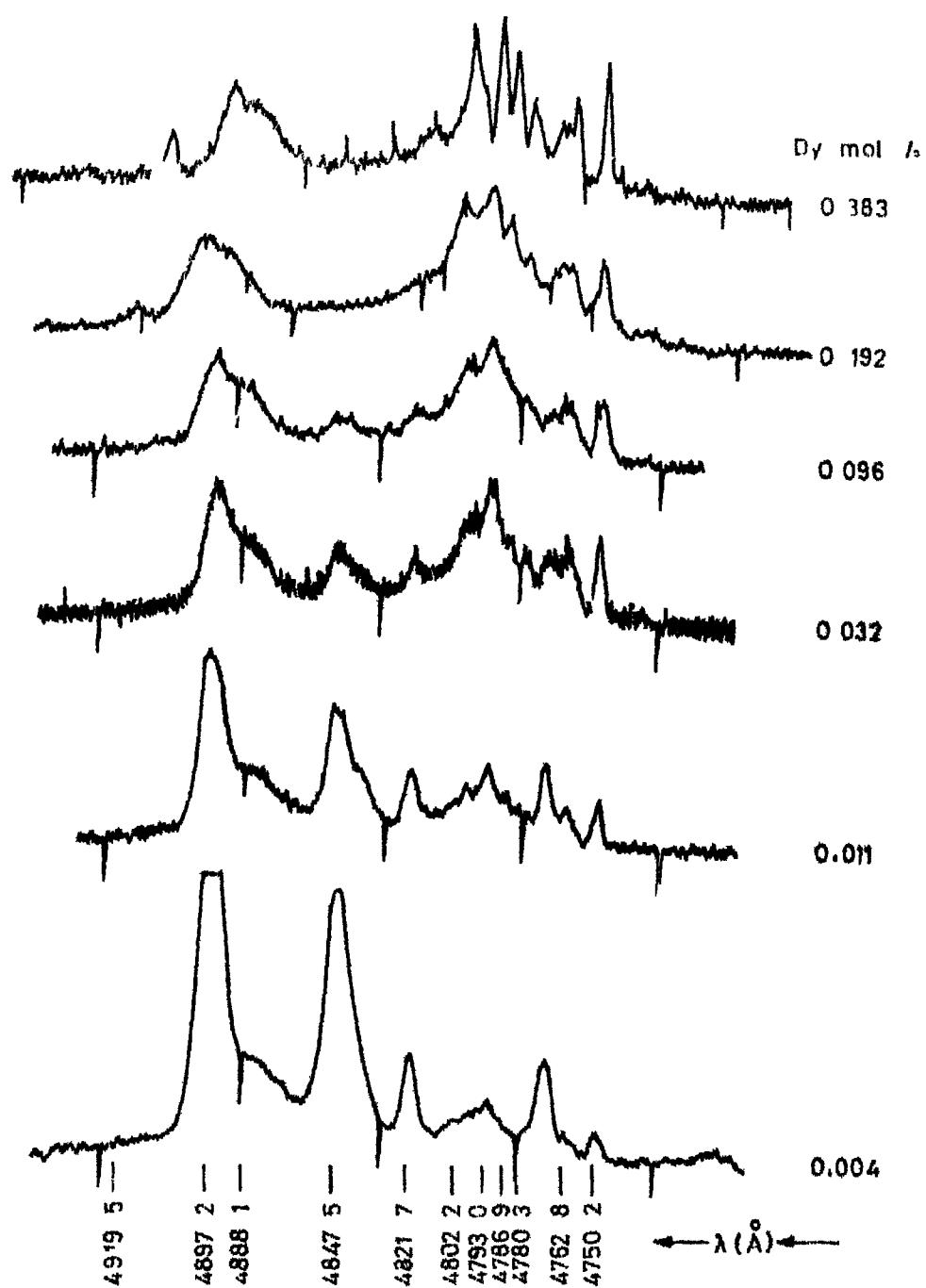


Fig 41 $\text{Dy}^{3+} \cdot \text{CaF}_2$ fluorescence at 77°K ,
 4580 \AA excitation, $F(^4F_{9/2}) \rightarrow Z(^6H_{15/2})$

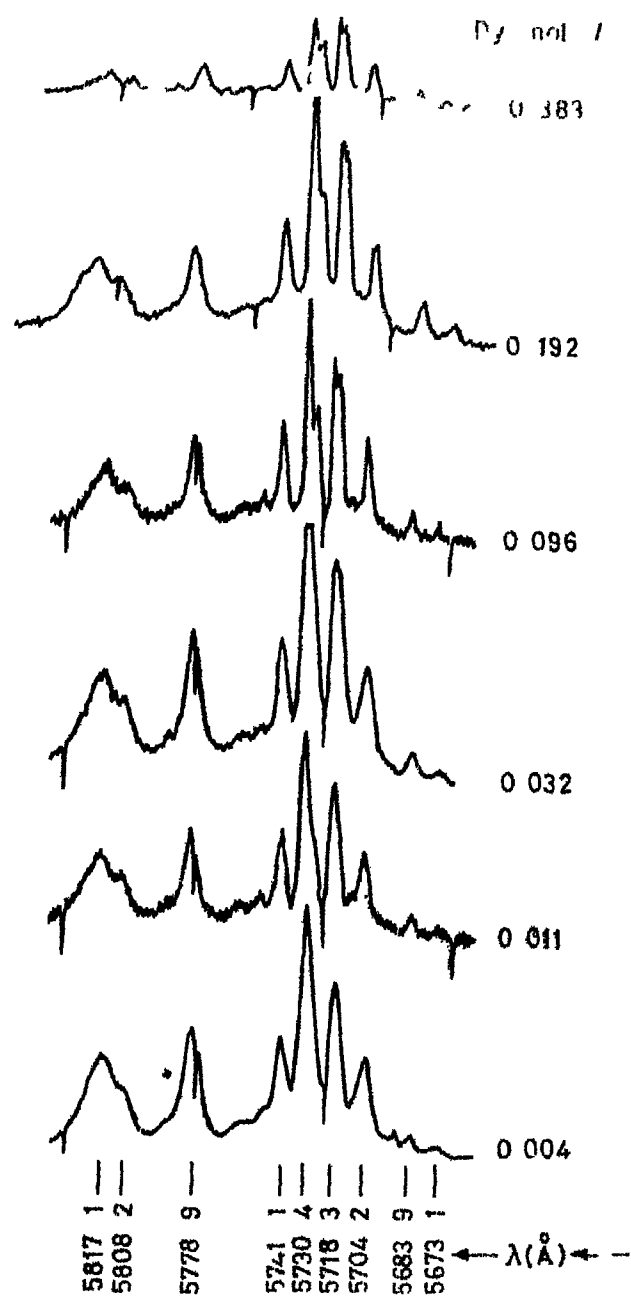


Fig 4 2 $\text{Dy}^{3+} \cdot \text{CaF}_2$ fluorescence at 77°K ,
 4765\AA excitation, $F(^4F_{9/2}) \rightarrow Y(^6H_{13/2})$.

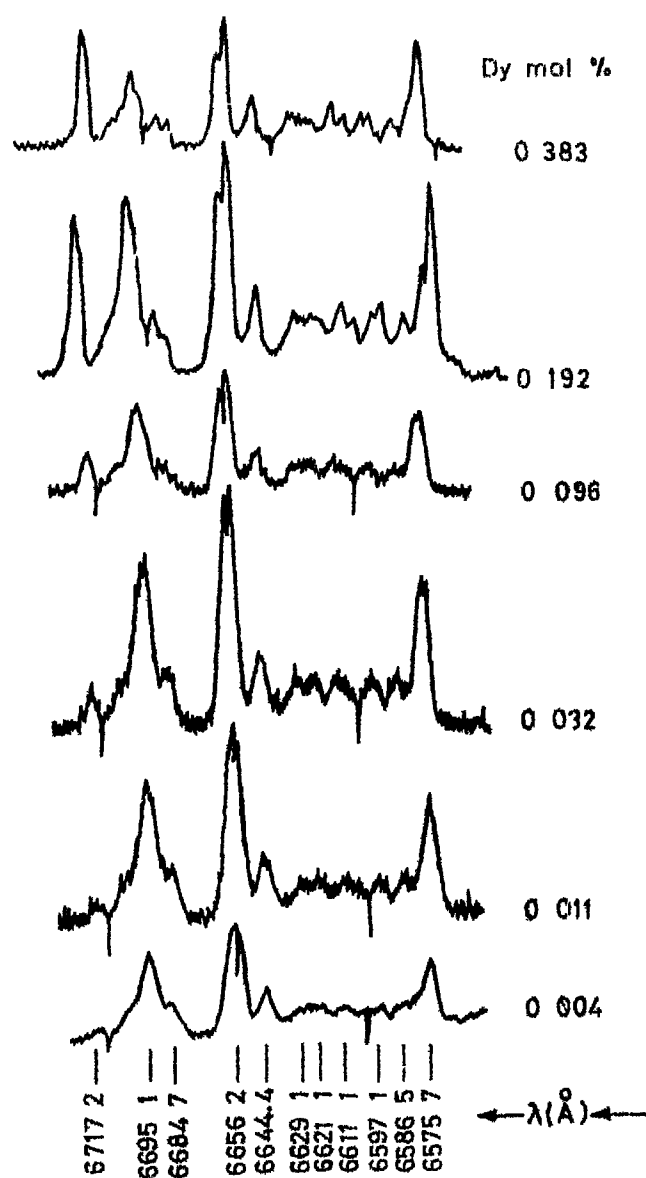


Fig 4.3 Dy³⁺ CaF₂ fluorescence at 77°K,
4765 Å excitation, $F(^4F_{9/2}) \rightarrow X(^6H_{11/2})$

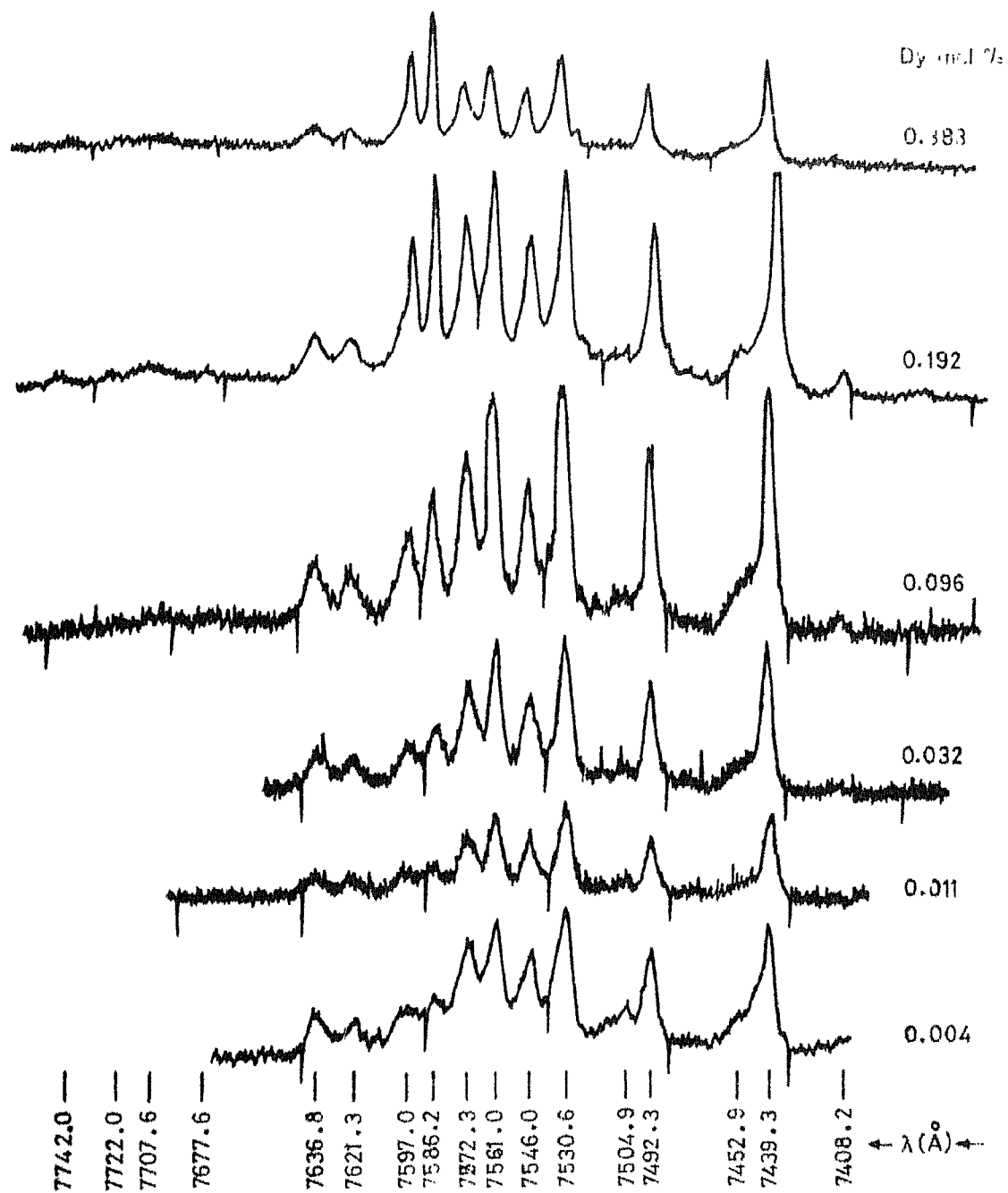


Fig. 4.4 $\text{Dy}^{3+}:\text{CaF}_2$ fluorescence at 77°K ;
 4765 \AA excitation; $F(^4F_{9/2}) \rightarrow W(^6H_{9/2}, ^5F_{7/2})$.

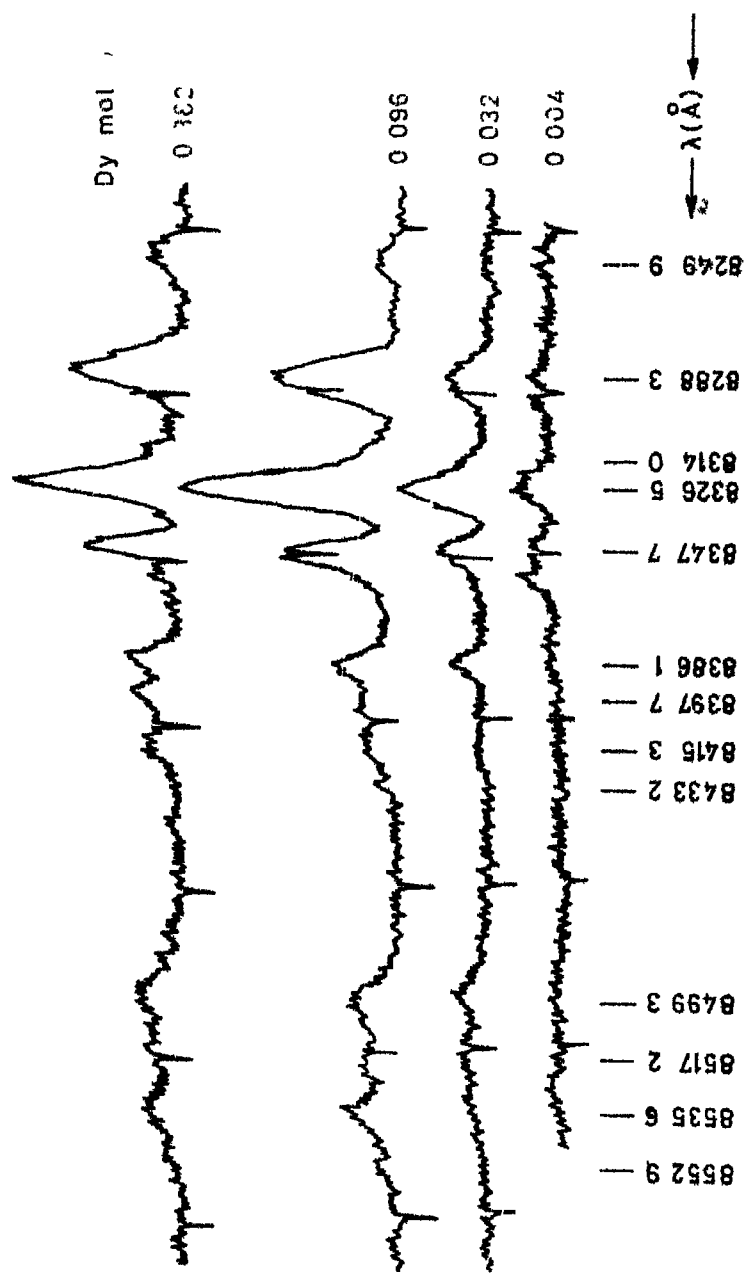


Fig. 4.5 $\text{Dy}^{3+}:\text{CaF}_2$ fluorescence at 77°K ;
 4765\AA excitation; $F(^4F_{9/2}) \rightarrow A(^6H_{7/2}, ^6F_{9/2})$

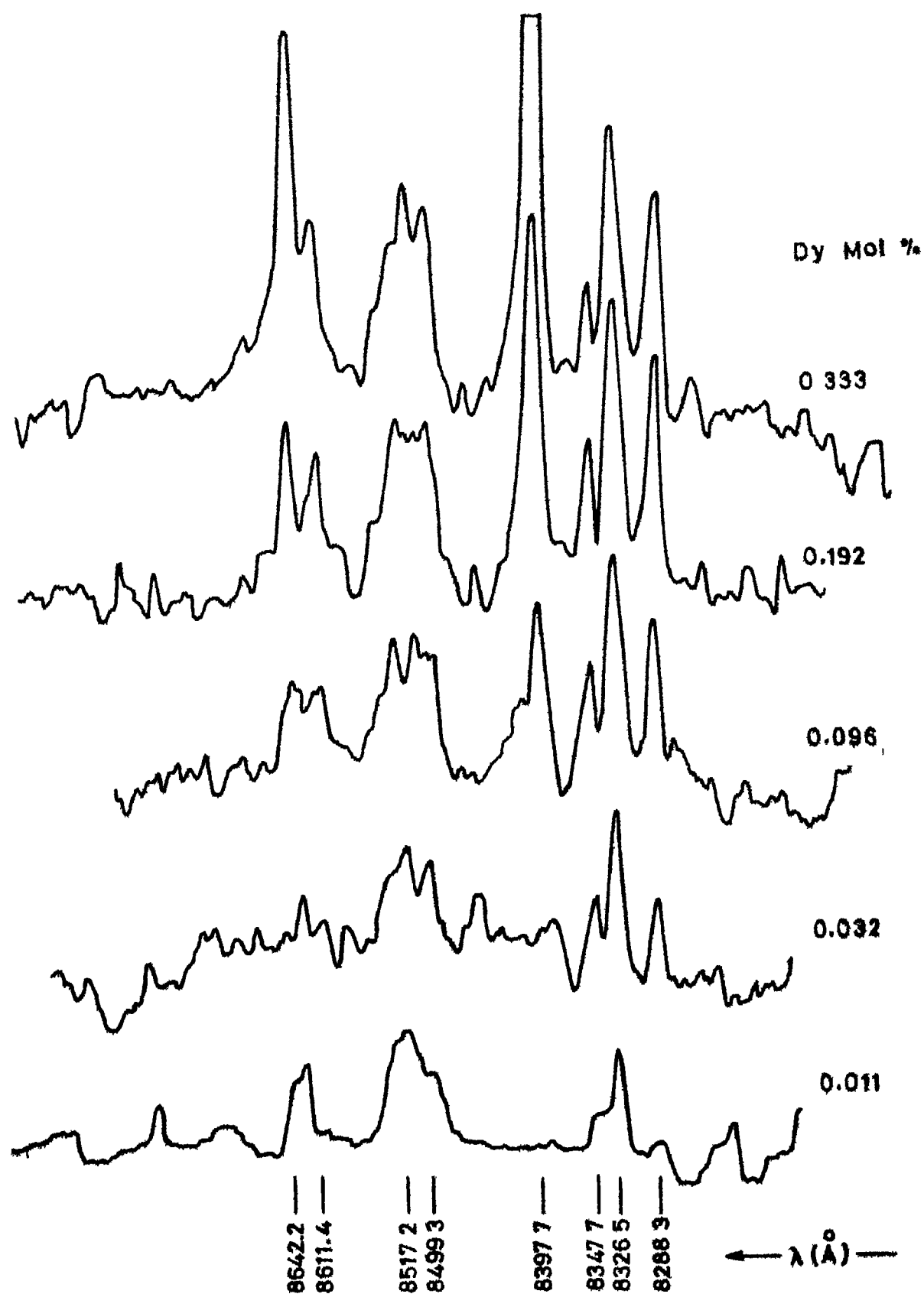


FIG 4 6 $\text{Dy}^{3+} \text{CaF}_2$ FLUORESCENCE AT 77°K , N_2 LASER EXCITATION, $\text{F}(^4\text{F}_{9/2}) \rightarrow \text{A}(^6\text{H}_{7/2}, ^6\text{F}_{9/2})$ GROUP (DENSITOMETER TRACES).

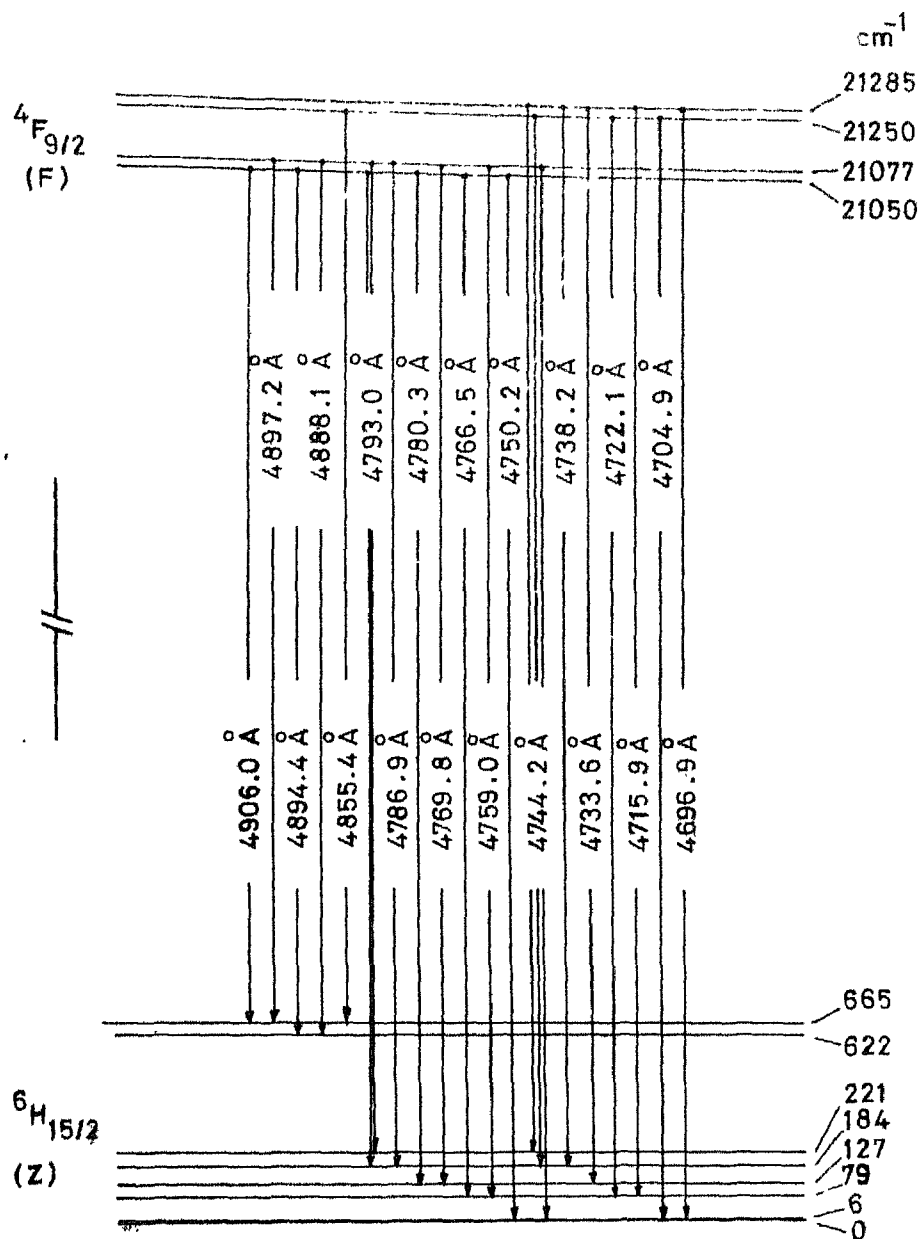


FIG. 4.7 PARTIAL ENERGY LEVEL DIAGRAM OF $\text{Dy}^{3+}:\text{CaF}_2$ FOR TETRAGONAL CENTERS SHOWING THE FLUORESCENCE GROUP OF 4800 \AA (F→Z) AT 77°K.

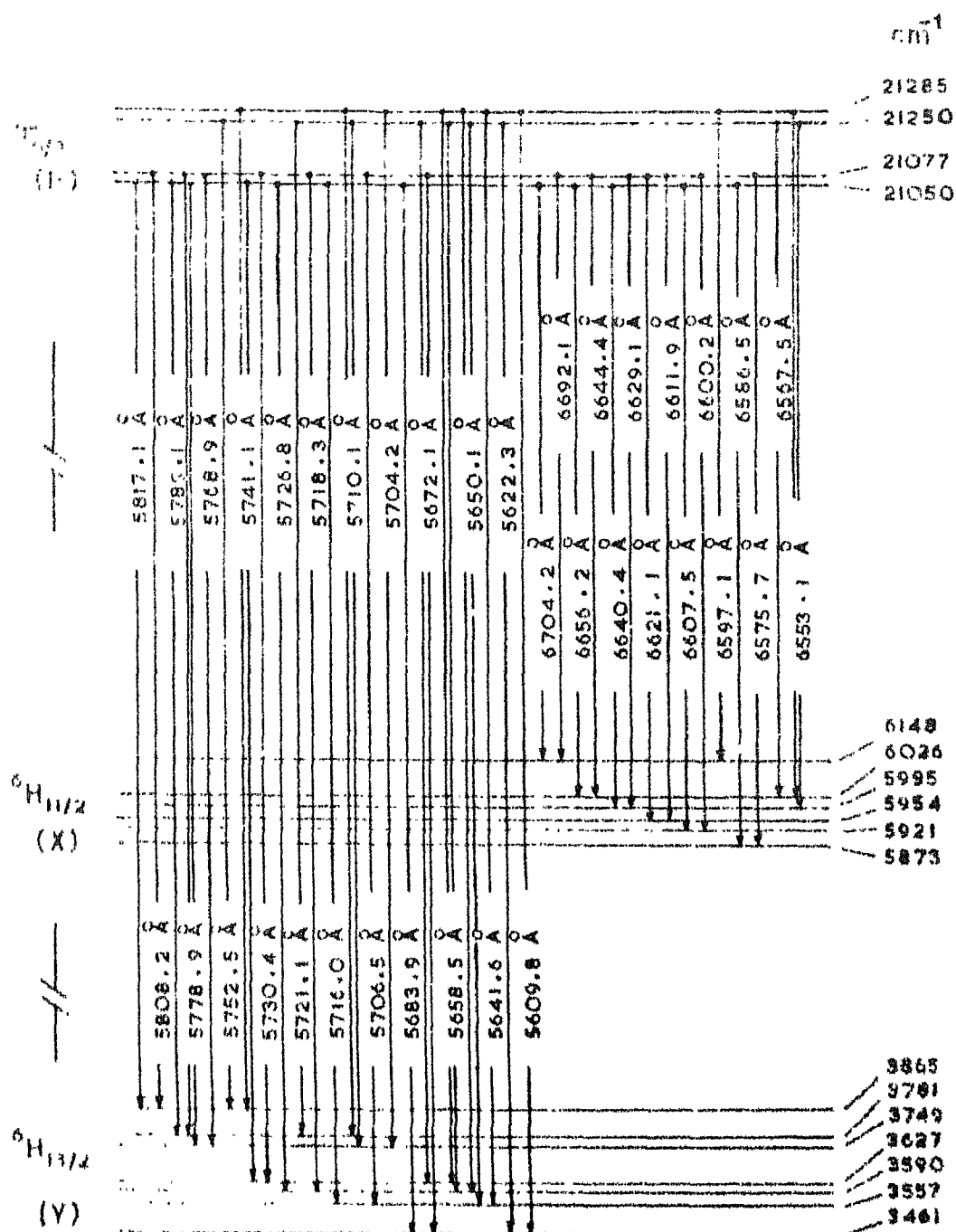


FIG. 4.8 PARTIAL ENERGY LEVEL DIAGRAM OF $\text{Dy}^{3+}:\text{CaF}_2$ FOR TETRAGONAL CENTERS SHOWING THE FLUORESCENCE GROUPS OF 5700 Å ($\text{F} \rightarrow \text{Y}$) AND 6500 Å ($\text{F} \rightarrow \text{X}$) AT 77°K.

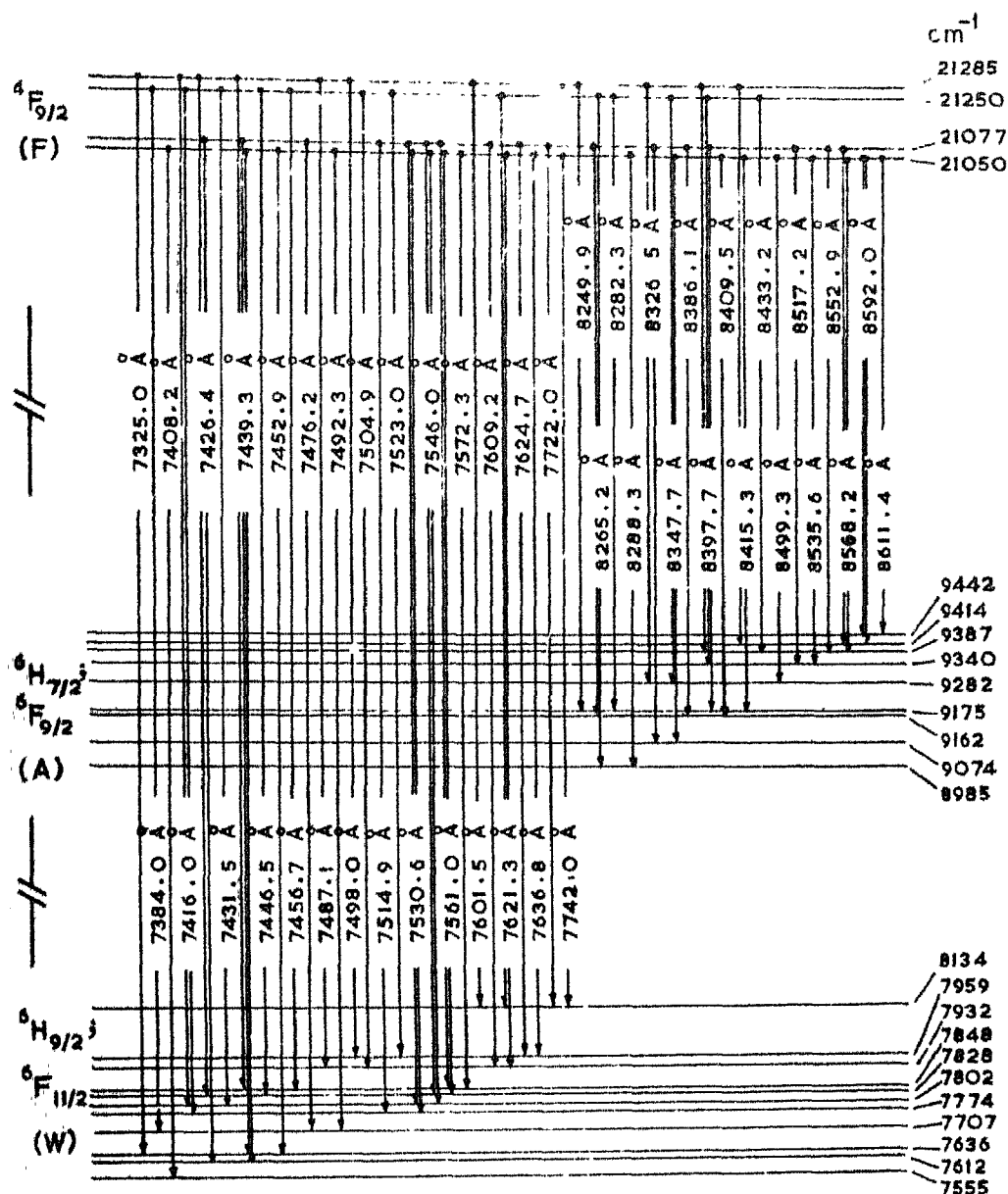


FIG.4.9 PARTIAL ENERGY LEVEL DIAGRAM OF $\text{Dy}^{3+}:\text{CaF}_2$ FOR TETRAGONAL CENTER SHOWING THE FLUORESCENCE GROUPS OF 7500 \AA (F→W) AND 8500 \AA (F→A) AT 77°K.

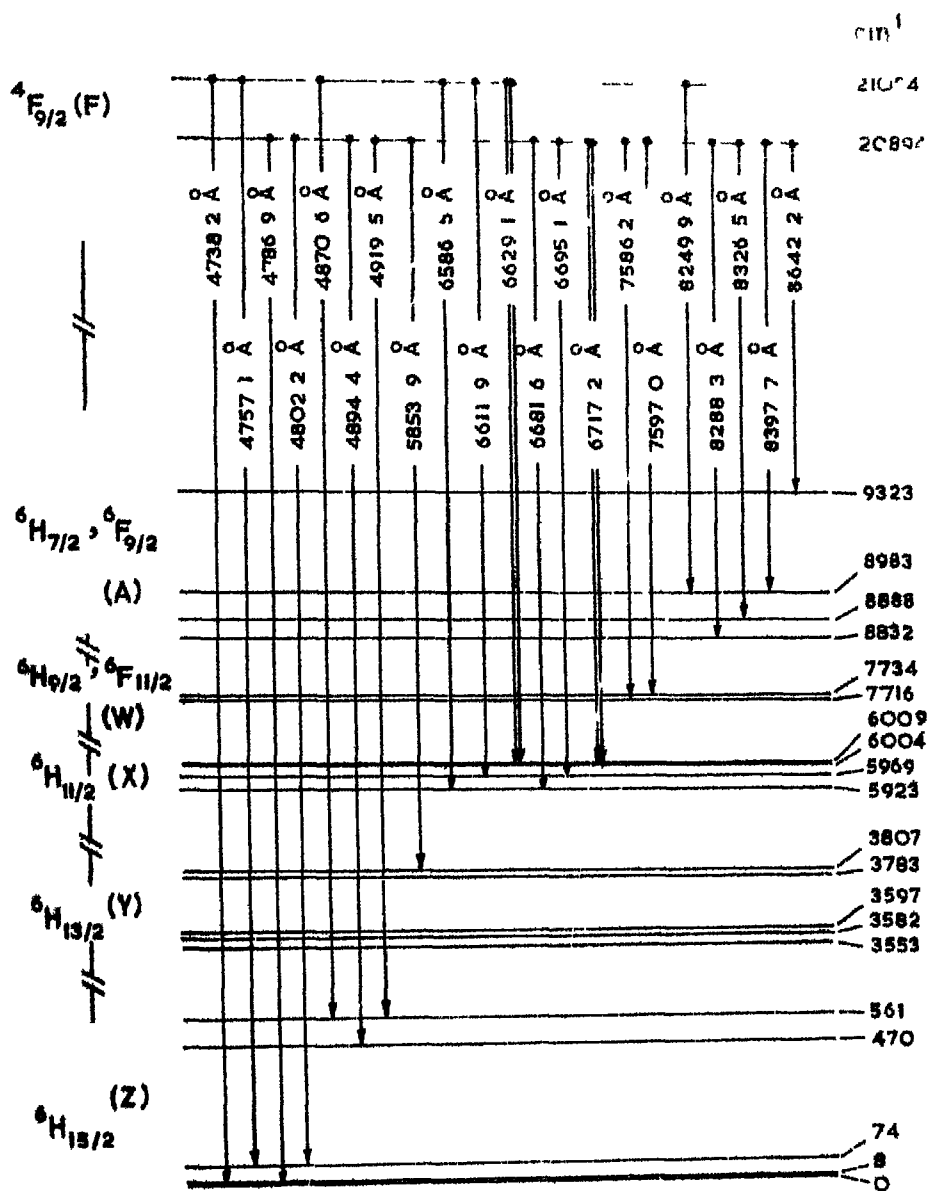


FIG 410 PARTIAL ENERGY LEVEL DIAGRAM OF Dy^{3+} CaF_2 FOR CUBIC CENTERS SHOWING THE OBSERVED FLUORESCENCE AT 77°K

Table + 1
Fluorescence spectrum of $\text{Dy}^{3+} \text{CaF}_2$ at 77° .

Wavelength (Å)	Energy (cm^{-1})	Intensity ¹ (arb units)	Transition assignments to [†]	
			Tetragonal center	Cubic center
4696.9*	21285		$4 \rightarrow Z_1, Z_2$	
4704.9*	21249		$4 \rightarrow Z_1, Z_2$	
4715.9*	21199		$4 \rightarrow Z_3$	
4722.1	21170	2VVB	$4 \rightarrow Z_3$	
4733.6	21120	5B	$4 \rightarrow Z_4, (4 \rightarrow Z_1, Z_2)'$	
4738.2*	21099		$4 \rightarrow Z_5$	$2 \rightarrow Z_1$
4744.2	21073	7SR	$2 \rightarrow Z_1, Z_2, 4 \rightarrow Z_5,$ $4 \rightarrow Z_6$	
4750.2	21046	44S	$1 \rightarrow Z_1, Z_2$	
4757.1*	21015			$2 \rightarrow Z_3$
4759.0	21007		$2 \rightarrow Z_3$	
4762.8	20990	32S	$2 \rightarrow Z_3, (4 \rightarrow Z_4)'$	
4766.5*	20974		$1 \rightarrow Z_3$	
4769.8	20959	22M	$2 \rightarrow Z_4, (4 \rightarrow Z_5)'$	$(2 \rightarrow Z_1)'$
4775.6	20934		$(2 \rightarrow Z_1, Z_2)'$, $(4 \rightarrow Z_5)'$, $(1 \rightarrow Z_6)'$	
4780.3	20913	32M	$1 \rightarrow Z_4, (1 \rightarrow Z_1, Z_2)'$	
4786.9	20885	46S	$2 \rightarrow Z_5$	$1 \rightarrow Z_1, Z_2;$ $(1 \rightarrow Z_3)'$
4793.0	20858	57S	$2 \rightarrow Z_6, 1 \rightarrow Z_5,$ $(2 \rightarrow Z_3)'$	

Table 4.1 (Contd)

Wavelength (Å)	Energy (cm ⁻¹)	Intensity ^φ (arb units)	Transition assignments to [‡]	
			Tetragonal center	Cubic center
4797.2	20840	34SR	($\Gamma_1 \rightarrow Z_3$)'	
4802.2	20818	54S	($\Gamma_2 \rightarrow Z_4$)'	$\Gamma_1 \rightarrow Z_3$
4809.1	20738	25SR	?	
4813.2	20770		($\Gamma_1 \rightarrow Z_4$)'	
4821.7 ⁸	20734	20B		
4826.9 ⁸	20712			
4836.2 ⁸	20672	13VB		
4839.7 ⁸	20657			
4847.5 ⁸	20624			
4850.5 ⁸	20612			
4855.4	20590	10VB	$\Gamma_3 \rightarrow Z_8$	
4861.0	20566	5VB	?	
4870.6	20526	13B		$\Gamma_2 \rightarrow Z_5$
4880.7	20485	22SR		($\Gamma_2 \rightarrow Z_4$)'
4883.1	20453	27	$\Gamma_2 \rightarrow Z_7, (\Gamma_3 \rightarrow Z_8)$ '	
4894.4 [*]	20426		$\Gamma_1 \rightarrow Z_7$	$\Gamma_1 \rightarrow Z_4$
4897.2	20414	33B	$\Gamma_2 \rightarrow Z_8$	
4906.0	20378	12SR	$\Gamma_1 \rightarrow Z_8$	
4913.0	20349		?	
4919.5	20322	17B		$\Gamma_1 \rightarrow Z_5$
4929.4 [*]	20281			($\Gamma_1 \rightarrow Z_4$)'
4934.6	20259	5VVB		

Table 4.1 (.Contd.)

Wavelength (Å)	Energy (cm ⁻¹)	Intensity ^φ (arb.units)	Transition assignments to Tetragonal center	Transition assignments to Cubic center [‡]
4952.9	20185	4VVB		($\bar{1} \rightarrow Z_5$)'
4966 7*	20129		?	
5609 8*	17821		$F_4 \rightarrow Y_1$	
5622.3*	17781		$F_3 \rightarrow Y_1$	
5641.6	17721		$F_4 \rightarrow Y_2$	
5650 1	17694		$F_3 \rightarrow Y_2, F_4 \rightarrow Y_3,$ ($F_4 \rightarrow Y_1$)'	
5658 5*	17668		$F_3 \rightarrow Y_3, F_4 \rightarrow Y_4$	
5672.1	17625	3VB	$F_2 \rightarrow Y_1, F_3 \rightarrow Y_4$	
5683 9	17589	10M	$\bar{1} \rightarrow Y_1, (F_4 \rightarrow Y_2)'$	
5692.8	17561		($F_3 \rightarrow Y_2$)', ($F_4 \rightarrow Y_3$)'	
5696 9	17549		?	
5700 5*	17538		($F_3 \rightarrow Y_3$)' ($F_4 \rightarrow Y_4$)'	
5704 2	17526	23..	$F_4 \rightarrow Y_5$	
5705 5	17519		$F_2 \rightarrow Y_2$	
5710.1	17508		$F_3 \rightarrow Y_5, F_4 \rightarrow Y_6$	
5716.0	17490	40M	$F_1 \rightarrow Y_2$	
5718.3	17483	52M	$F_2 \rightarrow Y_3$	
5721 1*	17474		$F_3 \rightarrow Y_6$	
5726.8	17457	42M	$F_1 \rightarrow Y_3$	
5730 4	17446	63S	$F_2 \rightarrow Y_4$	
5741.1	17414	27M	$F_1 \rightarrow Y_4, F_4 \rightarrow Y_7$	

Table 4.1 (Contd)

Wavelength (Å)	Energy (cm ⁻¹)	Intensity ^φ (arb units)	Transition assignments to [†]	
			Tetragonal center	Cubic center
5748.3	17392	12VB	(F ₂ →Y ₂)'	
5752.5	17379		F ₃ →Y ₇	
5758.2	17362	10VB	(Γ ₁ →Y ₂)'	
5768.9	17330		F ₂ →Y ₅	
5778.9	17300	27.1	F ₁ →Y ₅ , F ₂ →Y ₆	
5784.2	17234		(F ₁ →Y ₄)', (F ₄ →Y ₇)'	
5787.3	17274	10VB	(F ₁ →Y ₄)', (F ₄ →Y ₇)'	
5789.1	17269	7VB	F ₁ →Y ₆	
5799.4	17238		(F ₃ →Y ₇)'	
5803.2	17212	12L	F ₂ →Y ₇	?
5817.1	17186	15B	F ₁ →Y ₇	?
5822.9	17169	12SR	(F ₁ →Y ₅)', (F ₂ →Y ₆)'	(F ₁ →Y ₃)'
5823.9	17151			(Γ ₂ →Y ₅)'
5833.3	17137		(F ₁ →Y ₆)'	
5853.9	17078		(F ₂ →Y ₇)'	F ₁ →Y ₅
5859.1	17063		?	
5889.5*	16975		?	
5909.2	16918		?	
5926.5*	16869		?	
5934.2	16847		?	
5995.4	16675		?	

Table 4.1 (...Contd)

Wavelength (μ)	Energy (cm^{-1})	Intensity ^o (arb units)	Transition assignments to [†]	
			Tetragonal center	Cubic center
6068 5	16474		?	
6553.1	15256		$F_3 \rightarrow X_4, F_4 \rightarrow X_5$	
6567 5	15222	2VB	$F_3 \rightarrow X_5$	
6575 7	15203	34S	$F_2 \rightarrow Y_1$	
6579 4	15195	15SR	?	
6586 5	15178	8B	$F_1 \rightarrow X_1$	$F_2 \rightarrow X_1$
6597 1	15154	11M	$F_4 \rightarrow X_6$	
6600.2	15147	10M	$F_2 \rightarrow X_2$	
6607 5	15130	10M	$F_1 \rightarrow X_2$	$F_2 \rightarrow X_2$
6111 9	15120	13M	$F_2 \rightarrow X_3, (F_3 \rightarrow X_4)',$ $(F_4 \rightarrow X_5)'$	$F_2 \rightarrow X_2$
6621 1	15099	8VB	$F_1 \rightarrow X_3$	
6625 3	15090	9VVB	$(F_3 \rightarrow X_5)'$	$F_2 \rightarrow X_3$
6629.1	15081	10B	$F_2 \rightarrow X_4$	$F_2 \rightarrow X_4$
6640.4	15055		$F_1 \rightarrow X_4$	
6644 4	15046	15M	$F_2 \rightarrow X_5, (F_1 \rightarrow X_1)'$	$(F_2 \rightarrow X_1)'$
6656 2	15020	44S	$F_1 \rightarrow X_5, (F_2 \rightarrow X_2)'$	
6659 9	15011	30S	$(F_4 \rightarrow X_6)'$?
6673.2	14981		$(F_2 \rightarrow X_3)'$	
6681.6	14962	8M	$(F_1 \rightarrow X_3)'$	$F_1 \rightarrow X_1$
6684 7	14955	9M	$(F_1 \rightarrow X_3)'$	$(F_2 \rightarrow X_3)'$
6692 1	14939	16SR	$F_2 \rightarrow X_6$	$(F_2 \rightarrow X_4)'$

Table 4 1 (. Contd)

Wavelength (Å)	Energy (cm ⁻¹)	Intensity ^o (arb units)	Transition assignments to [†]	
			tetragonal center	cubic center
6695 1	14932	23F		$\Gamma_1 \rightarrow X_2$
6704.2	14912	8B	$\Gamma_1 \rightarrow X_6$	
6709 9	14899		$(\Gamma_2 \rightarrow X_5)'$	
6715 8	14836	100SR	$(\Gamma_1 \rightarrow X_5)$	$\Gamma_1 \rightarrow X_3$
6717 2	14393	33S		$\Gamma_1 \rightarrow X_4$
6722 7	14871		?	
6734 1	14846		?	
6762 9	14783			$(\Gamma_1 \rightarrow X_3)'$
7325 0	13648		$\Gamma_4 \rightarrow W_3$	
7350 1	13601		?	
7373 0	13559		?	
7384 0	13539		$\Gamma_3 \rightarrow W_4$	
7403 2	13495	5B	$\Gamma_1 \rightarrow W_1$	
7416 0	13481		$\Gamma_3 \rightarrow W_5, \Gamma_4 \rightarrow W_6$	
7426 4	13462		$\Gamma_2 \rightarrow W_2, \Gamma_4 \rightarrow W_7$	
7431.5	13453		$\Gamma_3 \rightarrow W_6$	
7439.3	13438	45S	$\Gamma_1 \rightarrow W_2, \Gamma_2 \rightarrow W_3, \Gamma_4 \rightarrow W_8$	
7446.5	13425		$\Gamma_3 \rightarrow W_7$	
7452 9	13414	10B	$\Gamma_1 \rightarrow W_3$	
7456.7	13407		$\Gamma_3 \rightarrow W_8, (\Gamma_3 \rightarrow W_4)'$	
7468.7	13386		?	
7476.2	13372	5B	$\Gamma_2 \rightarrow W_4$	

Table 4.1 (. Contd)

Wavelength (Å)	Energy (cm ⁻¹)	Intensity ^φ (arb units)	Transition assignments to [‡]	
			Tetragonal center	Cubic center
7437.1	13352		$F_4 \rightarrow W_9, (F_1 \rightarrow V_1)'$	
7452.3	13343	30M	$F_1 \rightarrow V_4, (F_3 \rightarrow W_5)'$, $(F_4 \rightarrow V_6)'$	
7493.0	13333		$F_4 \rightarrow V_{10}$	
7504.9	13321		$F_3 \rightarrow V_9, (F_2 \rightarrow V_2)'$, $(F_4 \rightarrow V_7)'$	
7514.9	13303		$F_2 \rightarrow V_5$	
7523.0	13289		$F_3 \rightarrow V_{10}$	
7530.6	13276	45S	$F_1 \rightarrow V_5, F_2 \rightarrow V_6$, $(F_1 \rightarrow V_3)'$	
7535.9	13266		$(F_3 \rightarrow V_8)'$	
7546.0	13248	33M	$F_1 \rightarrow V_6, F_2 \rightarrow V_7$	
7551.2	13239		$(F_2 \rightarrow V_4)'$	
7561.0	13222	45S	$F_1 \rightarrow V_7, F_2 \rightarrow W_8$, $(F_4 \rightarrow V_9)'$	
7572.3	13202	35M	$F_1 \rightarrow W_8, (F_1 \rightarrow V_4)'$, $(F_4 \rightarrow V_{10})'$	
7586.2	13178	60S		$F_1 \rightarrow V_1$
7597.0	13160	45S		$F_1 \rightarrow W_2$
7601.5	13152		$F_4 \rightarrow W_{11}, (F_3 \rightarrow W_{10})'$	
7609.2	13138		$F_2 \rightarrow W_9, (F_1 \rightarrow V_5)'$, $(F_2 \rightarrow W_6)'$	

Table 4.1 (Contd)

Wavelength (Å)	Energy (cm ⁻¹)	Intensity ^φ (arb units)	Transition assignments to [‡]	
			Tetragonal center	Cubic center
7614.8	13129		?	
7621.3	13118	12M	$F_1 \rightarrow W_9, F_3 \rightarrow W_{11}$	
7624.7	13112		$F_2 \rightarrow W_{10}, (F_1 \rightarrow W_6)',$ $(F_2 \rightarrow W_7)'$	
7636.8	13091	10M	$F_1 \rightarrow W_{10}, (F_1 \rightarrow W_7)',$ $(F_2 \rightarrow W_3)'$	
7656.3	13057		$(F_1 \rightarrow W_8)'$	
7677.6	13021	2VB	$(F_4 \rightarrow W_{11})'$	$(F_1 \rightarrow W_2)'$
7706.6	12972	5VB	$(F_2 \rightarrow W_{10})', (F_1 \rightarrow W_9)',$ $(F_3 \rightarrow W_{11})'$	
7722.0	12947	3VB	$F_2 \rightarrow W_{11}, (F_1 \rightarrow W_{10})'$	
7742.0	12913	2VB	$F_1 \rightarrow W_{11}$	
7763.7	12869		?	
7800.9	12815		$(F_2 \rightarrow W_{11})'$	
8249.9	12118	10B	$F_4 \rightarrow A_3$	$F_2 \rightarrow A_3$
8265.2	12096		$F_2 \rightarrow A_1, F_3 \rightarrow A_3$	
8322.3	12071	20SR	$F_3 \rightarrow A_4$	
8323.3	12062	40M	$F_1 \rightarrow A_1$	$F_1 \rightarrow A_1$
8314.0	12025	15SR	?	
8326.5	12006	55S	$F_2 \rightarrow A_2, F_4 \rightarrow A_5$	$F_1 \rightarrow A_2$

Table 4 1 (. Contd.)

Wavelength (Å)	Energy (cm ⁻¹)	Intensity ^o (arb units)	Transition assignments to [†]	
			Tetragonal center	Cubic center
8347.7	11976	30S	$F_1 \rightarrow A_2, F_3 \rightarrow A_5,$ $(F_4 \rightarrow A_3)'$	
8386.1	11921	20M	$F_2 \rightarrow A_3, (F_1 \rightarrow A_1)'$	
8397.7	11905	15M	$F_2 \rightarrow A_4, F_3 \rightarrow A_6,$ $F_4 \rightarrow A_7$	$F_1 \rightarrow A_3$
8409.5	11888		$F_1 \rightarrow A_3$	
8415.3	11880	10M	$F_1 \rightarrow A_4, F_4 \rightarrow A_3$	
8433.2	11855	5VB	$F_3 \rightarrow A_7$	
8499.3	11763	15B	$F_1 \rightarrow A_5, (F_2 \rightarrow A_4)'$, $(F_3 \rightarrow A_6)'$, $(F_4 \rightarrow A_7)'$	
8517.2	11738	10B	$F_2 \rightarrow A_6, (F_1 \rightarrow A_4)'$, $(F_4 \rightarrow A_8)'$	
8535.6	11712	10B	$F_1 \rightarrow A_6, (F_3 \rightarrow A_7)'$	
8552.9	11689	5B	$F_2 \rightarrow A_7$	
8563.2	11668		$F_1 \rightarrow A_7, F_2 \rightarrow A_8$	
8573.2	11654		?	
8592.0	11636		$F_1 \rightarrow A_8, F_2 \rightarrow A_9$	
8611.4	11609		$F_1 \rightarrow A_9, (F_2 \rightarrow A_6)'$	
8642.2*	11571		$(F_1 \rightarrow A_6)'$	$F_1 \rightarrow A_4$

Notes to Table 4.1

* Transition observed only with 3371 Å excitation

§ Lines due to Pr^{3+} -fluorescence

φ The numbers indicate relative intensities in an arbitrary scale for 0.383 mol percent concentration (i.e. 1.08 percent by wt of DyF_3 in CaF_2). The letters S, M, B, VB, VVB, SR stand for sharp, medium, broad, very broad, very very broad and shoulder transitions

‡ $(F_1 \rightarrow Z_J)'$ etc., stand for vibronic transitions corresponding to $(F_1 \rightarrow Z_J)$ etc respectively involving a 137 cm^{-1} phonon of the CaF_2 lattice (Ref 9)

Some of the transitions reported for the cubic centers have been observed. In addition, some additional lines in the shorter wavelength region are observed which could be due to transitions from the higher Stark levels of $^4F_{9/2}$ of the tetragonal center. The decay time measurements and the relative intensities of the transitions confirm this. Most of these transitions can be explained if two more Stark components of F-level at 21250 cm^{-1} and 21285 cm^{-1} (Fig. 4.7) and one more of Z-level at 665 cm^{-1} are assumed. The assignments of the observed transitions for the tetragonal center are shown in the Table 4.1 and Fig. 4.7.

Of the transitions from the cubic center, five of them could be easily identified. These are at 20385 , 20313 , 20426 , 20322 and 20135 cm^{-1} , the originating level being at 20394 cm^{-1} . The intensity variation of the first two transitions confirm this. The third and fourth transitions are overlapping transitions from both cubic and tetragonal centers. The observation of the decay time which is intermediate between that of cubic and tetragonal centers is a good confirmation. The fifth transition can be a vibronic line associated with 20322 cm^{-1} transition ($\Delta E = 137\text{ cm}^{-1}$)⁹. The transitions along with the other possible assignments are shown in Table 4.1 and the partial energy level diagram, Fig. 4.10.

5700 Å Group

A total of forty one transitions are observed in this group (Fig 4.2) The wavelengths and the intensities are shown in Table 4.1 This group has also been reported by LSS Assuming their values for the Stark levels of $Y(^6H_{13/2})$, some of the presently observed transitions including one intense transition at 17526 cm^{-1} could not be accounted satisfactorily When an alternate set of values are taken for the Stark levels of Y as 3461, 3557, 3590, 3627, 3749, 3731 and 3365 cm^{-1} , almost all the transitions excepting the very weak transitions beyond 16975 cm^{-1} are well accounted for The possible assignments are shown in Table 4.1 and are shown in Fig 4.8.

The transitions belonging to cubic centers are not many in this group. Only three transitions at 17169, 17151 and 17078 cm^{-1} could be identified with the decay time measurements These transitions are overlapping transitions (Table 4.1 and Fig 4.10) The remaining transitions at 17212, 17186 cm^{-1} observed as overlapping transitions however, could not be assigned.

6500 Å Group

Al'tshuler et al⁹⁾ have reported this group for cubic centers. The spectrum due to tetragonal centers in this region is not known. In the present study twenty-

eight transitions are observed in this group (Fig. 4.3). A good number of transitions belonging to cubic centers could be identified from the measured decay times and the relative intensity variations. These transitions are at 15130, 15011, 14962, 14932, 14386 and 14325 cm^{-1} . The intensities and the assignments are shown in the Table 4.1 and the transitions are depicted in Fig. 4.10.

Most of the transitions observed in the shorter wavelength region of this group belong to the tetragonal center. The position of the Stark components of the lower level $X(^6H_{11/2})$ are obtained by subtracting the energy of the transitions from the energy of the originating Stark levels of $^4F_{9/2}$. Fifteen of the observed transitions can be accounted for if the following set of values are used, 5873, 5921, 5954, 5995, 6026 and 6143 cm^{-1} for the six Stark levels of $^6H_{11/2}$. The assignments of the transitions are shown in the Table 4.1 and Fig. 4.8.

7500 Å Group

A study of the optical absorption and fluorescence of $\text{Dy}^{3+} \text{LaF}_3$ at 4.2°K by Fry et al.²⁵⁾ showed the existence of eleven energy levels in the region of 7600-8100 cm^{-1} which were attributed to the overlapping group of Stark levels of the $^6H_{9/2}$ and $^6F_{11/2}$ levels. The eleven fluorescence lines from $^4F_{9/2}$ to $(^6H_{9/2}, ^6F_{11/2})$ in $\text{Dy}^{3+} \text{LaF}_3$ spectrum lie in the region

12900 to 13450 cm^{-1} . In the same region, the fluorescence spectrum of $\text{Dy}^{3+} \text{CaF}_2$ includes the transitions from both cubic and tetragonal centers (Fig 4.4)

From the measured decay times and the relative intensities of the transitions, only two transitions belonging to cubic centers at 13178 and 13150 cm^{-1} are identified (Table 4.1). These are possibly originating from the lowest Stark component at 20894 cm^{-1} of $4F_{9/2}$ and terminating at 7716 and 7734 cm^{-1} of $6F_{11/2}$ level (Fig 4.10). The remaining transitions are from tetragonal centers. Assuming that most of the intense transitions originate from the lowest level 21050 cm^{-1} of $4F_{9/2}$, the eleven possible components of the level $6F_{11/2}$ of the tetragonal center are at 7555, 7612, 7636, 7707, 7774, 7802, 7828, 7848, 7932, 7959 and 8134 cm^{-1} . The relative intensities and the assignments are shown in Table 4.1 and Fig. 4.9

8500 Å Group

Fry et al.²⁵⁾ obtained nine absorption lines in the region 8990 to 9450 cm^{-1} at 4.2°K in $\text{Dy}^{3+} \text{LaF}_3$. Also, nine fluorescence lines are observed in the region of 11900 cm^{-1} , all of them originating from the lowest Stark level of $4F_{9/2}$ (at 21059 cm^{-1}), corresponding to nine Stark levels of $6H_{7/2}$ and $6F_{9/2}$ levels

In CaF_2 Dy^{3+} , twentyone transitions are observed in this fluorescence group (Figs 4 5 and 4 6) which include transitions from both tetragonal and cubic centers. The group as a whole is much weaker than the other fluorescence groups. Hence, the decay times could not be measured. From the intensity variations observed with the change in Dy^{3+} -concentration, five possible transitions from cubic centers at 12113, 12062, 12006, 11905 and 11571 cm^{-1} are identified and are shown in Fig 4.10. Of these the first three transitions may be overlapping transitions (Table 4.1). The remaining sixteen transitions are accounted for by assuming the nine Stark components of $A(^6\text{H}_{7/2}, ^6\text{F}_{9/2})$ level to be at 8985, 9074, 9162, 9175, 9282, 9340, 9387, 9414 and 9442 cm^{-1} for the tetragonal center. The relative intensities and the assignments are shown in Table 4 1 and Fig 4 9.

4.5 Temperature Dependence of the 'Cubic Spectrum'

It is to be noted from the previous section that the transitions due to cubic centers increase in intensity relative to 'tetragonal transitions' with an increase in Dy-concentration. A similar variation in the ratio of cubic to tetragonal centers with rare earth ion concentration has been observed earlier in Gd^{3+} in CaF_2 and SrF_2 crystals²⁶⁻²⁸). In the present study, in addition to this, an increase in intensity of 'cubic

transitions' with increase in temperature is observed. This can be seen in Fig. 4.11 where the fluorescence group at 7500 Å is shown at four different temperatures for the 0.383 Dy-mol percent crystal. This group is chosen as a representative because the 'cubic transitions' observed at 7586.2 and 7597.0 Å do not show any contribution from the tetragonal centers as evidenced from the decay time measurements (Sec. 4.4.1 and Fig. 4.4). The integrated intensities for the cubic and tetragonal transitions at different temperatures are shown in Table 4.2.

The distribution of the different sites in rare earth doped single crystals has been studied by many workers. Several statistical theories have been proposed¹⁸⁻²¹). The dominant centers observed in magnetic resonance and optical studies are tetragonal with the compensating $F^{\cdot-}$ ion in the nearest neighbour positions and trigonal with $F^{\cdot-}$ ion in the (1,1,1) positions²⁹). The cubic centers are assumed to be due to the non-local charge compensation by $F^{\cdot-}$ ion. All the centers are possible at low concentrations and the statistical theories predict a distribution of sites which is independent of rare earth concentrations³⁰). At high concentrations, the sites available for non-local compensation are less and hence, the cubic sites are expected

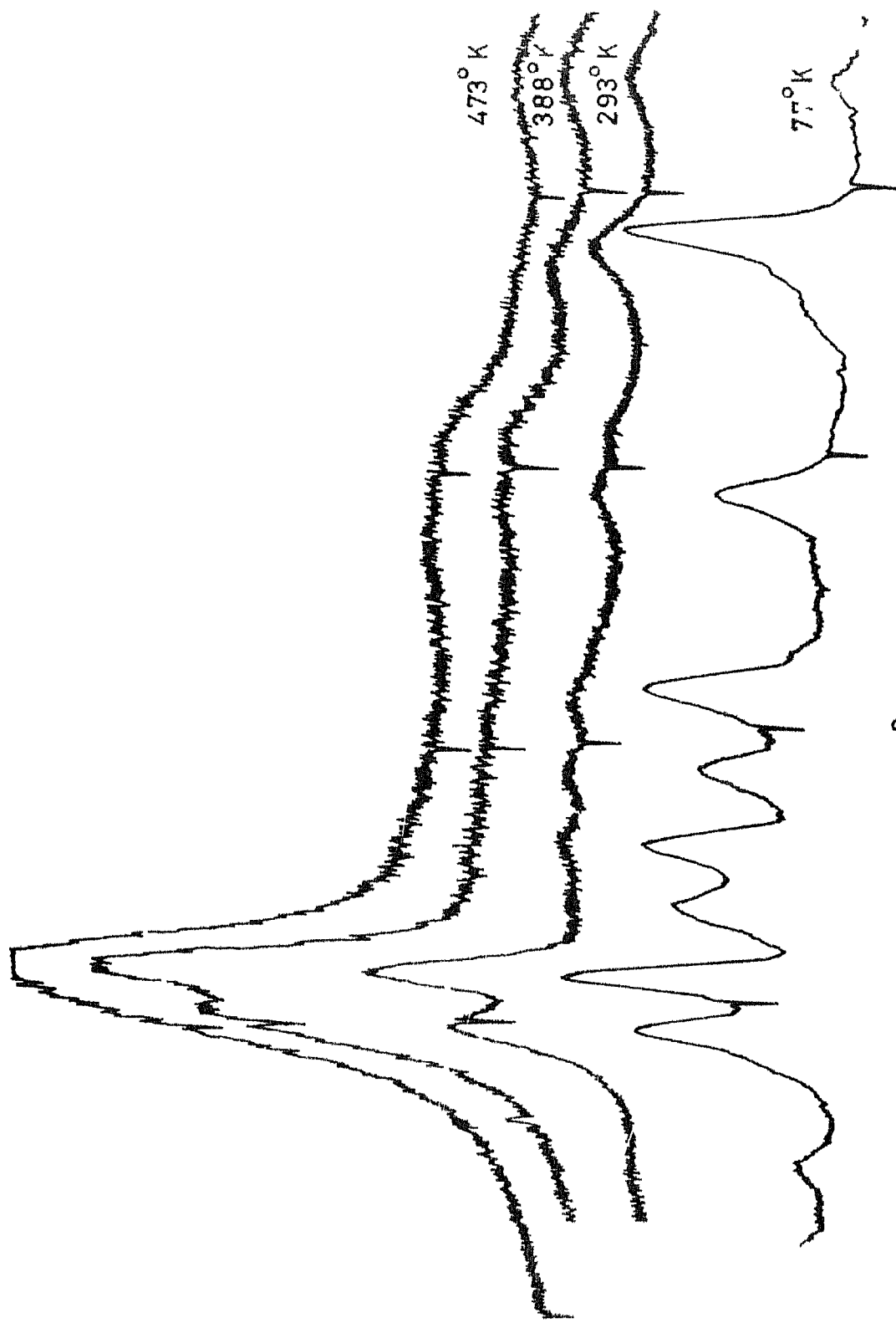


FIG 4.11 VARIATION OF THE 7500 Å (F → W) FLUORESCENCE SPECTRUM WITH TEMPERATURE

Table 4.2

Integrated intensities of cubic and tetragonal transitions
of 7500 Å group (F+W) at different temperatures

Temperature (°C)	Intensity (arbitrary units) of	
	Cubic transitions	Tetragonal transitions
77	8	26
293	13	27
338	28	46
476	41	47

to decrease in number¹⁹⁾ The dimerization and trimerization of centers are also possible at high concentrations which have their characteristic spectra¹⁸⁾ however, experimentally it has been observed from both the PL and optical studies in $\text{Gd}^{3+}:\text{CaF}_2$ and $\text{Nd}^{3+}:\text{LiF}$ systems, that the number of cubic centers increases with concentration. The same is not found to be true for $\text{Er}^{3+}:\text{CaF}_2$ in which the non-locally compensated cubic centers have been found to be absent, but the dimers and trimers formed from the tetragonal centers increase with concentration²⁴⁾. The spectrum due to clusters generally consists of broader lines compared to that due to single pairs³¹⁾

In the present study, the cubic transitions are found to increase in intensity with concentration as well as with temperature relative to tetragonal transitions. Because the observed cubic transitions are found to be sharp, these are probably not due to clusters³¹⁾

The observed variation of intensity of cubic transitions with temperature can be due to the following reasons (i) The laser radiation (4765 Å) does not excite the Dy^{3+} ion resonantly and thus the F-level population is a function of temperature and the energy mismatch. Since the density of lattice phonons increases with temperature, the phonon assisted excitation is also a function of temperature. Thus, in general, an increase

in intensity of the fluorescence can be expected at higher temperatures and this increase can be different for different centers (11) The interstitials and vacancies in a crystal migrate due to diffusion. Since, the diffusion constant increases with temperature, the charge compensating F^- ions in the local compensating sites can be expected to move out to non-local sites with higher temperatures. The probability of this process depends on the binding energy of the rare earth ion and the compensating ion. At high temperatures, therefore, one can expect an increase in the non-locally compensated sites at the cost of the locally compensated sites.

These arguments can be substantiated or negated only by studying the fluorescence spectrum at various temperatures with resonant excitation (Sec. 4.2).

4.6 Variation of the Fluorescence Spectrum with Excitation Wavelength

The fluorescence spectrum of Dy^{3+} ion excited by different wavelengths of Ar^+ laser (4765, 4727, 4658 and 4580 Å) and N_2 laser (3371 Å) shows variation in the ratios of tetragonal to cubic centers. With 4658 Å and 4727 Å, the spectra in the regions of 5700 Å and 6500 Å (Figs. 4.12 and 4.13) show variation in the intensities of the transitions towards shorter wavelength (Sec. 4.4). The positions of these transitions

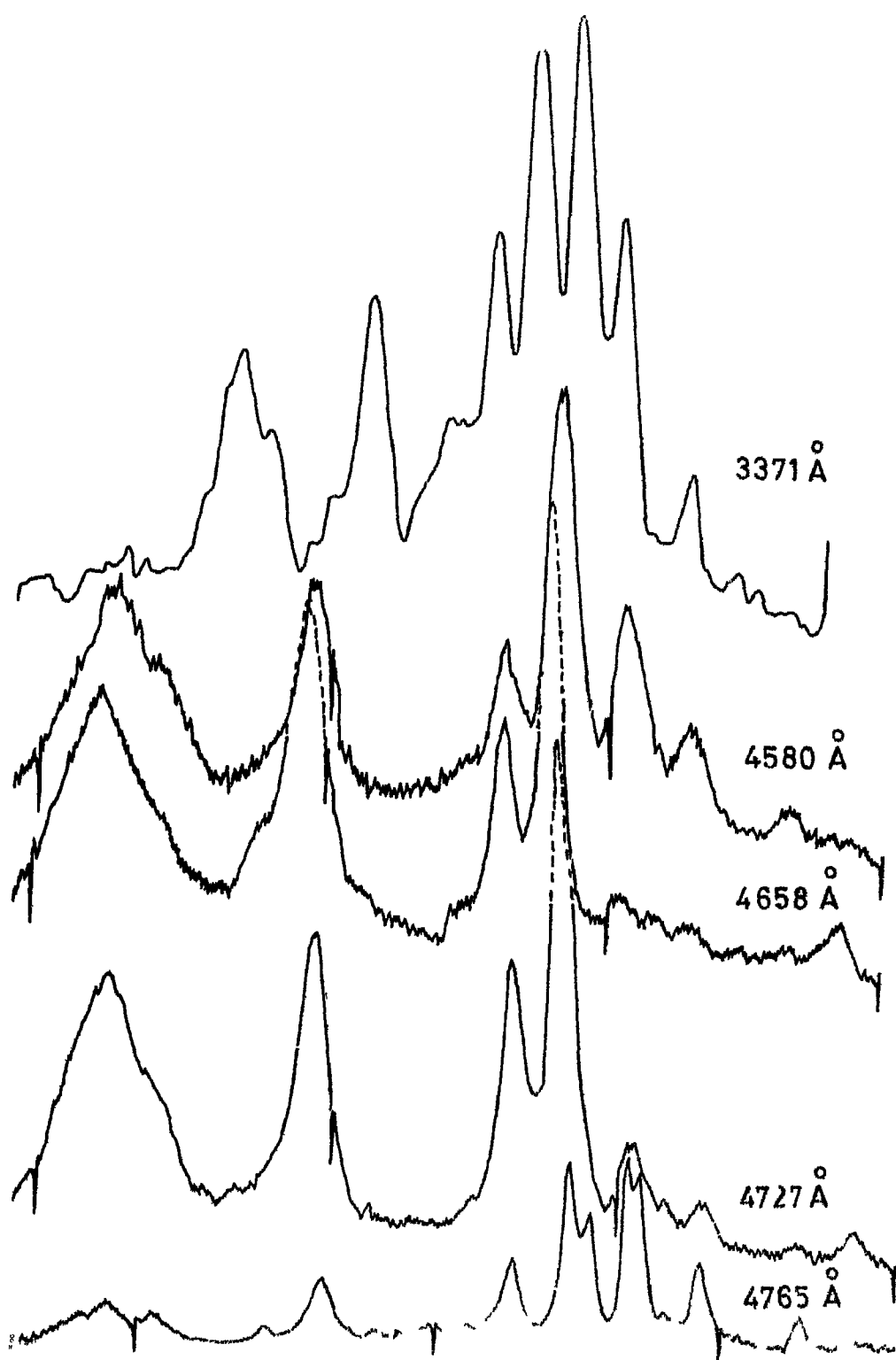


FIG. 4.12 VARIATION OF 5700 Å GROUP (F → Y) OF $\text{Dy}^{3+}(\text{aq})$,
(0.383 MOL %) WITH EXCITATION AT 77°K

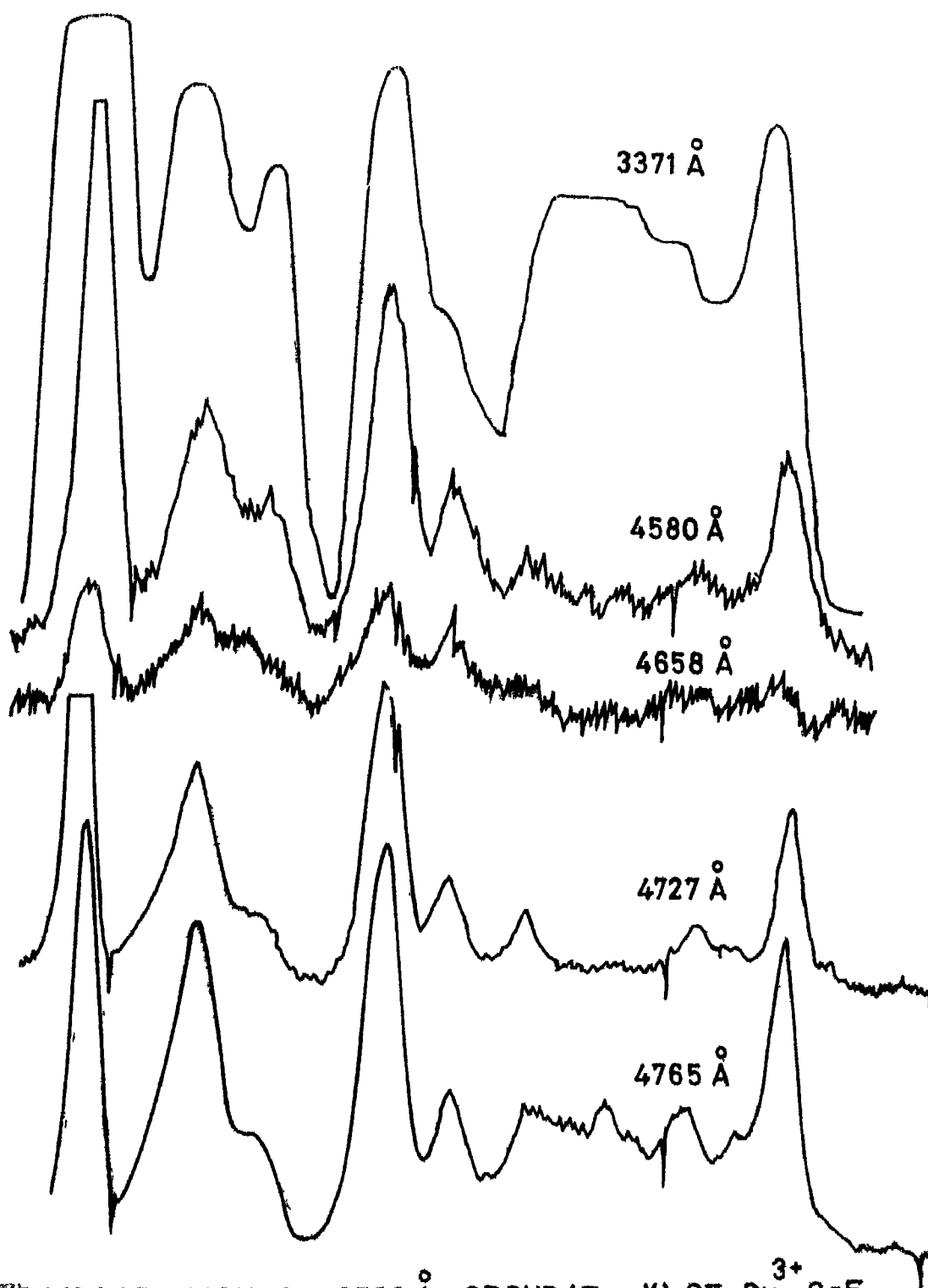


FIG 4.13 VARIATION OF 6500 Å GROUP (F→X) OF $\text{Dy}^{3+}:\text{CaF}_2$
(0.383 MOL %) WITH EXCITATION AT 77°K

are identical to those obtained with 4765 Å excitation. Also, these are found to be due to tetragonal centers (Sec 4.4.1). All the above observations suggest the possibility of these transitions being due to overlapping transitions from levels with approximately the same decay time. The identification of these centers is only possible by using higher dispersion and performing the experiments at lower temperatures (than 77°K). Resonant excitation method (Sec 4.2) also might be useful for proper identification.

4.7 High Temperature Fluorescence Spectrum

As in the case of $\text{Dy}^{3+} \text{LaF}_3$ (Sec 3.5), fluorescence from the G-level is also observed in $\text{Dy}^{3+} \text{CaF}_2$ at 300°K and higher temperatures. The overall intensity is however, much weaker than in the case of $\text{Dy}^{3+} \text{LaF}_3$. Only $\text{G} \rightarrow \text{Z}$ fluorescence could be observed and its variation with temperature is shown in Fig. 4.14. The study is done using the 0.383 Dy. Mol percent crystal (i.e. the crystal containing 1.08 percent by wt of DyF_3 in CaF_2). The decay times (τ) are measured and the 'intermediate' τ -values obtained signify the overlap of transitions belonging to tetragonal as well as cubic centers. It is found that the decay times are constant throughout the temperature range of study (300 to 673°K). Similar to the observation made in $\text{Dy}^{3+} \text{LaF}_3$, (Chap. 3) the

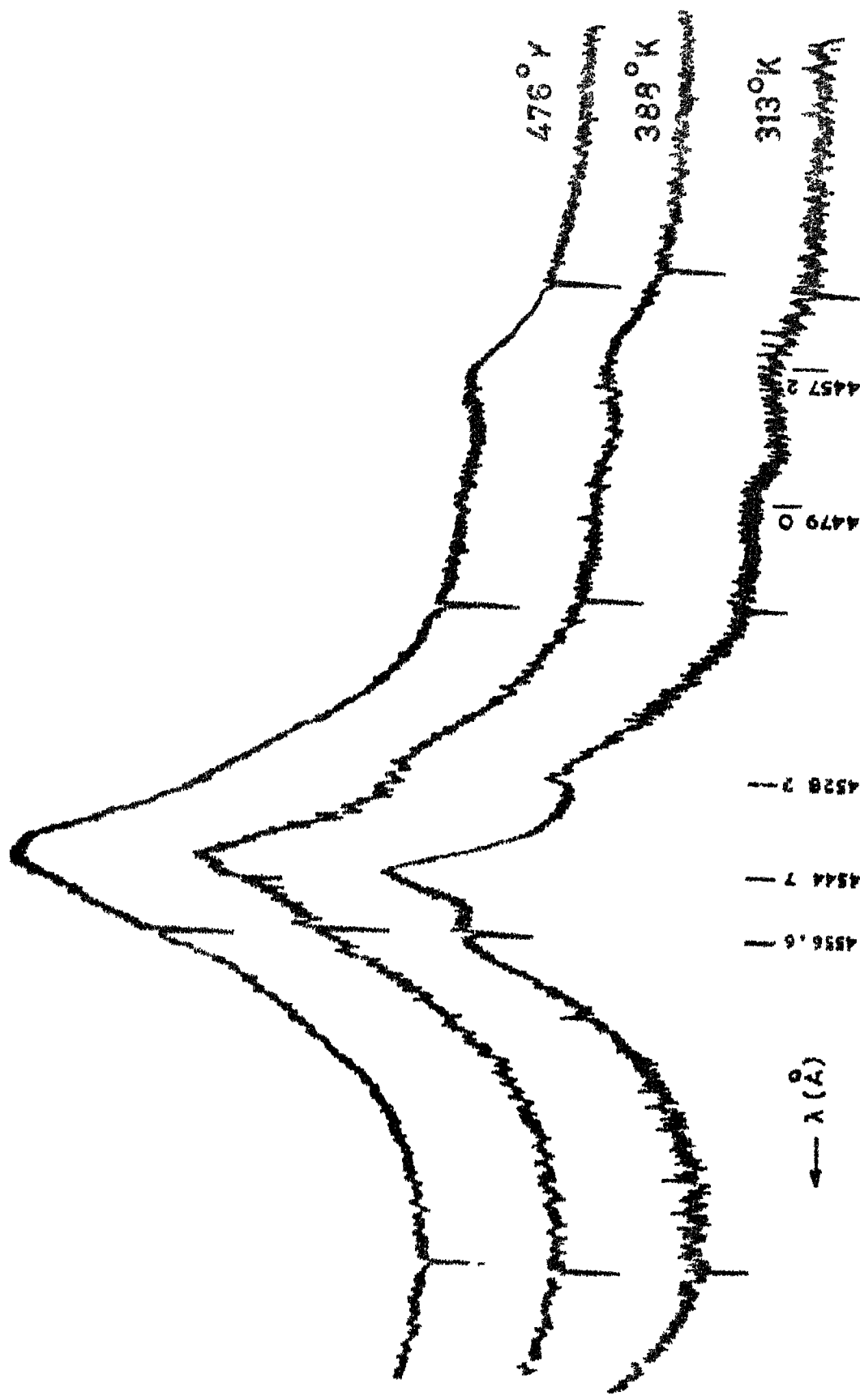


Fig 4 14 High temperature fluorescence of Dy^{3+} : CaF_2 ; 4765 Å excitation;
 $\text{G}({}^4\text{I}_{15/2}) \longrightarrow \text{Z}({}^6\text{H}_{15/2})$ Group.

F-level is also found to show a constant decay time throughout the temperature range of 77 to 673°K for the two centers, indicating the purely radiative nature of the F-fluorescence from the two centers as well as the thermal mixing of F and G levels

The transition assignments for the G → Z fluorescence are done with the help of a 'Summation-Matrix' shown in Table 4.3. The wave numbers of the five observed fluorescence lines are noted in the first column. The known energies of the Stark components of the lower level $Z(^6H_{15/2})$ are noted on top of the rest of the columns. The table is now filled as a matrix of 'sums' of energies of the lower Stark components (Z_1) and the observed lines. These 'sums' correspond to possible Stark components of the upper level $G(^4I_{15/2})$ and since a particular upper level can be involved in more than one transition, some of these numbers must coincide with one another. Because of the broad fluorescence lines, the positions are accurate to within ± 3 to 4 Å. Thus, a 'match' or 'coincidence' is taken to occur if any two numbers are within $\sim 15 \text{ cm}^{-1}$ of each other. Fifteen such 'matches' could be seen for tetragonal center, out of which the set '4' occurs four times, '14' occur three times and the rest twice. For cubic center, seven sets could be noted out of which only the sets '2' and '3'

Table 4 3

'Summation-matrix' for G 4 fluorescence of $\text{Dy}^{3+} \text{Ca}_2$

(a) Tetragonal center

Starting com- ponents of Z in cm^{-1}		Observed transitions (cm^{-1})				
		21940	21997	22073	22520	22520
Z_1	0	21940 ¹	21997 ²	22078 ⁴	22520 ³	22520 ⁹
Z_2	6	21946 ¹	22003 ^{2,5}	22034 ⁴	22526 ³	22555 ^{5,10}
Z_3	79	22019 ³	22076 ⁴	22157 ⁶	22539	22563 ¹¹
Z_4	127	22067 ⁴	22124 ⁵	22205 ⁷	22447 ¹⁰	22556 ^{12,13}
Z_5	134	22124 ⁵	22181	22262	22504 ¹¹	22613 ¹⁴
Z_6	221	22161 ⁶	22218 ⁷	22299	22541 ¹²	22650 ¹⁵
Z_7	662	22562 ¹³	22619 ¹⁴	22700	22942	23051
Z_8	665	22605 ¹⁴	22662 ¹⁵	22743	22985	23094

Note The superscripts indicate sets of matching numbers within $\sim 15 \text{ cm}^{-1}$.

Table 4 3 (Contd)

(b) Cubic center

Stark compo-

nents of
Z in cm^{-1} Observed transitions (cm^{-1})

		21940	21997	22073	22320	22429
ϵ_1	0	21940 ¹	21997 ²	22073 ³	22320 ⁴	22429 ⁵
ϵ_2	3	21948 ¹	22005 ²	22036 ³	22323 ⁴	22437 ⁵
ϵ_3	74	22014 ²	22071 ⁵	22152	22394	22503 ⁶
ϵ_4	470	22410	22467	22548 ⁷	22790	22899
ϵ_5	561	22501 ⁶	22558 ⁷	22639	22881	22990

Note The superscripts indicate sets of matching numbers within $\sim 15 \text{ cm}^{-1}$

Table 4.4
 High-temperature fluorescence spectra of $\text{Dy}^{3+} \text{CaF}_2$
 and the probable assignments

Wavelength (Å)	Energy (cm^{-1})	Intensity (arb units)	Probable assignments to	
			Tetragonal center	Cubic center
457.2	22429	9	22612-184	?
479.0	22320	13	?	?
4528.2	22078	46	22076-0, 22076-6	22078-0 22078-3
4544.9	21997	75	22076-79, 22612-622	22005-0, 22005-3, 22073-74
4556.6	21940	62	22076-127, 22612-665	22005-74

occur more than twice. The probable assignments for the observed transitions are shown in Table 4. It is to be noted that the observed G-level positions match well with the excitation spectrum reported by Schlesinger and Kwan¹¹⁾. Because of the presence of more than one Dy^{3+} -center in CaF_2 and also because all the level positions of F and G are not known for either center, the radiative relaxation rates of G levels could not be calculated (Sec 3.6) from the present data.

4.8 Conclusion

From the steady state and transient fluorescence study of Dy^{3+} CaF_2 , two centers of Dy^{3+} are identified and the energy level schemes are proposed. High temperature study yielded fluorescence from G-level and approximate Stark level positions of G obtained from this study match well with the excitation spectrum reported earlier. The observed dependence of the 'cubic spectrum' on temperature as well as the fluorescence from G-level can be better understood by recording the spectra at lower temperatures ($< 77^\circ\text{K}$) and by using resonant excitation.

REFERENCES

1. M. Rabbiner, Phys Rev. 132, 224 (1965).
2. Yu. K. Voron'ko, V. V. Osiko, V. T. Udovenchik and M. M. Pirsikov, Sov Phys Solid State 7, 204 (1965).
3. Z. J. Kiss and D. L. Staebler, Phys Rev. Lett 14, 691 (1965).
4. K. R. Lea, M. J. M. Leask and W. P. Wolf, J Phys Chem Solids 23, 1381 (1962).
5. J. L. Merz and P. S. Pershan, Phys Rev. 162, 235 (1967).
6. R. K. Luks, I. G. Saatkulov and A. L. Stolov, Sov Phys. Solid State 11, 210 (1969).
7. F. Z. Gilfanov, L. D. Livanova and A. L. Stolov, Sov Phys. Solid State 8, 108 (1966).
8. R. K. Luks and A. L. Stolov, Opt and Spec. 29, 170 (1970).
9. M. S. Al'tshuler, M. V. Eremin, R. K. Luks and A. L. Stolov, Sov Phys Solid State 11, 2921 (1970).
10. A. A. Antipin, M. P. Davydova, M. V. Eremin, R. K. Luks and A. L. Stolov, Opt and Spec. 33, 372 (1972).
11. M. Schlesinger and C. T. Kwan, Phys Rev B3, 2852 (1971).
12. H. Nara and M. Schlesinger, Solid State Commun 9, 1247 (1971).
13. H. Nara and M. Schlesinger, J Phys C5, 606 (1972).
14. Ralph W. G. Wyckoff, 'Crystal Structures', Vol. 1, Interscience Publ, NY (1971).
15. K. Nassau, 'The Chemistry of Laser Crystals', Applied Solid State Science, Vol. 2 (Ed. R. Wolfe), Academic Press, NY (1971).
16. J. C. Toledano, J. Chem. Phys 57, 4468 (1972).

- 17 R C Newman, 'Infrared Studies of Crystal Defects',
Taylor and Francis Ltd , London (1973)
- 18 V V. Osiko, Sov Phys Solid State 7, 1047 (1965)
- 19 J. Jakovsky, J Chem Phys . 46, 390 (1967)
- 20 J H. Heist and F.K Lyons, Phys Rev B1, 2970 (1970)
- 21 J C Toledano, J. Chem. Phys 57, 1046 (1972)
- 22 W A Hargreaves, Phys. Rev B6, 5417 (1972)
- 23 L Friedman and W Low, J Chem Phys 33, 1275 (1960).
24. D R. Tallant and J.C Wright, J. Chem Phys. 63, 2074
(1975).
25. J L. Fry, H.H. Caspers, H.E Rast and S.A. Miller,
J Chem. Phys. 48, 2342 (1968).
- 26 G.K. Miner, T P Graham and G T Johnston, J Chem
Phys. 57, 1263 (1972)
27. J A. Detrio, M W. Ferralli, P P Yaney, D M Ware and
V.L. Donlan, J. Chem. Phys. 53, 4372 (1970)
28. M.R. Brown, K.G Roots, J.M Williams, W.A Shand,
C Grater and H.F Kay, J. Chem Phys 50, 391 (1969)
- 29 H.J. Weber and R. V Bierl, Phys Rev. 134A, 1462 (1964).
- 30 W. Low, Phys. Rev 109, 265 (1958).
31. J B Fenn, J.C Wright and F K Fong, J Chem. Phys.
59, 5591 (1973).

CHAPTER 5

THE STEADY STATE AND TRANSIENT FLUORESCENCE SPECTRUM
OF LiF:UO_2^{4+} SINGLE CRYSTAL

ABSTRACT

The fluorescence and lifetime studies of uranium activated LiF single crystal have been carried out in the temperature range of 77 to 673°K. The fluorescence spectrum is recorded using Ar^+ and N_2 lasers in the 4500 to 8500 Å region. The spectrum in the 4700 to 6200 Å region is similar to the one reported by earlier workers. In the present study four vibrational quanta (e_1, e_2, e_3, e_4) of the 'electric dipole series' from level F and three of the 'magnetic dipole series' (m_1, m_2, m_3) from level C are observed with $\Delta\nu \sim 800 \text{ cm}^{-1}$. From the observed self-absorption of the Zero-Phonon line e_0 , the oscillator strength is calculated to be $> 2.0 \times 10^{-6}$. New fluorescence is observed in the 7500 to 8400 Å region which also shows vibrational structure with $\Delta\nu \sim 750 \text{ cm}^{-1}$. Possible excitation processes for this fluorescence are discussed.

The decay times of all fluorescence lines are found to decrease with increase in temperature. An attempt is made to explain the observed decrease in the decay times of F and C levels on the basis of simplified four level model.

5 1 Introduction

The absorption and fluorescence spectra of uranium activated alkali fluorides ($Al^+ U$) have been studied by many workers. The absorption spectrum is found to have a wide region of resonance overlap with the luminescence spectrum¹⁾ At low temperature ($< 100^\circ K$), the emission spectrum consists of a large number of narrow line-like bands and could be separated into two regions. The longer wavelength region, which is reproducible with the same relative intensities in all samples can be resolved into at least two series, both involving principal lines and their vibronic satellites. Also, the relative intensities remain the same with different excitations. The shorter wavelength region, however is different in different samples and the relative intensities of the lines are found to change with excitation wavelength also. The long wavelength region is thus attributed as due to one 'main' center and the shorter wavelength region as due to different kinds of uranium centers. The need of oxygen atmosphere while growing the luminescent samples indicates that all the luminescent centers must contain oxygen. Also, the similarity of the long wavelength spectra of $Al^+ U$ and those of uranyl salts suggests the possibility of the main center of uranium being in the form of uranyl ion (UO_2^{++})³⁾.

The first systematic study of AF U was by Runciman¹⁾ who recorded the absorption and fluorescence spectra of NaF:U phosphor at 77 and 4°K. On the basis of his observations, he proposed a model according to which the source of luminescence is a symmetrical complex, UO_6^{6-} (Fig. 5.1a). The uranyl ion (UO_2^{++}) in this model, has four O^{2-} ions perpendicular to its axis and the excess negative charge is compensated by the anion vacancy in the $\langle 111 \rangle$ direction. However, this model was ruled out by Feofilov²⁾ who studied the polarization features of the luminescence using single crystals of LiF:U. The luminescence lines were found to be due to magnetic dipole and electric dipole transitions and he could conclude from the observed polarization that the 'main' luminescent center must possess a four-fold axis of symmetry. Kaplyanskii and his co-workers³⁾ investigated the influence of unidirectional elastic deformation (Piezospectroscopic effect) and of the electric field (Stark effect) on the luminescence spectra of single crystals of LiF:U and NaF:U. They concluded that the 'main' luminescence center must possess a C_{4v} symmetry. They suggested that the uranyl ion model has to have a non-centro symmetrical distortion like a shift along $\langle 100 \rangle$ to obtain C_{4v} symmetry. The complex UO_5^+ (Fig. 5.1c) proposed by Feofilov was found to have the exact C_{4v} symmetry. Also, they could identify

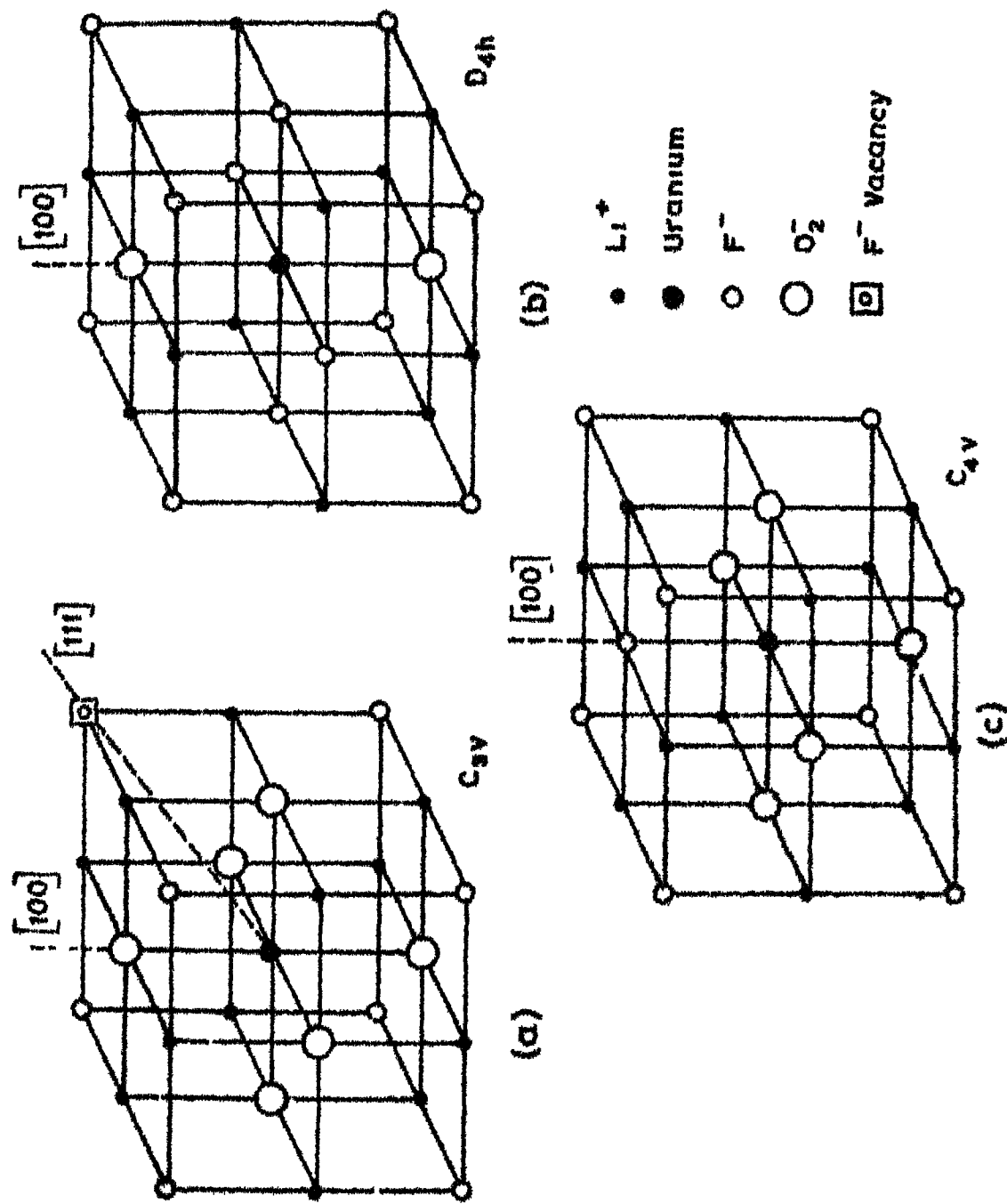


FIG. 5.1 DIFFERENT MODELS PROPOSED FOR $LiF : U$ MAIN CENTER.
(REF. 3)

two 'series' from the main center in both the crystals. The longer wavelength principal line (m_0) was associated with a magnetic dipole transition and the shorter wavelength principal line (e_0) with an electric dipole transition. Thus the corresponding vibrational series were called magnetic and electric series respectively. When the crystals were heated above 77°K , a gradual strengthening of electric series and a weakening of the magnetic series was found to take place and magnetic series disappear above 150°K . At 4.2°K , resonance absorption was found only for e_0 and not for m_0 . From the observed temperature dependence and the polarization data, they could conclude that the magnetic series must be originating from a level situated at $\sim 350\text{ cm}^{-1}$ lower than the level from which the lines of electric series originate.

The decay times (τ) of luminescence lines were measured by Tolstoi et. al.⁴⁾ who found that the lines in the longer wavelength region decay slower than those in the shorter wavelength region. At 100°K , τ was found to vary along the spectrum by a factor of four (160 μsec to 650 μsec while scanning from 4800 to 5500 \AA). Also, τ increased with the thickness of the crystal and this phenomenon due to self absorption of the luminescence was more pronounced for higher concentrations of uranium. It was also noted that for low concentrations, τ was

exponential while for high concentrations it was non-exponential. Pant and his co-workers⁵⁾ studied the absorption and luminescence of LiF, NaF and KF phosphors activated with uranium and identified several 'series'. They have also observed the temperature shift of the luminescence lines as reported by Kaplyanskii et al³⁾ The decay times were found to be non-exponential and they tried to explain their experimental observations assuming a UO_4^{2-} as the active complex. Recently Bagai and Warrior⁶⁾ reported the visible, UV and VUV absorption spectra of LiUO_4 single crystal and proposed an energy level structure based on the molecular orbital model of UO_2^{++} suggested by McGlynn and Smith⁷⁾

The spectra of uranyl salts and solutions as well as some single crystals are very well known and the energy level structures for the uranyl ion are available in literature⁸⁻¹⁰⁾.

In the present study, the luminescence and lifetimes of LiUO_4 single crystal are studied in the temperature range of 77 to 673°K using Ar^+ and N_2 lasers as the excitation sources. The author could identify four vibrational quanta ($\Delta\nu = 800 \text{ cm}^{-1}$) in electric dipole series (e_1, e_2, e_3, e_4) and three in magnetic dipole series (m_1, m_2, m_3) in addition to the principal lines (e_0 and m_0). It is found that line e_0 shows self-absorption and from the

cathetometer is 0.01 mm, but the inaccuracy in the measured value of x is slightly more than this because of the finite width of the fluorescence 'streak'.

The LiF:U single crystal is kindly loaned to the author by AVR Warrier of Solid State Physics Laboratory, Delhi. The crystal has a characteristic green glow on irradiation with UV light indicating the presence of UO_2^{++} ion. The crystal is cleaved so as to have (100) faces. The concentration of uranium in the crystal under study is found to be <250 ppm as per a semi-quantitative analysis by the Spectroscopy Division of BARC, Bombay.

5.3 Fluorescence Spectrum at 77°K

The fluorescence spectrum of LiF:U single crystal shows three distinct groups at 77°K in the regions of 4700 to 5150 Å, 5150 to 6200 Å and 6700 to 8350 Å. The fluorescence group in the short wavelength region (4700 to 5150 Å) which is probably due to different uranium centers as reported by earlier workers contains a large number of lines, the relative intensities of which show considerable change with the excitation wavelength. Some typical spectra with different excitations are shown in Fig. 5.2 and the relative intensities of the observed lines are shown in Table 5.1. The group in the long wavelength region (5150 to 6200 Å) which is also reported by earlier workers is found to be completely independent

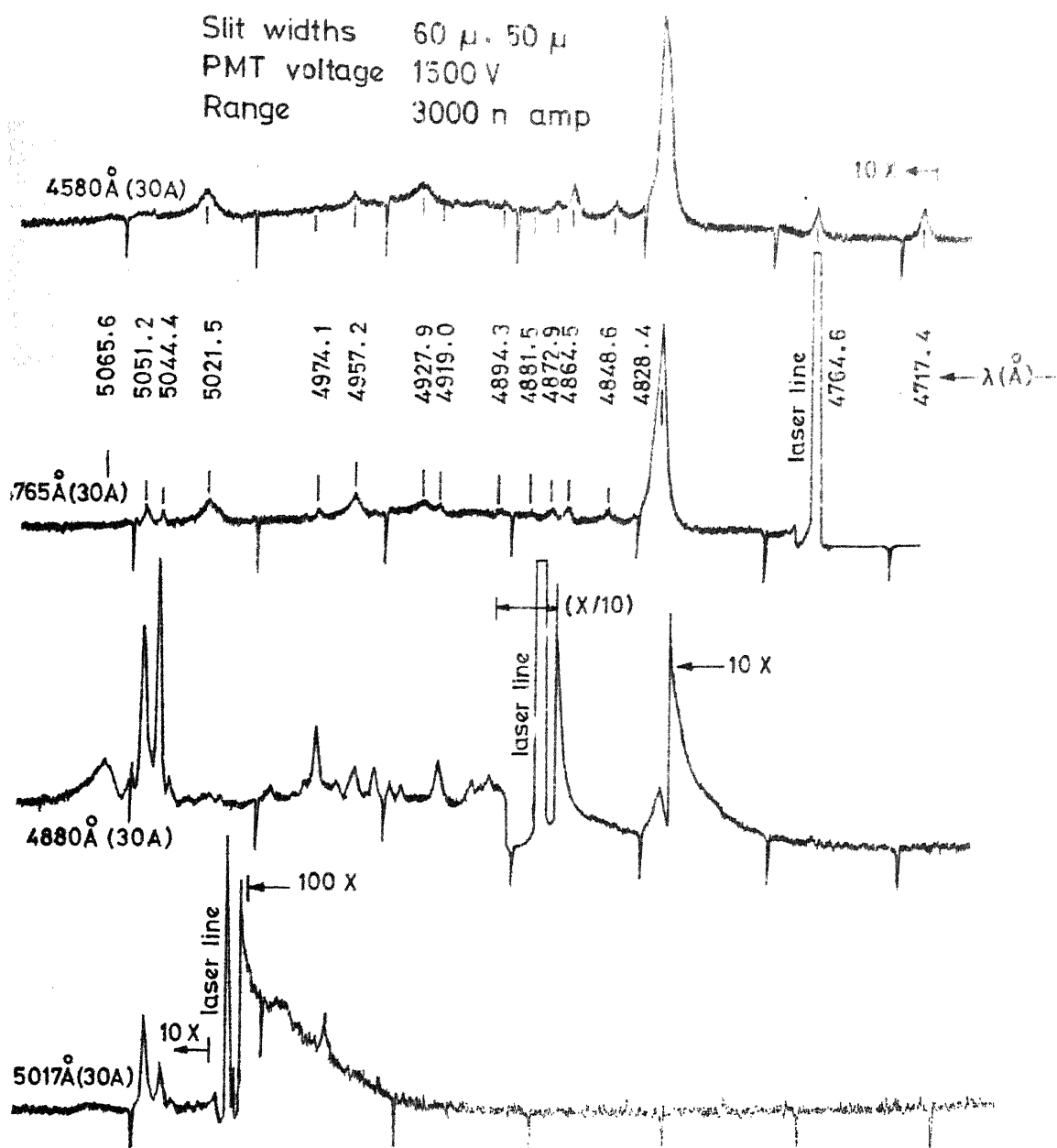


Fig.5.2 LiF :U fluorescence at 77°K, low wavelength region .

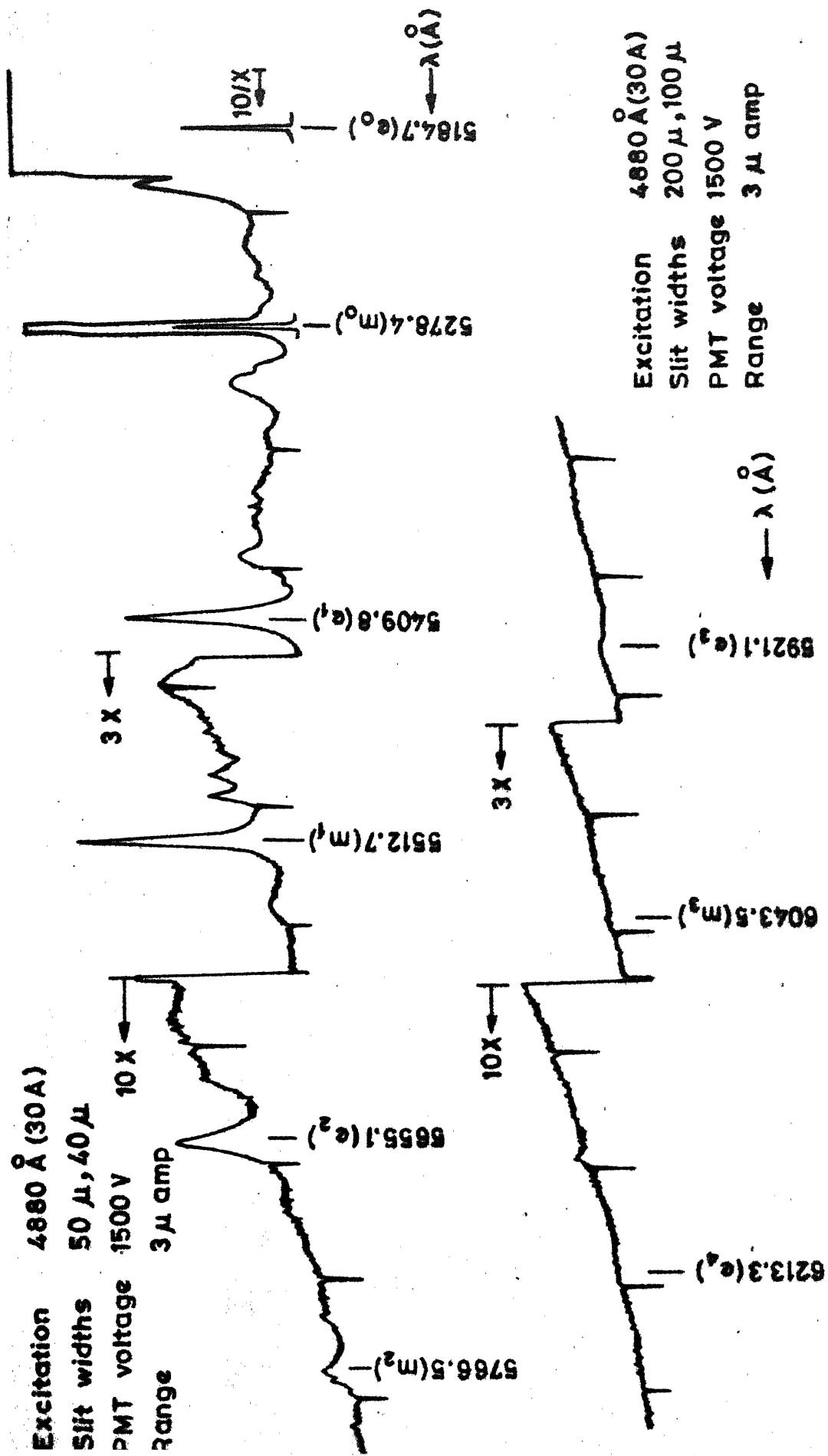


FIG.5.3 LiF :U FLUORESCENCE FROM THE MAIN CENTER AT 77°K.

Table 5.1
Fluorescence spectrum from the main center of
LiF:U single crystal

Wavelength* (Å)	Energy (cm ⁻¹)	Intensity (arb.units)	Decaytime (μsec)		Remarks
			77°K	300°K	
5184.7	19232	19000	450	50	e ₀ , showing self-absorption
5211.7	19182	1340	605		
5226.4	19128	600			
5239.3	19079	600			
5255.0	19024	430			
5259.9	19007	360			
5269.1	18973	460			
5278.4	18940	19600	570		m ₀
5296.3	18876	530			
5305.4	18844	310	595	55	
5327.7	18765	410			
5346.6	18698	430			
5354.1	18672	570			
5358.6	18656	620			
5364.4	19636	550			
5367.7	18625	550			
5374.8	18600	515			
5382.7	18673	740	595	48	

le 5.1 (.....Contd.)

Wavelength (Å)	Energy (cm ⁻¹)	Intensity (arb.units)	Decaytime (μsec)		Remarks
			77°K	300°K	
5394.3	13533	240			
5409.8	13484	2030	625	53	e ₁
5438.5	18382	520	603		
5453.9	18330	370			
5462.2	18303	360			
5481.2	18239	340			
5491.9	18204	340			
5512.7	18135	930	611	50	m ₁
5541.2	18042	120			
5595.4	17867	240			
5624.1	17776	200			
5655.1	17678	235	590		e ₂
5683.7	17589	110			
5731.5	17443	70			
5740.9	17414	67			
5766.5	17337	67			m ₂
5851.7	17084	26			
5885.5	16986	17			
5921.1	16884	15			e ₃
6016.6	16616	7			
6043.5	16542	5			m ₃
6156.9	16238	4			
6213.3	16090	2			e ₄

* observed fluorescence lines at 77°K.

m_2 at $\sim 5767 \text{ \AA}$ (17335 cm^{-1}), and m_3 at $\sim 6044 \text{ \AA}$ (16540 cm^{-1}) could be observed. It is to be noted that the structure of lines found around the principal lines (e_0, m_0) is also repeated with identical relative intensities around the vibrational lines (e_1 and $m_1, 1 \neq 0$) (Fig. 5.3). The observed separations of lines match well with the energy level structure suggested by Kaplyanskii et. al.³⁾ in which the magnetic dipole series originates from a level $\sim 340 \text{ cm}^{-1}$ lower than that from which electric dipole series originates and the ground state vibrational quantum is $\sim 800 \text{ cm}^{-1}$. Also it's to be noted that only the e_0 line shows self absorption³⁾ (Sec. 5.5).

The new group of fluorescence which is observed beyond 7500 \AA (7500 to 8400 \AA) consists of several lines the relative intensities of which remain the same with all excitations. The two lines at 7940.0 \AA (12591 cm^{-1}) and 7952.6 \AA (12571 cm^{-1}) seem to have almost the same relative intensity and structure as well as the separation when compared with the two lines at 7494.3 \AA (13340 cm^{-1}) and 7505.2 \AA (13321 cm^{-1}). The separation between these two sets is $\sim 750 \text{ cm}^{-1}$. From the Fig. 5.4 and the Table 5.2, one can identify similar sets of lines separated by $\sim 750 \text{ cm}^{-1}$ (for ex., the lines at 13050 and 12296 cm^{-1}). One will then be tempted to conclude that this fluorescence involves vibrations associated with an excited state of the

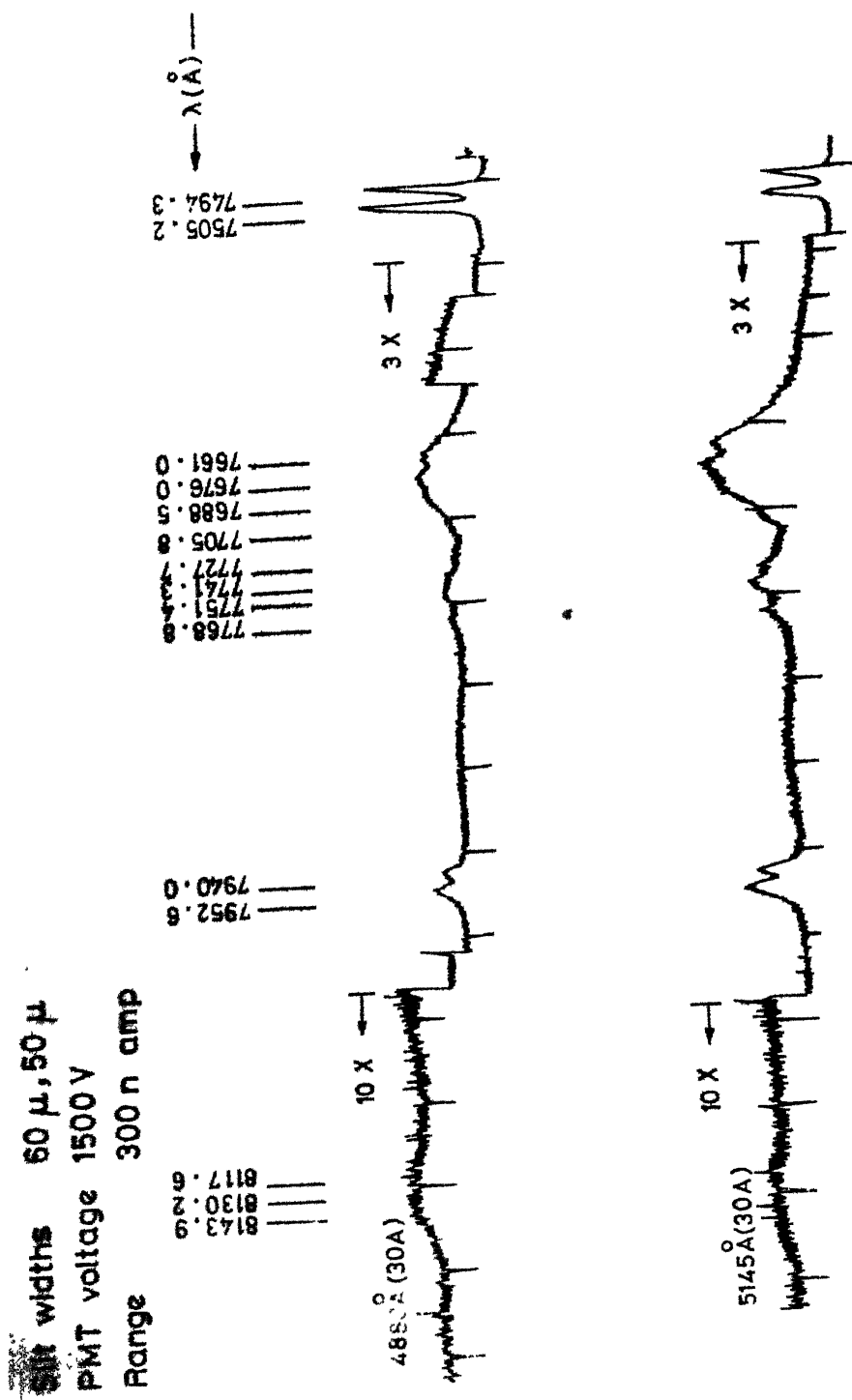


Fig. 5.4 LiF:U fluorescence at 77°K; 7500 Å group.

